JAERI-M
8286

SECOND PRELIMINARY DESIGN OF JAERI EXPERIMENTAL FUSION REACTOR (JXFR)

(INTERIM REPORT)

June 1979

Kiyoshi SAKO, Tatsuzo TONE, Yasushi SEKI, Hiromasa IIDA,
Harumi YAMATO*[1], Koichi MAKI*[2], Kimihiro IOKI*[3],
Takashi YAMAMOTO*[4], Akio MINATO*[5], Michinori YAMAUCHI*[1],
Kensuke SHIRAISHI

日本原子力研究所
Japan Atomic Energy Research Institute

この報告書は，日本原子力研究所がJAERI-Mレポートとして，不定期に刊行している研究報告書です．入手，複製などのお問合わせは，日本原子力研究所技術情報部（茨城県那珂郡東海村）あて，お申しこしください．

JAERI-M reports, issued irregularly, describe the results of research works carried out in JAERI. Inquiries about the availability of reports and their reproduction should be addressed to Division of Technical Information, Japan Atomic Energy Research Institute, Tokai-mura, Naka-gun, Ibaraki-ken, Japan.

JAERI - M 8286

Second Preliminary Design of JAERI Experimental Fusion Reactor (JXFR)

(Interim Report)

K. SAKO, T. TONE, Y. SEKI, H. IIDA,
H. YAMATO*1, K. MAKI*2, K. IOKI*3, T. YAMAMOTO*4
A. MINATO*5, M. YAMAUCHI*1, K. SHIRAISHI+

Division of Thermonuclear Fusion Research
Tokai Research Establishment, JAERI

(Received May 25, 1979)

Second preliminary design of a tokamak experimental fusion reactor to be built in the near future has been performed. This design covers overall reactor system including plasma characteristics, reactor structure, blanket neutronics radiation shielding, superconducting magnets, neutral beam injector, electric power supply system, fuel recirculating system, reactor cooling and tritium recovery systems and maintenance scheme. Safety analyses of the reactor system have been also performed. This paper gives a brief description of the design as of January, 1979. The feasibility study of raising the power density has been also studied and is shown as appendix.

Keywords: Tokamak Experimental Reactor, Design Study, Plasma Characteristics, Reactor Structure, Blanket Neutronics, Fuel Circulating System, Reactor Cooling Systems, Superconducting Magnets, Neutral Beam Injector, Radiation Shielding, Tritium Recovery System

---

*1 On leave from Tokyo Shibaura Electric Co. Ltd., Kawasaki, Japan
*2 On leave from Hitachi, Ltd., Tokyo, Japan
*3 On leave from Mitsubishi Atomic Power Industries Inc., Omiya, Japan
*4 On leave from Fuji Electric Co. Ltd., Kawasaki, Japan
*5 On leave from Kawasaki Heavy Industries, Ltd., Tokyo, Japan
+ Division of Nuclear Fuel Research, Tokai, JAERI

JAERI－M　8286

核融合実験炉第２次予備設計（中間報告書）

日本原子力研究所東海研究所核融合研究部

迫　　淳・東稔　達三・関　　泰・飯田　浩正

大和　春海[*1]・真木　紘一[*2]・伊尾木公裕[*3]・山本　　孝[*4]

湊　　章男[*5]・山内　通則[*1]・白石　健介[+]

（1979年5月25日受理）

近い将来建設が期待されるトカマク型核融合実験炉の第２次予備設計が実施された。この設計は炉システム全般に亘るものであり，プラズマ特性，炉構造，ブランケットニュートロニクス，遮蔽，超電導マグネット，中性粒子入射装置，電源系，燃料循環系，炉冷却系，トリチウム回収系ならびに保守計画を含む。炉システムの安全性解析も行った。

本報告書は上記各項目を含む設計概要を述べたものである。また，出力密度を上げた場合の可能性評価も行ない，附録で述べている。

*1　外来研究員：東京芝浦電気Ｋ．Ｋ．

*2　　〃　　：日立製作所

*3　　〃　　：三菱原子力工業Ｋ．Ｋ．

*4　　〃　　：富士電機製造Ｋ．Ｋ．

*5　　〃　　：川崎重工業Ｋ．Ｋ．

+　日本原子力研究所東海研究所燃料工学部

CONTENTS

目　　次

1. Introduction

The first preliminary design of a tokamak experimental fusion reactor to be built in near future started in April 1975 and finished in March 1977. The design report has been completed and published as JAERI-M 7300 (Sept. 1977). It was also presented at the IAEA Technical Committee and Workshop on Fusion Reactor Design (1977, Madison). This design covered the overall reactor system including plasma characteristics, reactor structure, blanket neutronics, shielding, superconducting magnets, neutral beam injector, electric power system, fuel(D and T) circulating system, reactor cooling and tritium recovery systems and maintenance scheme. By this design many problems to be overcome have been identified.

The second preliminary design with special emphasis placed on developing realistic and credible solutions to the design problems started in April 1977 and finished in March 1979. Then an overall evaluation of the design will be carried out for another year. The main design parameters are summarized in Table 1.1. The overview and the cross sectional view of JXFR is shown in Figs. 1.1 and 1.2, respectively. Some figuers in this paper are not updated but are sufficient to show the basic idea of the design.

1.1 Purposes of Design

(1) Elucidate the concept of the experimental fusion reactor.

(2) Clarify the request to the plasma physics research.

(3) Investigate the problems associated with the development of main components and subsystems of the reactor and provide bases for R & D planning.

(4) Improve the designing techniques.

Emphasis of this design is in defining problem areas rather than in the optimization from the economical point of view.

1.2 Goals of JXFR

The goals of JXFR as the facility to be built prior to the utilization of fusion power reactor are set as follows:

(1) Demonstrate the duration of fusion reaction and its control.

(2) Solve the problems in the design and construction of main components of the reactor.

(3) Solve the problems in the operation and maintenance which are essential for the realization of power reactors.

1.3 Design Bases

The following design bases are provided:

(1) The fusion power is to be at the reasonable level of 100 MW.

(2) A long operation period and a high load factor are to be achieved.

(3) The size of reactor should be as compact as possible from an economical point of view.

(4) Niobium tin (NB_3Sn) superconductor is to be available for toroidal field magnets.

(5) The cross-section of the plasma is circular, and gas blanket and mechanical limiters are employed.

(6) In order to make the best use of the toroidal magnetic field, the thickness of the blanket and shield on the inside of the torus is minimized at the cost of reduced tritium breeding ratio.

(7) The blanket is loaded with lithium oxide (Li_2O) and cooled by helium gas so as to simplify the reactor structure and maintenance scheme also to attain low tritium inventory.

(8) Stainless steel (AISI-316) is used as the main structural material.

Table 1.1 Main design parameters of JXFR (2nd preliminary design)

Power	
Fusion power (MW)	125
Thermal power (MW)	140
Electrical power (MW) ,Gross	-
Net	-
Net thermal efficiency	-
Wall loading (MW/m^2)	0.3
Operation mode	
Operation period (s)	180
Burn time (Flat top) (s)	100
Duty factor	0.6
Plant availability	0.5
Load factor	0.3
Reactor dimensions	
Major radius (m)	6.75
Plasma radius (m)	1.5
First wall radius (m)	1.75
Plasma volume (m^3)	300
Plasma	
Mean temperature (keV)	7
Mean ion density ($10^{14} cm^{-3}$)	1.1
Mean electron density ($10^{14} cm^{-3}$)	1.4
Effective charge	1.9
Confinement time (s)	7.2
Injection power (MW)	26
Toroidal field (T)	5.5
Safety factor	2.5
Poloidal beta	2.2
Toroidal beta	0.025
Plasma current (MA)	4.4
Blanket structure	
Blanket module/Reactor	8
Blanket cells/Blanket module	284
Injection and evacuation hole/Blanket module	1
Nominal max. 1-st wall temp. (°C)	520
Materials	
Structural material	316SS
Blanket fertile material	Li_2O
Reflector material	Stainless steel & W
Neutronics	
Neutron current at 1-st wall ($n\ cm^{-2} s^{-1}$)	9.5×10^{12}
Neutron wall loading ($MW\ m^{-2}$)	0.2
First wall displacement damage rate ($dpa\ y^{-1}$)	0.8
Max. helium production rate in 1-st wall ($appm\ y^{-1}$)	9.4
Max. hydrogen production rate in 1-st wall ($appm\ y^{-1}$)	29
Tritium breeding ratio	0.9
Nuclear heating per DT neutron ($MeV\ n^{-1}$)	16.1
Total induced activity at one hour after shutdown (Ci) (after one year operation)	9.1×10^7
Toroidal field magnet	
Number of coils	16
Bore, width/height (m)	7/11
Magnetomotive force (MAT)	186
Max. field strength (T)	11
Stored energy (GJ)	50
SCM material	Nb_3Sn
Neutral beam injector	
Number of ion sources	24
Deuterium beam energy (keV)	200
Injection power (MW)	32
Power efficiency	0.3
Cooling system	
Number of loops	4
Coolant, pressure ($kg\ cm^{-2}$)	He,10
Inlet/outlet temp. (°C)	300/500
Flow rate (kg/s)	143
Secondary system	He
Third system	Air cooler
Tritium inventory (kg)	
Fuel recirculating system	0.3
Tritium recovery system including blanket	0.1
Total inventory including storage	0.5

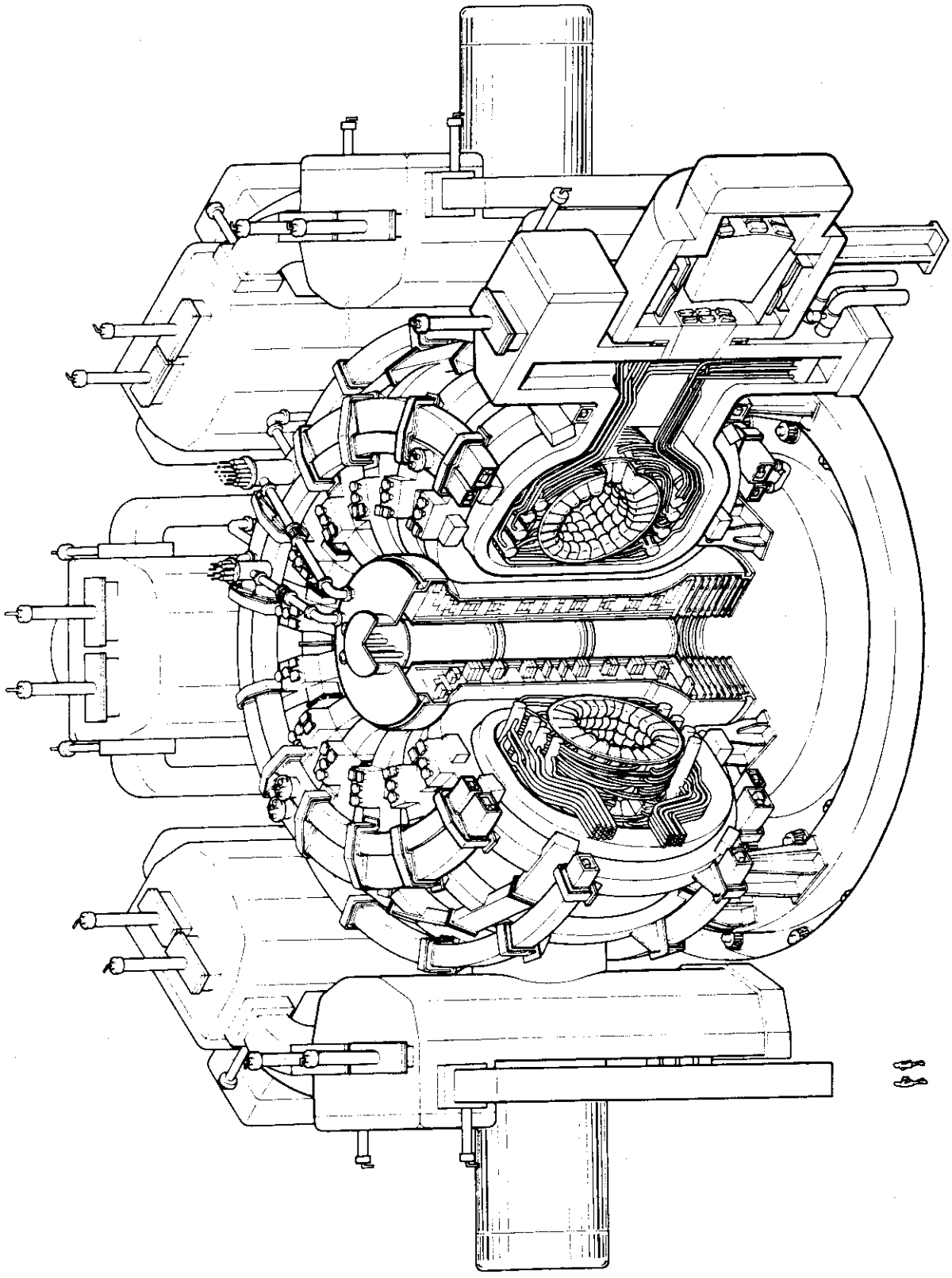

Fig.1.1 Overview of the reactor (the first preliminary design)

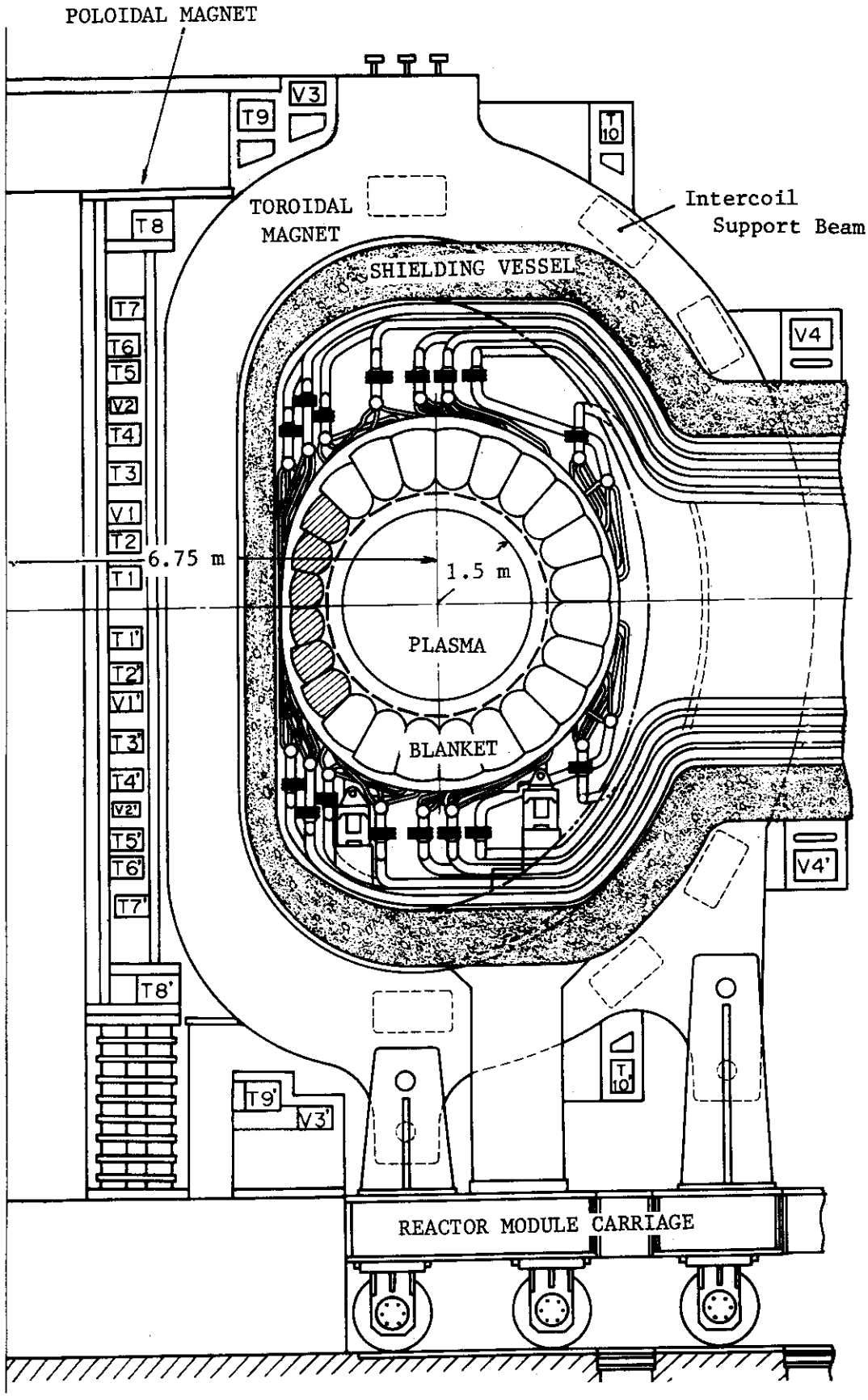

Fig.1.2 Cross-sectional view of JXFR

2. Plasma

It is difficult to obtain a self-ignition plasma at a power level of 100 MW with the plasma dimension and the toroidal field strength. Plasma operates in a beam driven mode with stationary heating by 200 keV neutral deuteron beam. The power amplification by the TCT effect gives about 10 % of total fusion power. The driven mode operation adopted is considered to be reasonable in view of the injection power and the controllability of long-time burning. The external heating broadens a thermally stable region and decreases the growth rate due to the thermal instability. Operation cycle is shown in Fig. 2.1. In the figure beam heating starts just after current rise phase, but presently a start of beam heating during current rise phase is being considered so as to optimize the start-up phase.

2.1 MHD Equilibrium

MHD equilibrium calculations for various values of poloidal beta (β_p) and plasma current (I_p) were made by the fixed boundary method. The plasma pressure and toroidal flux function profiles used are given as

$$P(\psi)=P_0\psi^{\alpha}$$

$$F^2(\psi)=F_0^2(1+\eta\psi^{\alpha})$$

$$\psi=\begin{cases} 0 & \text{at plasma surface} \\ \psi_{max} & \text{at magnetic axis .} \end{cases}$$

The exponent α which characterizes the functional form of toroidal current density is chosen to satisfy a constraint $q(0)>1$ for the safety factor.

Figs. 2.2 to 2.4 show the MHD equilibrium parameters (β_p, $q(a)$, α and I_p) which were obtained for the toroidal field B_t=5.5 T. Current reversal occurs at the points on the dashed line in Figs. 2.2 and 2.3. The value of β_t required from the plasma power balance for the reference case is 2.5 %. The lower limit of $q(a)$ chosen in view of stability is 2.5.

From the results obtained, we have chosen the plasma current 4.4 MA and the poloidal beta 2.2 as reference design parameters. The safety factor at the plasma surface q(a) and the current profile exponent α for the above parameters are 2.55 and 1.5, respectively. The flux function, plasma pressure and current density profiles along the mid-plane for the reference case are shown in Figs. 2.5 to 2.7.

2.2 Power Balance

The power balance analysis was made at a power level of 100 MW with the same injection power as the first-phase design value and the toroidal field of 5.5 T reduced from the previous 6 T. These constraints require higher beta-value and longer confinement time than those in the first-phase design. The plasma parameters listed in Table 1.1 were determined by the trapped-ion instability scaling for particle and energy confinement times. A numerical factor of the scaling law formula was enhanced twice as much as the value used in the first design, though the new value is about half as low as that given by WASH-1295 [1].

The impurity considered is carbon which is the surface material of the first wall and the estimated concentration is 3 %. Radiation losses due to ionization, recombination and excitation were estimated to be nearly equal to the bremsstrahlung loss. This estimation might be large, and a further detailed analysis is being under way. The toroidal beta was set to 2.5 % which was obtained from an MHD equilibrium analysis. The required injection power to maintain the power balance is 26 MW.

Recent experiments in PLT show that the Alcator scaling holds even in the regime of trapped-ion instability. The scaling law currently obtained is given as $\tau_E^*=5\times10^{-15}na^2q^{1/2}$ [2][3] or $5\times10^{-15}na^2$ [4] according to impurity concentration. If the scaling $5\times10^{-15}na^2$ for high impurity concentration could be applicable to our plasma conditions, it gives

1.6 sec. The required energy confinement time being consistent to its definition in experiments in which the energy loss due to impurities is considered becomes 2.5 sec. At higher plasma temperature than 7 keV also, the empirical scaling cannot satisfy the required value. If the present empirical scaling is improved about 1.5 times in the future, the power balance is maintained.

2. 3 Fuel Supply

Fueling by means of neutral gas surrounding the plasma was proposed in this reactor. The fuel must be circulated with proper pumping speed in order to decrease α-particles produced by fusion reactions and other impurities from the wall. It was found that the impurity level in the plasma could be reduced by keeping low surface plasma temperature by neutral gas cooling if impurities were produced by physical sputtering of the limiter and the first wall. The surface material of graphite is assumed in this reactor. Some other material must be selected if chemical sputtering is serious.

The neutral gas density required to obtain a steady state of the plasma density is a function of neutral gas temperature and diffusion coefficient of of plasma particles which are ambiguous at present. The plasma density of 10^{14} cm^{-3} is obtained by neutral gas of about $2x10^{12}$ cm^{-2} uniformly distributed arroud the plasma when the neutral temperature of 1eV and the diffusion coefficient of $2x10^{3}$ cm^{2}/s is assumed.

When the fusion power output is 100MW, production rate of α-particle is $3.6x10^{19}$ s^{-1}. Evacuation of about 10^{6} ℓ/s is necessary to keep content of α-particles of 2%. It is not so difficult to achieve this pumping speed in this reactor. Pumping of the gas may become much easier by placing pumping ports near the limiter because gas pressure near the limiter is higher than other part of the scrape off region.

REFERENCES

[1] DEAN, S.O., et al. : WASH-1295 (1974).

[2] KONOSHIMA, S., et al. : J. Nuclear Materials, 76 & 77 (1978) 581.

[3] SHIMOMURA, Y., MAEDA, H. : ibid., 76 & 77 (1978) 45.

[4] GOTTLIEB, M.B. : PPPL-1296 (1976).

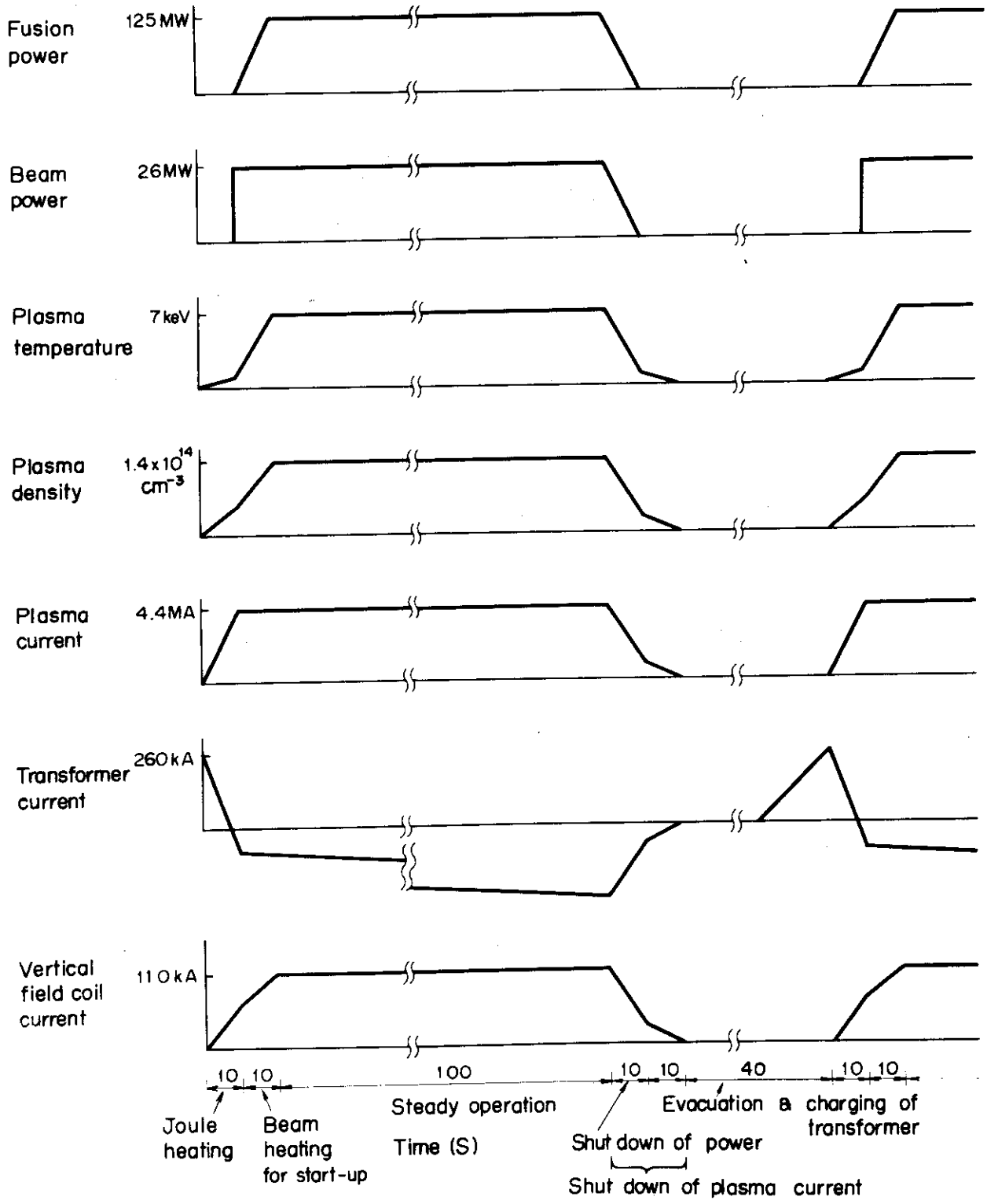

Fig. 2.1 Operation cycle

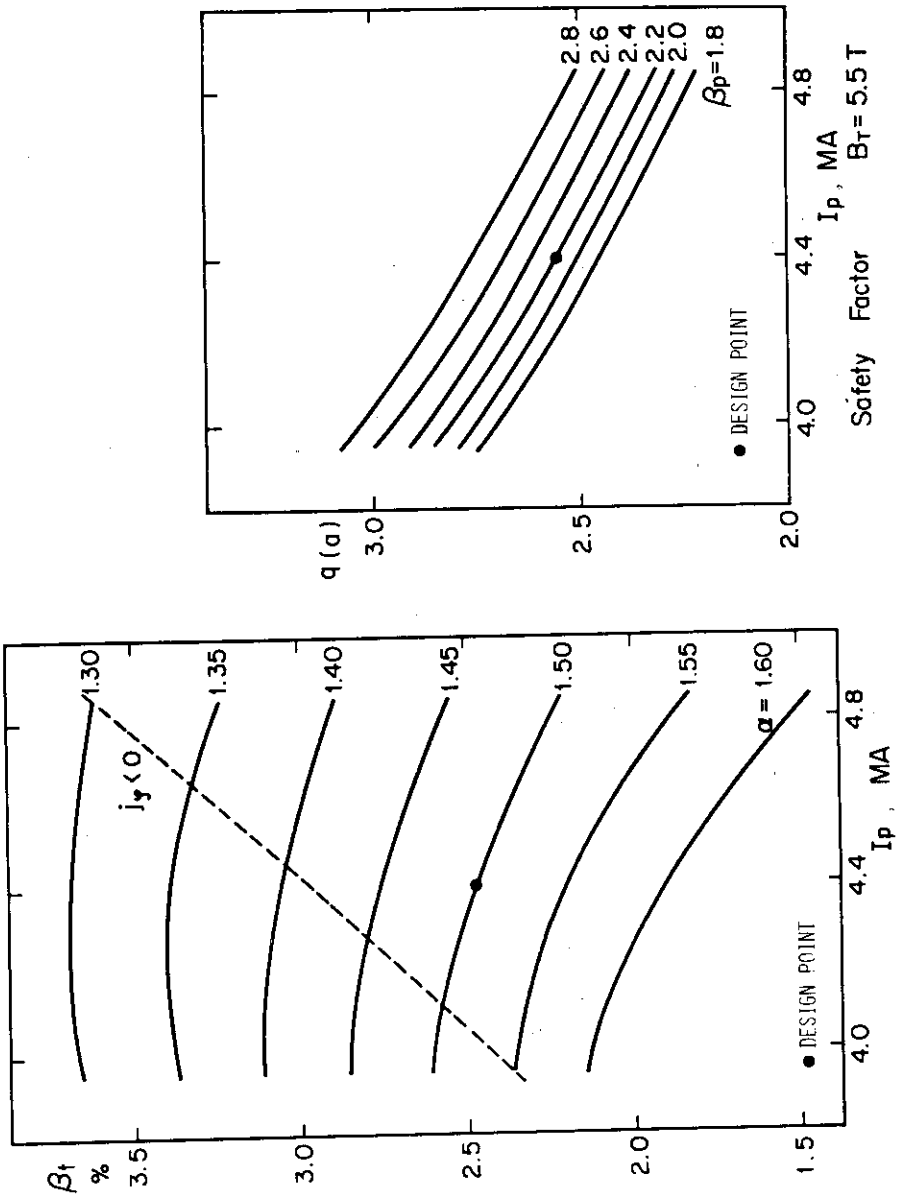

Fig. 2.2 Poloidal beta versus plasma current for B_t=5.5 T

Fig. 2.3 Toroidal beta versus plasma current for B_t=5.5 T

Fig. 2.4 Safety factor versus plasma current for B_t=5.5 T

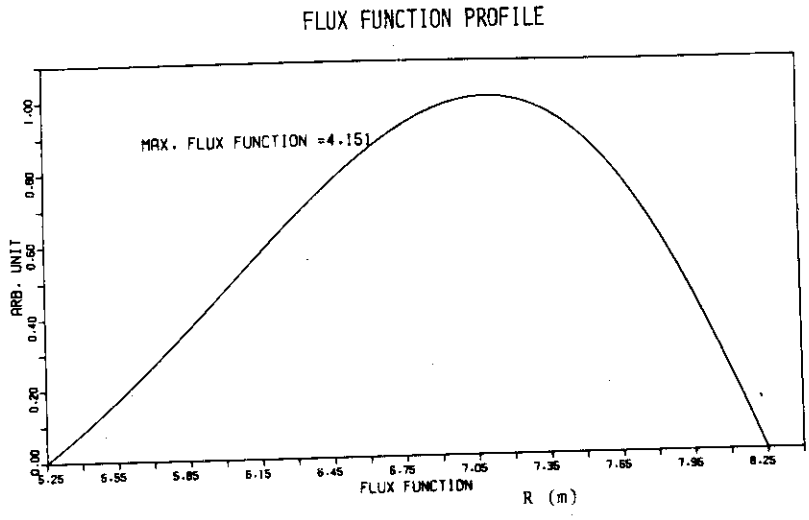

Fig. 2.5 Flux function profile along the mid-plane

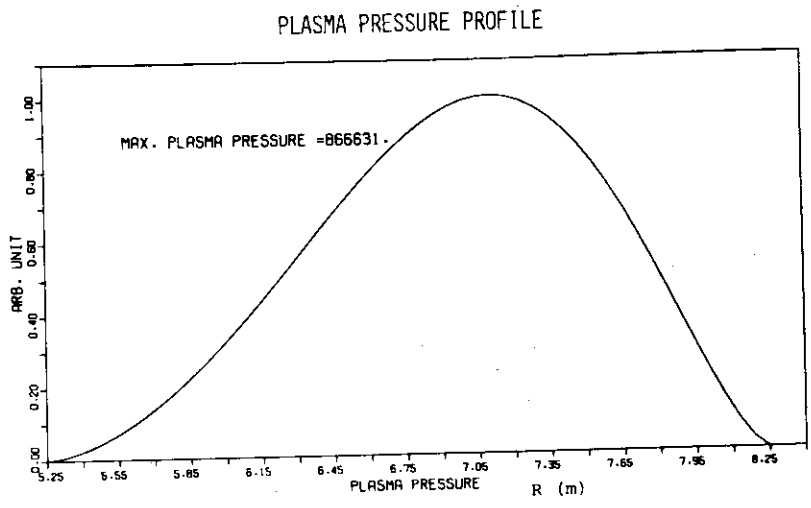

Fig. 2.6 Plasma pressure profile along the mid-plane

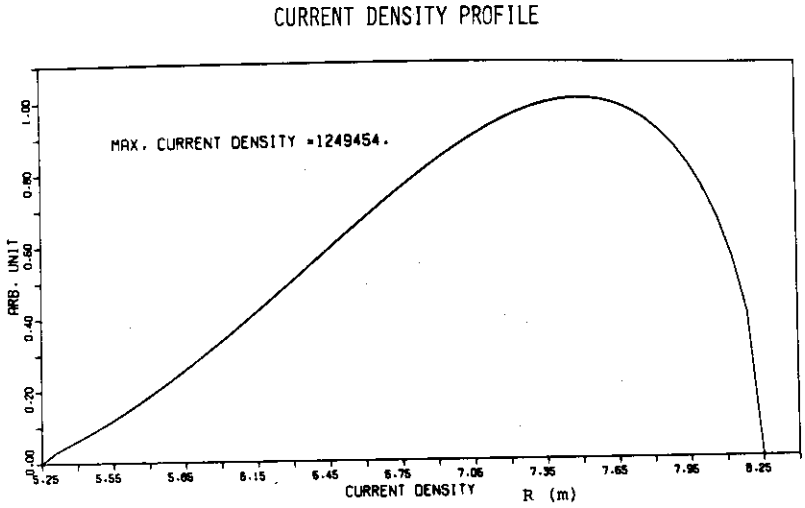

Fig. 2.7 Toroidal current density profile along the mid-plane

3. Reactor Structure

Arrangement of the reactor components is shown in Fig.1.1. The reactor consists of 8 reactor modules which may be withdraw in the radial direction for repair. Each module has a blanket module which consists of 284 blanket vessels and 1.2 meter equivalent dia. hole for the neutral beam injection and evacuation. Mechanical limiters employed are so designed that they may be withdrawn in case of failure. 4 limiters and 4 Injectors are alternately installed. Two vacuum pumps (cryo-pumps) are installed to every reactor module.

3.1 Blanket Structure

Blanket structure whose weight is about 2500 tons (including piping) in a vacuum vessel and is linked with toroidal magnets as shown in Fig. 1. It consists of 8 blanket modules. As shown in Fig.3.1, the module is formed with 12 blanket rings which consists of 24 blanket vessels each with two pieces of flanges. The hatched portion of blanket in Fig.1.2 serves exclusively for shielding purpose and the rest of the blanket includes Li_2O for tritium breeding.

The blanket structure consists of about 2,300 blanket vessels with round cornered rectangular cross sections (twelve slightly different shapes) and is placed in a vacuum vessel. Each blanket vessel is a double-walled thin-shell structure made of Type 316 stainless steel with a spherical domed surface at the plasma side. A typical blanket vessel is shown in Fig.3.2. The blanket vessel contains Li_2O pebbles and blocks for tritium breeding and stainless steel blocks for neutron reflection. The Li_2O pebbles and blocks are packed in the stainless steel canning to prevent their deformations. Ribs for coolant channel are provided between inner and outer walls. A coolant is helium gas at 10 ata (0.98MPa) and

its inlet and outlet temperature are 300°C and 500°C. The maxima of heat flux and nuclear heating rate at the first wall are 12W/cm^{2}and 2W/cc.

The volume fraction of structural material which is Type 316 SS in the blanket is limited from the requirement to obtain sufficient tritium breeding. There arise some difficult problems in the structure design of blanket vessels such as reducing pressure of wall to sufficient low level. Sufficient consideration is also required on the creep and fatigue of structural materials, because the number of thermal stress (6 kgf/mm^2, 58.8MPa) cycles on the first wall becomes 9×10^4 per year.

The following items are studied in this design : (1) mechanical stress due to internal pressure in a blanket vessel which a rectangular cross section and the effect of neighboring blanket vessels, (2) change of temperature distribution in a blanket vessel and effect of flow control, (3) high temperature (500°C) and effect of thermal cycles on the first wall of the blanket vessel, (4) change of the first wall temperature during plasma burst and effect of protection wall, (5) electromagnetic force on a blanket vessel, and (6) integrity of a blanket module.

3.1.1 Thermal and Hydraulic Design

(1) Steady State Analysis

Figure 3.3 shows the temperature distribution of the blanket vessel. At the top of the dome the temperature of outer surface is 509°C while that of inner surface is 480°C. The temperature difference between inner and outer surface (ΔT) is 29°C which causes thermal stress of 6 kg/mm^2. The temperature of dome skirt where dome is welded with body is about 330°C which may not present much problem.

(2) Transient Analysis with Protection Wall

The concept of the protection wall is shown in Fig.3.4. This wall is not cooled and the heat is removed only by radiation. The protection wall is relatively easy to repair. The material such as TZM with low Z material coating is a promising candidate for the first wall.

The variation of the protection wall temperature T_1 after start-up and the radiation heat flux Q_R to the first wall are shown in Fig.3.5, where F is overall emissivity between the protection wall to the blanket 1st wall. It indicates that the protection wall is very effective in reducing the variation of Q_R. Even if F is the low value of 0.25, the temperature of the protection wall is about 1,400°C, which is under the limitation for the application of TZM.

Furthermore, as it is possible to maintain the temperature above 1,000°C in operation after first start-up, the chemical sputtering of low Z material such as carbon coated on the wall may be reduced.

When protection wall is present, the temperature variation of the first wall after 300 sec is shown in Fig.3.6. Even without any flow control, the temperature varies slowly. The variation of the temperature drop in the first wall is shown Fig.3.7. The variation range is small and the changes are slow.

The above mentioned analyses were carried out for the first preliminary design of JXFR[1]. The analysis for the second design should lead to nearly the same results.

3.1.2 Stress Analysis of Blanket Structure

A design philosophy of the blanket structure is based on high tritium breeding ratio and more effective shielding performance. The shin-shell vessel with a rectangular cross section satisfies the design philosophy. We have designed the blanket structure so that the neighboring vessels are mutually supporting in order to decrease the large deflection and stress due to internal pressure in case of the thin-shell vessel.

An elastic analysis was carried out on a typical blanket vessel (a square cross section : 60 × 60 cm) with a three-dimensional model using a finite element method. The three-dimensional model is shown in Fig.3.8.

In the stress analysis, the design pressure of 12 ata (1.18MPa) is used as internal pressure. A gap between neighboring blanket vessels is 2.0 mm which was determined by previous study[1] and the outer wall (excluding the rib height) and the spherical dome are 10 mm and 5 mm in thickness. Fig.3.9 shows the stress intensity at the outside surface of O-A'-A section (shown in Fig.3.8) in the cases of free-standing type and mutually supporting type.

The evaluation of the stress obtained is based on the ASME. Code Case 1592. The analyses in preliminary stage revealed that the blanket vessel have enough margin against a primary stress (membrane stress plus bending stress).

3.2 Primary Shielding (Vacuum Chamber)

The functions of the shielding vessel are radiation shielding for the magnet, vacuum barrier, and support for the blanket. The shielding vessel is tubular torus and located between the blanket and TF magnet. Its major radius and inner bore are 6.75 m, 5.8m × 9.3m, respectively. From the consideration of the spacial arrangement, the thickness of the shielding vessel is determined to be 0.45 m at the smaller radius part, and 0.85 m at the larger radius part. The shielding vessel is divided into 8 sectors along the torus for assembling and disassembling the reactor. The structure of the one-eighth sector of the shielding vessel is shown in Fig.3.10. As shown in the figure, one NBI port is attached to the outer radius part of the one-eighth shielding vessel.

The main structure of the shielding vessel is formed by the stainless steel panels and is filled up with heavy concrete (stainless steel-heavy concrete). About 10 v% of water channels are buried in the heavy concrete to remove the nuclear heat (maximum 0.023 w/cm^3) and to obtain the required shielding characteristics. Maximum operation temperature and temperature gradient in the heavy concrete are settled to be 80°C and 1°C/cm, respectively.

To form the vacuum barrier, stainless steel lining is fixed to the inside (blanket side) of the stainless steel-heavy concrete structure. Part of this lining consists of bellows to acquire the electrical resistivity (more than 0.5 mΩ) along the torus. Ceramic breaks are also inserted within the stainless steel-heavy concrete structure at the position corresponding to the bellows. Seal welding at the flange of each one-eighth sector is employed for vacuum seal. The vacuum lining except the bellows is cooled by water to remove the thermal radiation heat from the blanket ($\sim$0.5 w/cm^2). The bellows are protected from the thermal radiation by the protection plate. The permeated tritium through the vacuum lining is purged by helium gas flow

in the gap between the lining and the stainless steel-heavy concrete structure. At the outside of the stainless steel-heavy concrete structure, lead layer is fixed for gamma-shielding. But at the smaller radius part, this lead layer is excluded for spacial arrangement requirement. Eight blanket support legs for one-eighth sector are fixed to stainless steel-heavy concrete structure through the vacuum lining. The maximum load on the leg is estimated to be 74 ton.

3.3 Materials

3.3.1 Structural Material

As the structural material for the JXFR, 316 stainless steel is selected on the basis of industrial capability and extensive data for the design. Although radiation damage of the steel has been extensively studied for LMFBR materials, the damage in fusion reactor environment is not well understood. Ductility loss and void swelling in the steel are supposed to be enhanced by He-production when the temperature exceeds 500°C under severe irradiation. In case of the low wall loading reactor, the radiation damage can be predicted from extrapolation of existing data. In addition, refractory metal first wall with low-Z material coating is used to protect the blanket structural material against thermal radiation from plasma.

The effects of radiation damage should be considered for blanket structural material of the higher wall loading reactor. Dimensional change and mechanical properties such as ductility, fatigue and creep under fusion reactor environment is required to be predicted as a function of radiation temperature and neutron fluence. In addition to engineering data available from fission reactor irradiation, fundamental studies are necessary to establish the correlation among damages 14 MeV produced by neutron, fission neutron, ion and electron irradiation. An advanced austenitic stainless steel is expected to be developed as blanket structural material for the higher wall loading reactor.

3.3.2 Breeding material

Solid blanket breeding materials have certain advantages concerning reactor structure and maintenance, and tritium inventory in comparison with liquid metal or fused salts in a fusion reactor, and lithium oxide

(Li_2O) pellets had been selected as a solid blanket material in the JXFR because its high lithium density (8.2×10^{22} atoms cm^{-3}) and high melting temperature (1420°C). At that time, any data on Li_2O compacts had not been available. In this circumstance, studies of Li_2O have been carried out to clarify properties and irradiation behaviors of Li_2O pellets and to establish excellent and economical preparation methods of sintered Li_2O pellets. The following research items were already finished.

1. Preparation of sintered Li_2O pellet

Sintered Li_2O pellets of a wide range of density from 70 to 99 % theoretical were prepared by a usual press-sintered method [2] and by an isostatic high pressure high temperature hot pressing method. Photomicrographs of polished and etched sections and scanning electron micrographs of the fracture surface of sintered Li_2O pellets were successfully taken to clarify the sintering behavior and properties [3].

2. Thermal properties

Thermal conductivity of sintered Li_2O pellets was measured in the temperature range from 200 to 900°C, and its porosity dependence was determind using the Maxwell-Euckan formula [4] (Fig.3.11), whereas thermal expansion coefficient (Fig.3.12) and heat capacity [5] (Fig.3.13) were also measured in the same temperature range. In addition, vapor pressure of Li_2O was measured in the temperature range from 1000°C to 1300°C using a mass-spectrometer.

3. Compatibility of Li_2O with metals and alloys

Preliminary experiments on the compatibility of Li_2O pellets with commercially available metals and alloys (316 stainless steel, Incolloy 800, Hastelloy X-R, Inconnel 600, Ni, Mo, TZM) were carried out using the reaction couple method, and some results were obtained for weight losses (Fig.3.14),

reaction depth (Fig.3.15) and activation energies of the reaction [6,7]. Studies of the vaporization of the reaction products such as Li_4FeO_5 [8] (Fig.3.16) and $LiCrO_2$ [9] (Fig.3.17) were also done.

4. Tritium release and irradiation effects

Tritium releases from neutron irradiated Li_2O pellets due to diffusion process as well as due to recoil process were studied, and preliminary results of density dependence of tritium release and chemical forms of released tritium[10] (Fig.3.18) and of recoil range were obtained. Studies of dose dependence of the Vickers microhardness of Li_2O pellets and its recovery were also measured at room temperature [11] (Figs. 3.19 and 3.20).

The following research items are now in progress.

1. Experiments on dose dependence of bulk density and lattice parameter changes in Li_2O pellets.
2. ESR and optical absorption studies of neutron irradiated Li_2O pellets.
3. Studies of neutron flux depletion and temperature distribution in Li_2O pellets under pile irradiation.

REFERENCE

[1] SAKO,K.,MINATO,A., 7th Symposium on Engineering Problems of Fusion Research, Vol.II, 1977, pp. 1490.

[2] TAKAHASHI, T., KIKUCHI, T., JAERI-M 7518 (1978).

[3] FUKAI, K., NASU, S., J. Nucl. Mater. 74 (1978) 351.

[4] TAKAHASHI, T., KIKUCHI, T., internal memo (1979), in Japanese.

[5] TANIFUJI, T., SHIOZAWA, K., NASU, S., J. Nucl. Mater. 78 (1978) 422.

[6] KURASAWA, T., TAKESHITA, H., MURAOKA, S., NASU, S., MIYAKE, M., SANO, T., J. Nucl. Mater., in press.

[7] TAKESHITA, H., KURASAWA, T., MURAOKA, S., NASU, S., MIYAKE, M., SANO, T., J. Nucl. Mater., in press.

[8] TAKESHITA, H., OHMICHI, T., NASU, S., WATANABE, H., SASAYAMA, T., MAEDA, A., MIYAKE, M., SANO, T., J. Nucl. Mater. 78 (1978) 281.

[9] OHMICHI, T., TAKESHITA, H., NASU, S., SASAYAMA, T., MAEDA, A., MIYAKE, M., SANO, T., J. Nucl. Mater., submitted.

[10] NASU, S., KUDO, H., SHIOZAWA, K., TAKAHASHI, T., KURAWAWA, T., TACHIKI, M., TANAKA, K., J. Nucl. Mater. 68 (1977) 261.

[11] NASU, S., FUKAI, K., TANIFUJI, T., J. Nucl. Mater. 78 (1978) 254.

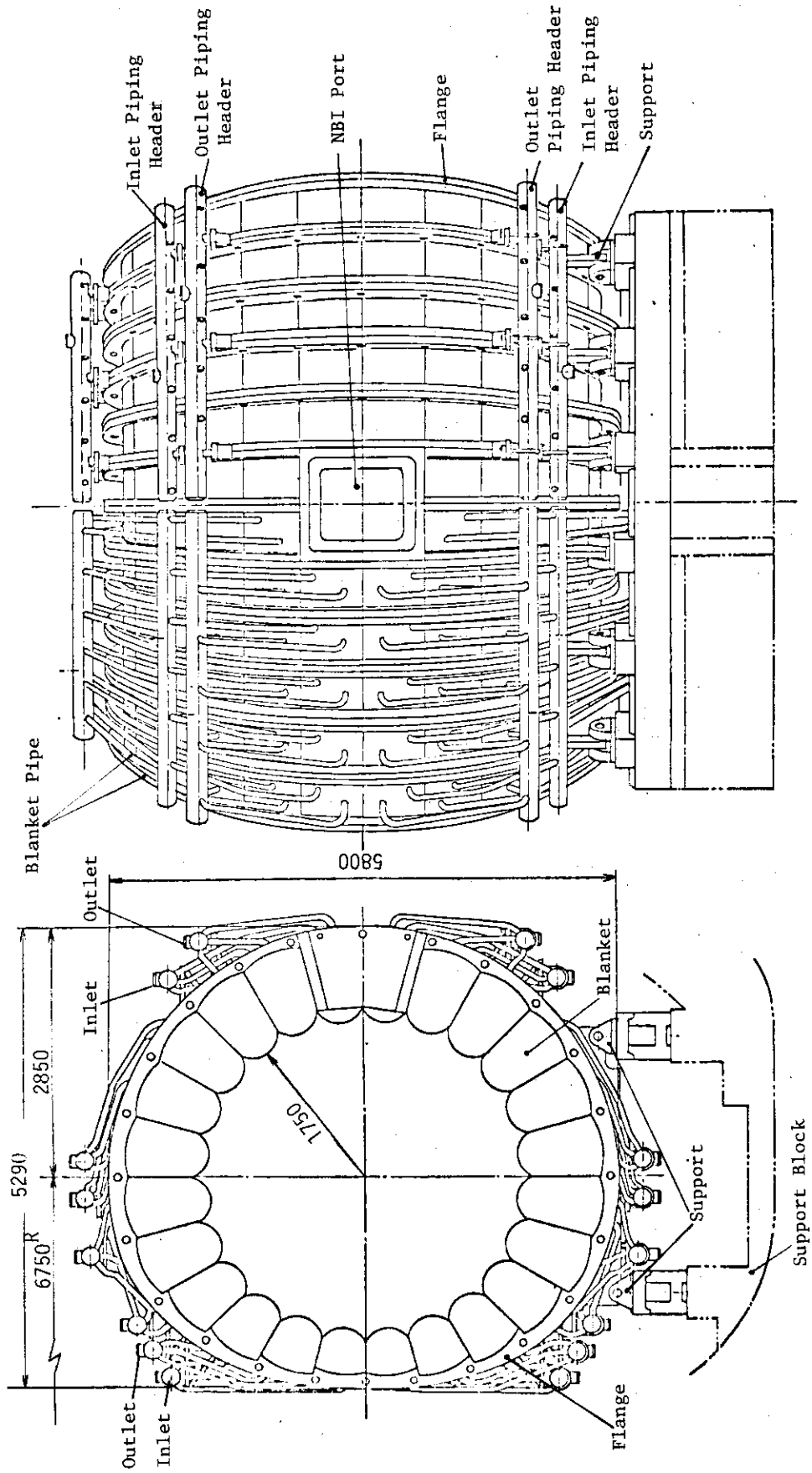

Fig. 3.1 Blanket module

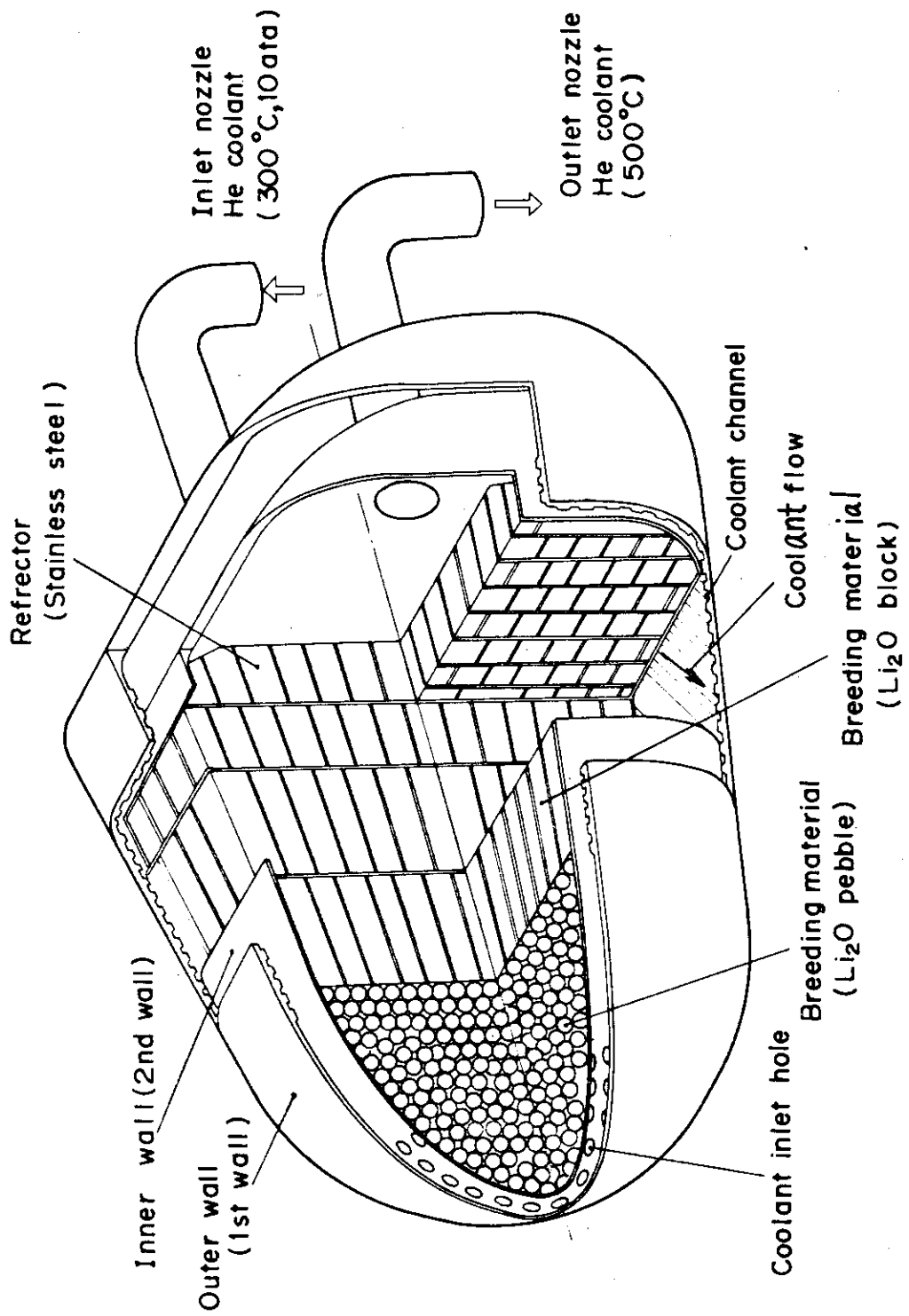

Fig. 3.2 A typical blanket vessel

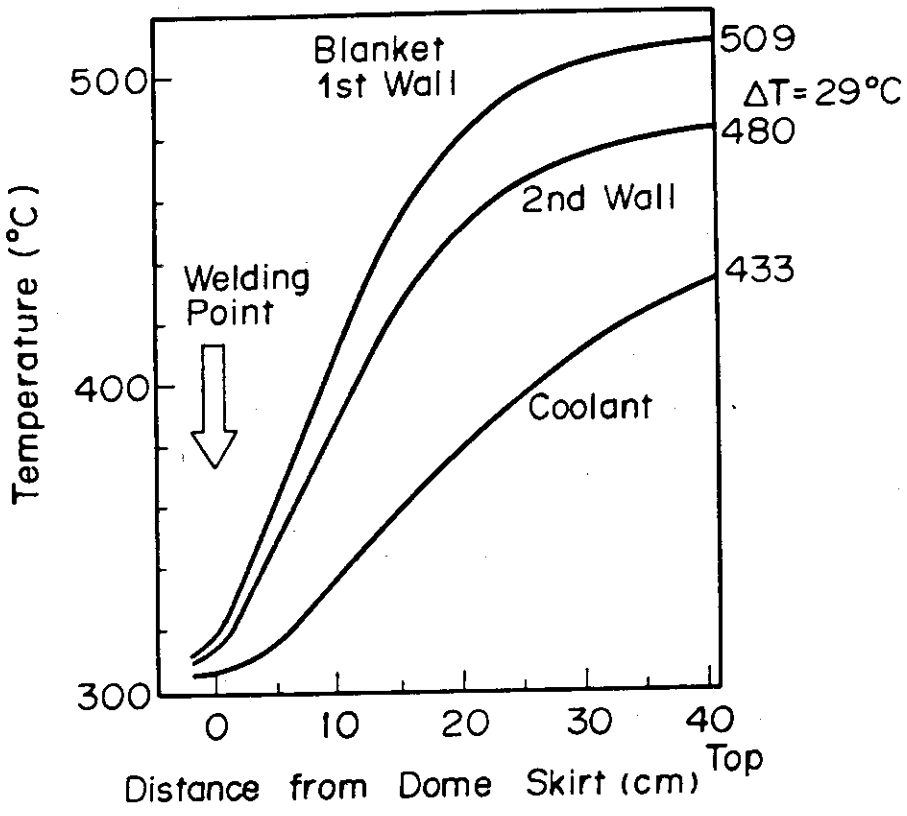

Fig.3.3 Temperture distribution of the blanket vessel

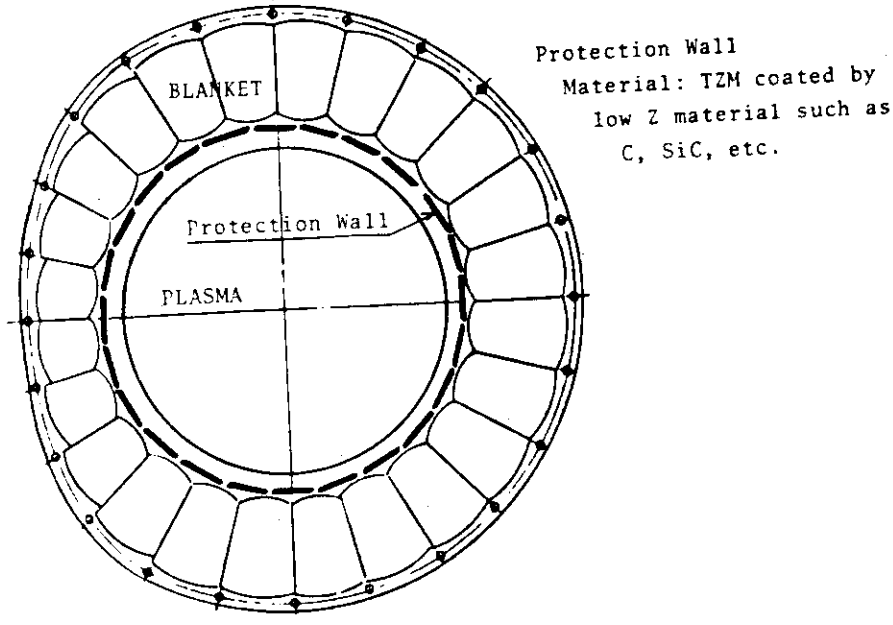

Fig.3.4 Concept of protection wall

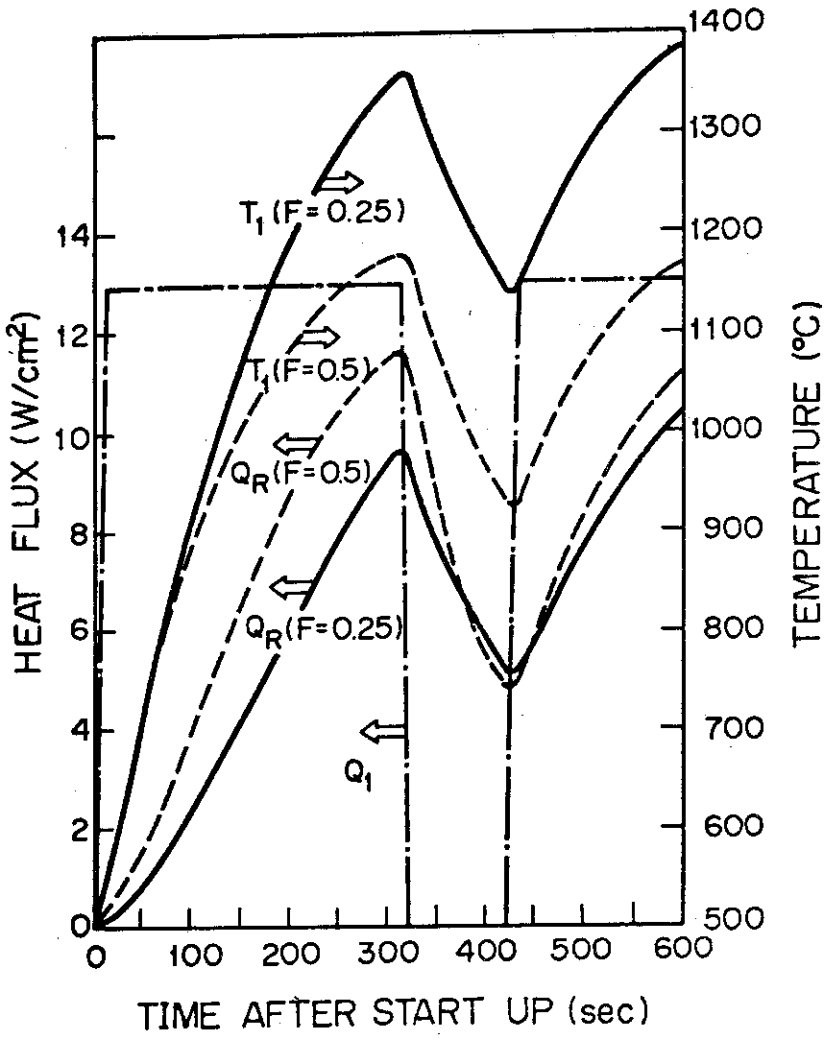

Fig.3.5 Temperature and heat flux variation with protection wall

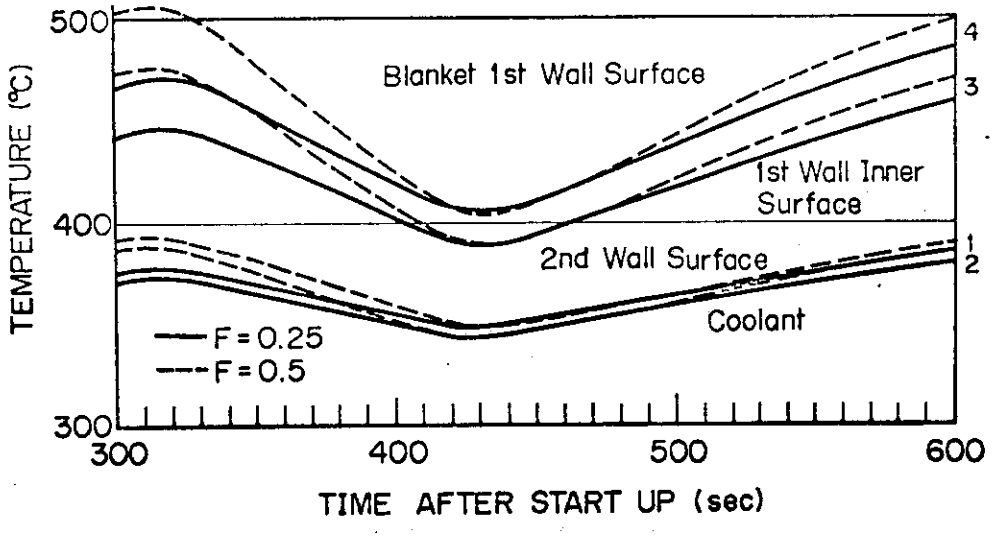

Fig.3.6 Temperature variation with protection wall

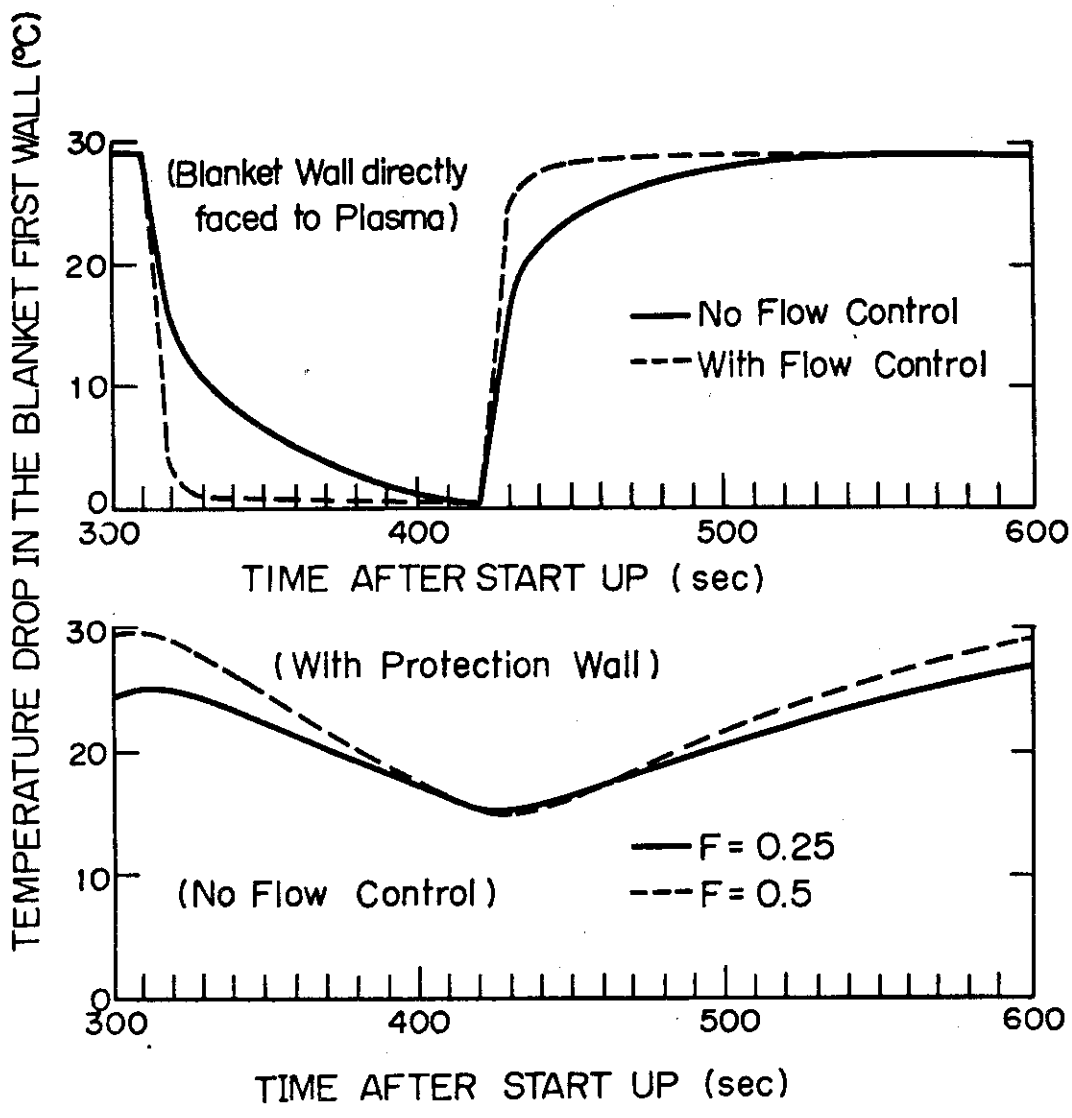

Fig.3.7 Temperature drop in the blanket first wall

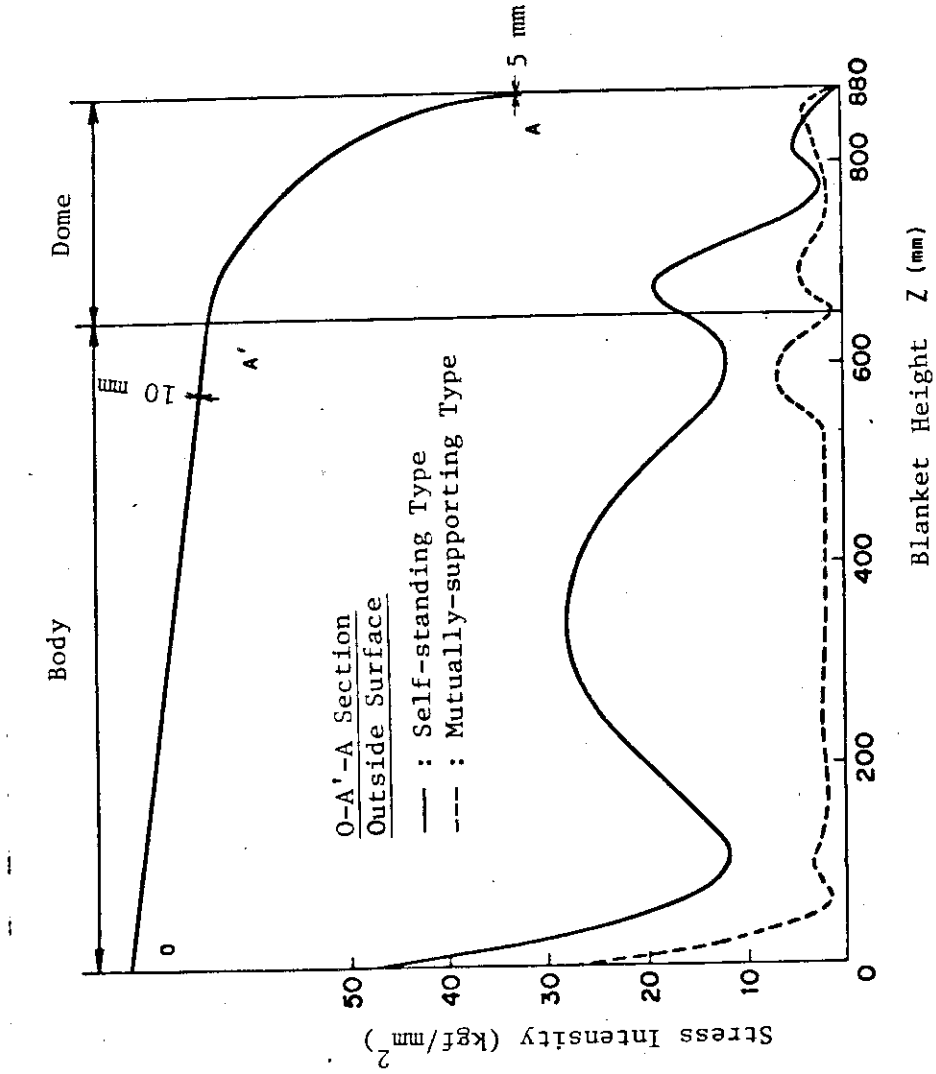

Fig.3.9 Distribution of Stress Intensity at Outside Surface of O-A'-A Section

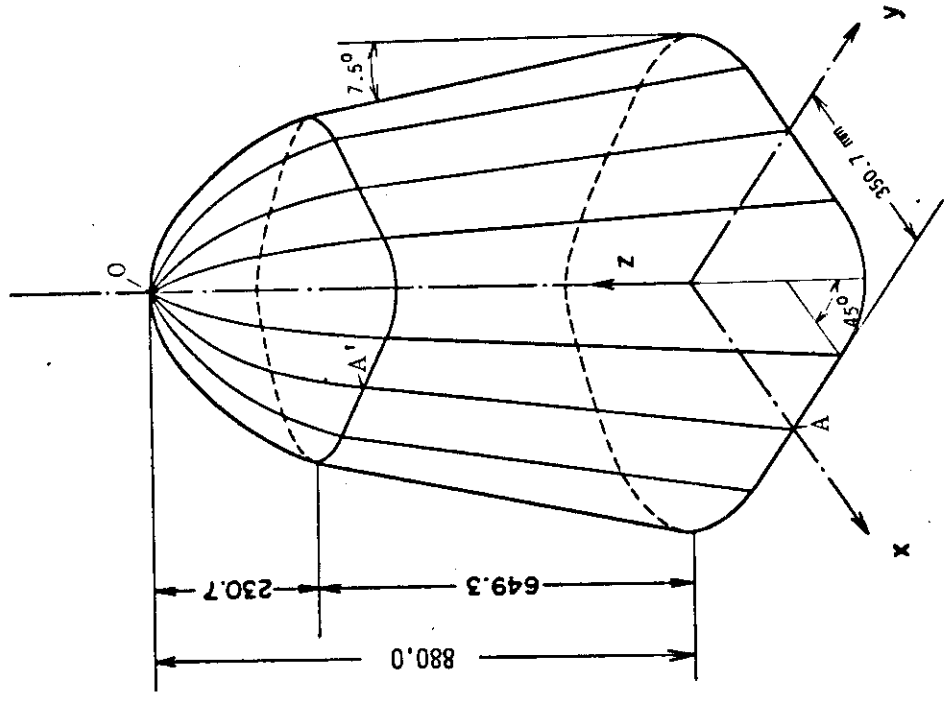

Fig.3.8 Three-dimensional Model of Blanket Vessel

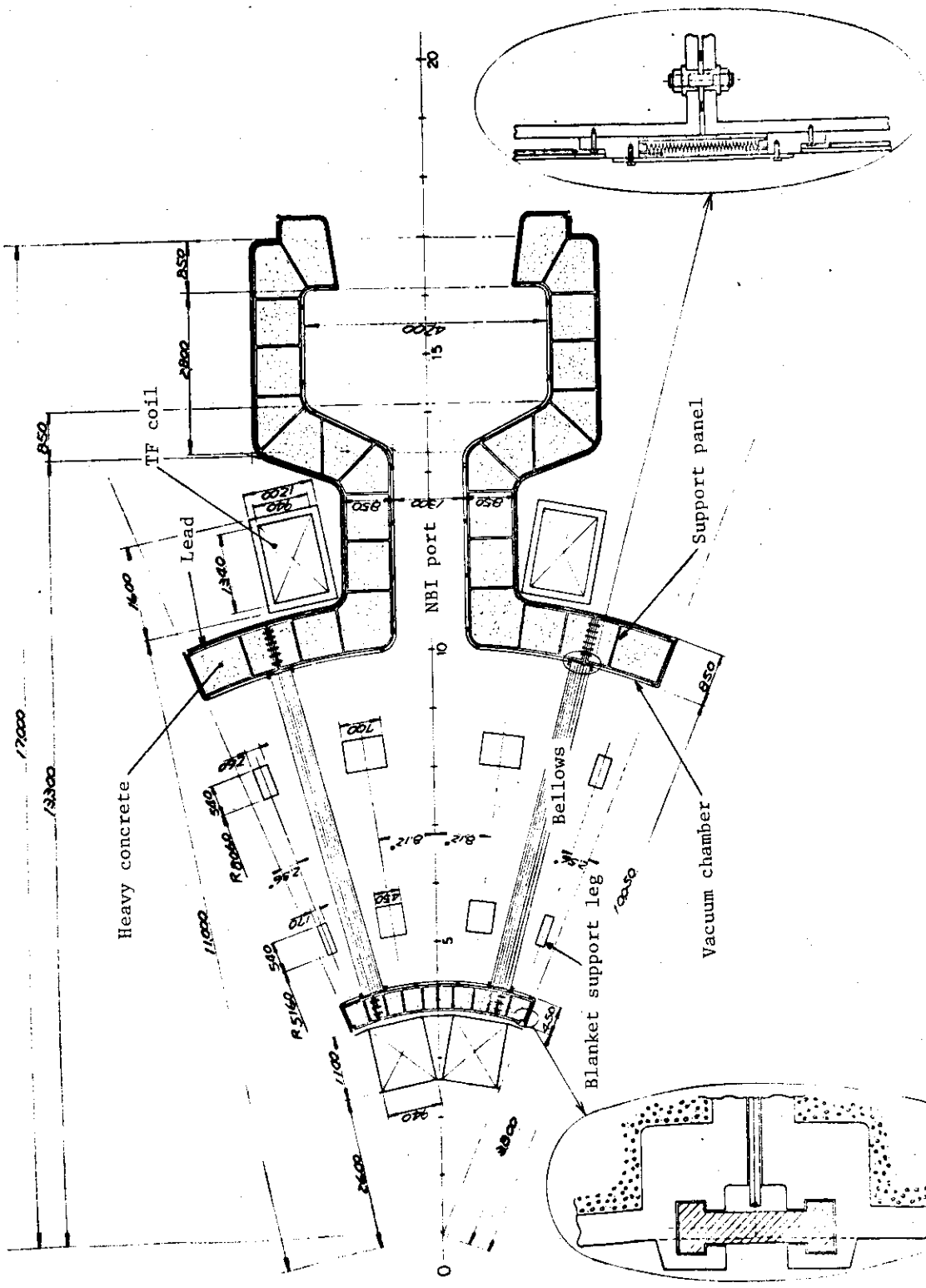

Fig.3.10 Magnetic shielding (Vacuum chamber)

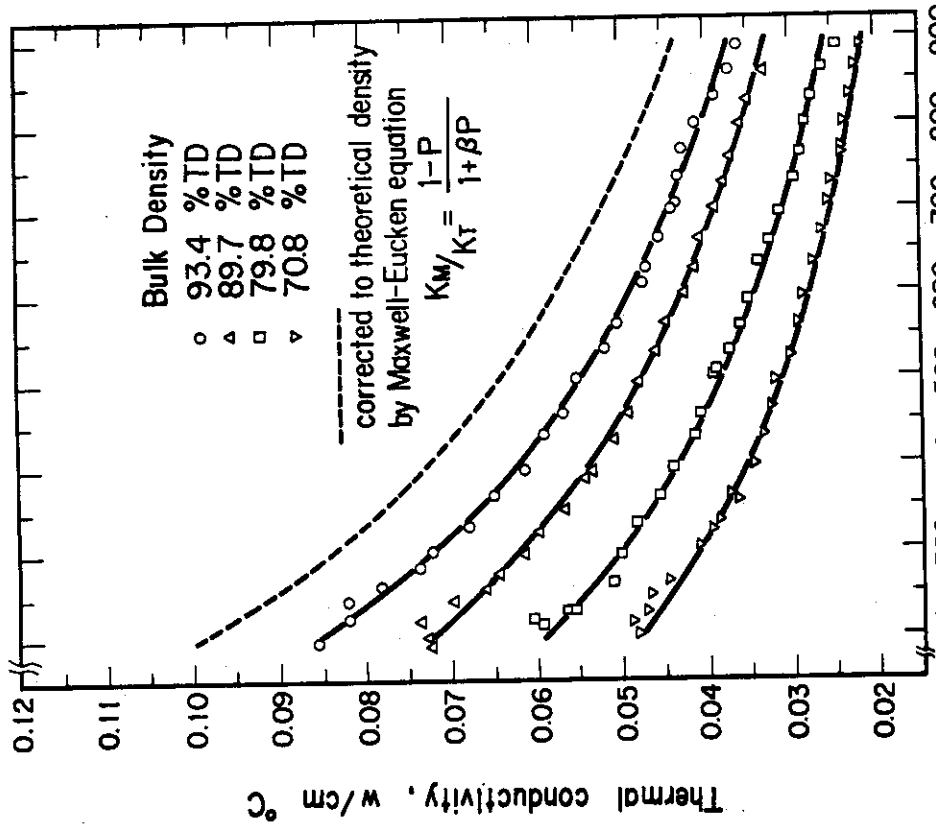

Fig.3.11 Temperature dependence of thermal conductivity of Li_2O pellets of various densities. Data points are fitted to a set of the $k=(a+bT)^{-1}$ equation for each density.

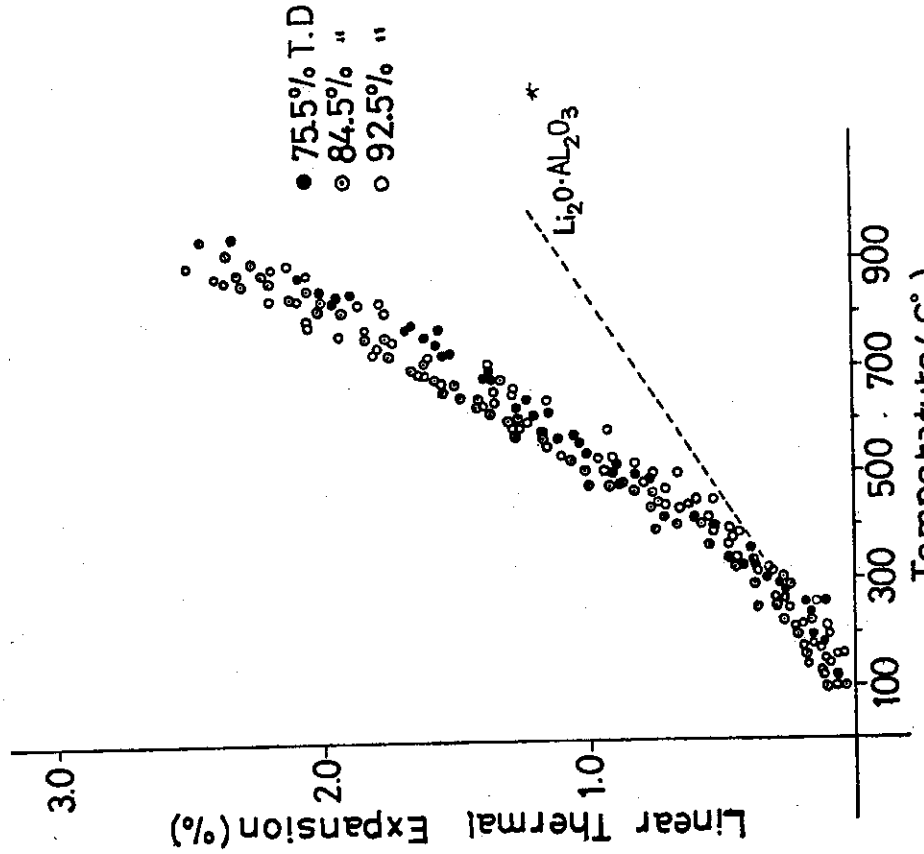

Fig.3.12 Thermal expansion of Li_2O pellets of various densities.

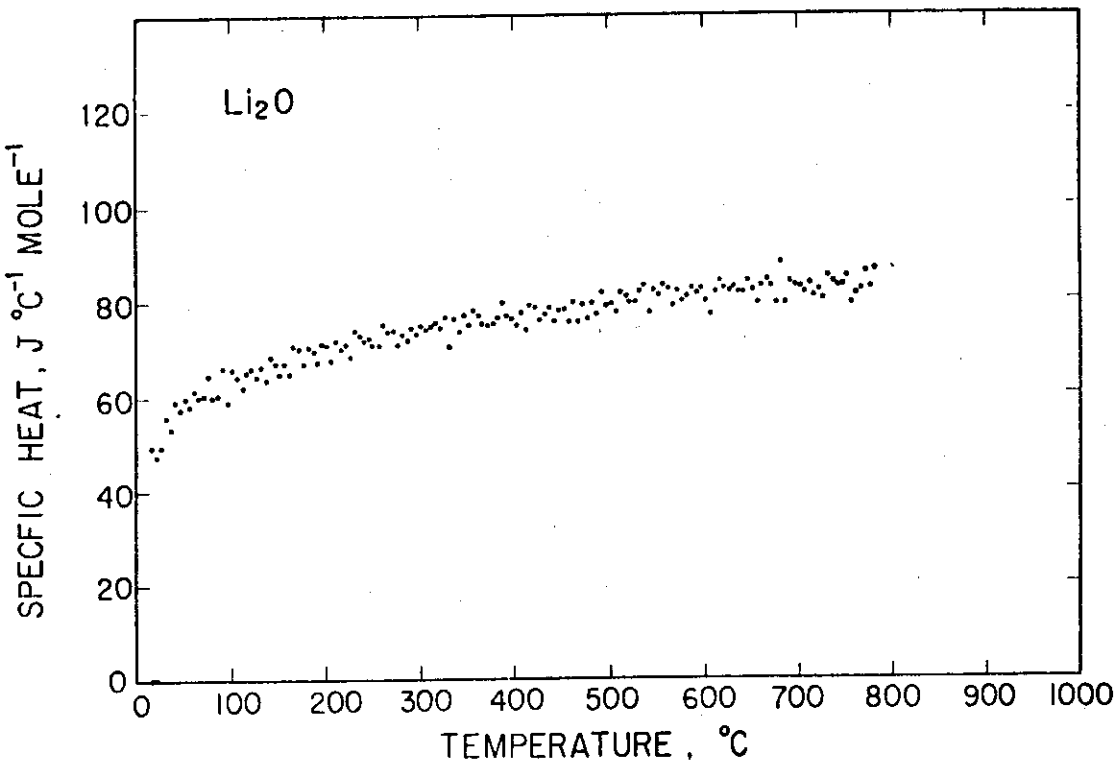

Fig.3.13 Heat capacity of Li_2O.

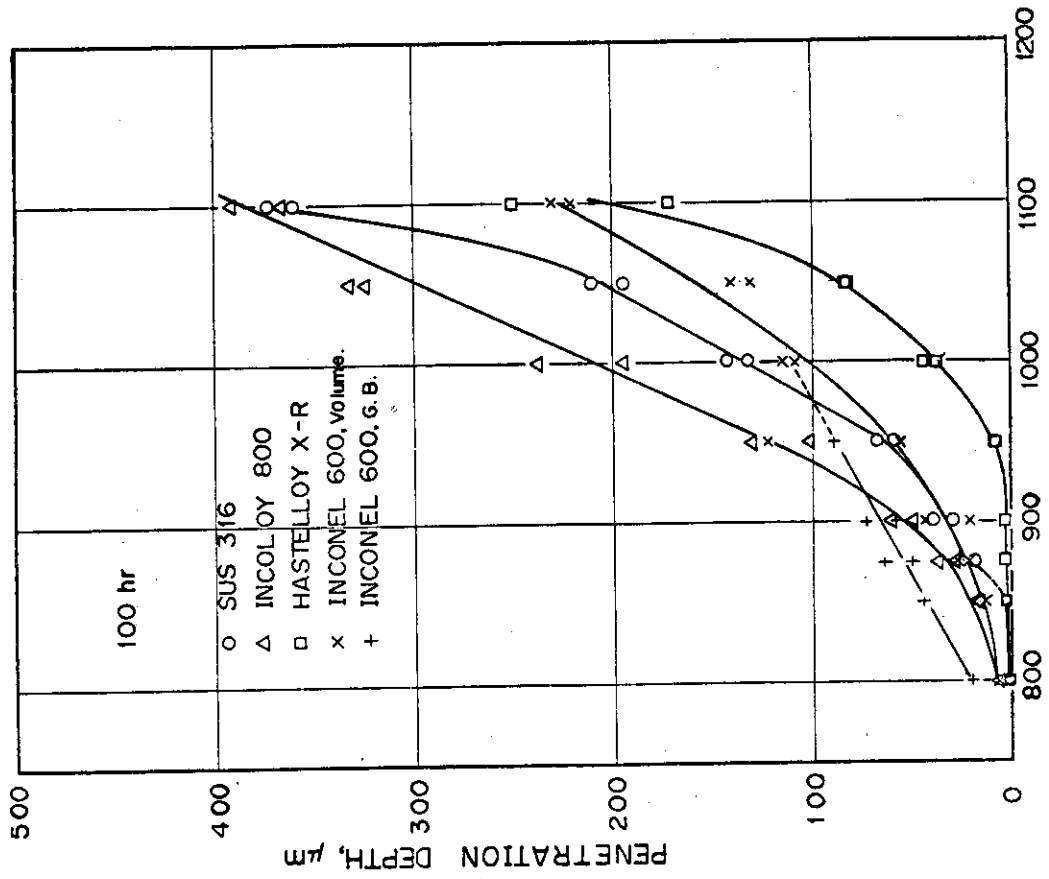

Fig.3.15 Relationship between attacked depth and temperature for a reaction period of 100 h.

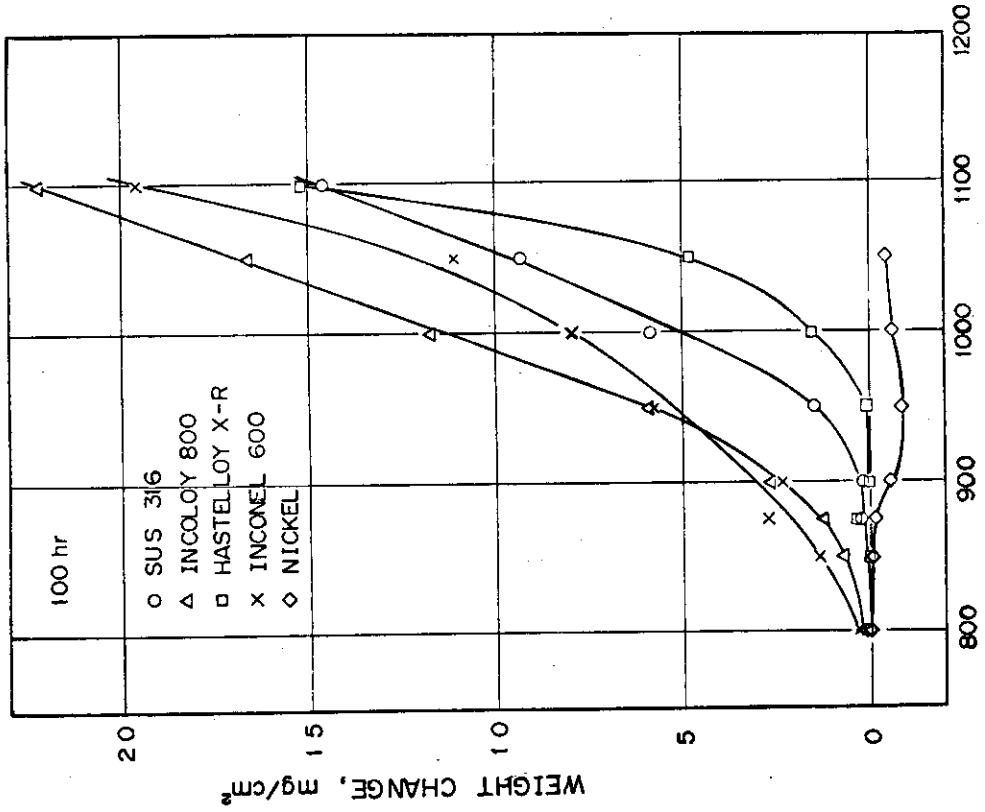

Fig.3.14 Relationship between weight change and temperature for a reaction period of 100 h.

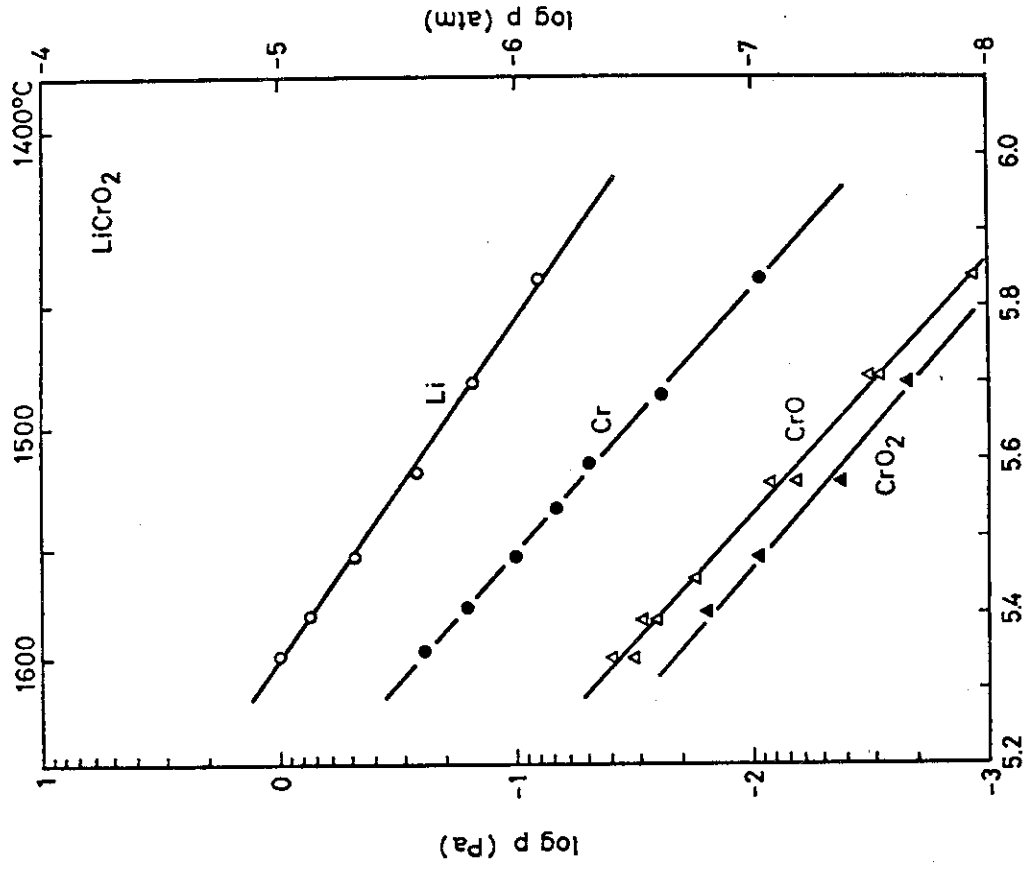

Fig.3.17 Partial pressure of Li(g), Cr(g), CrO(g) and CrO_2(g) over $LiCrO_2$.

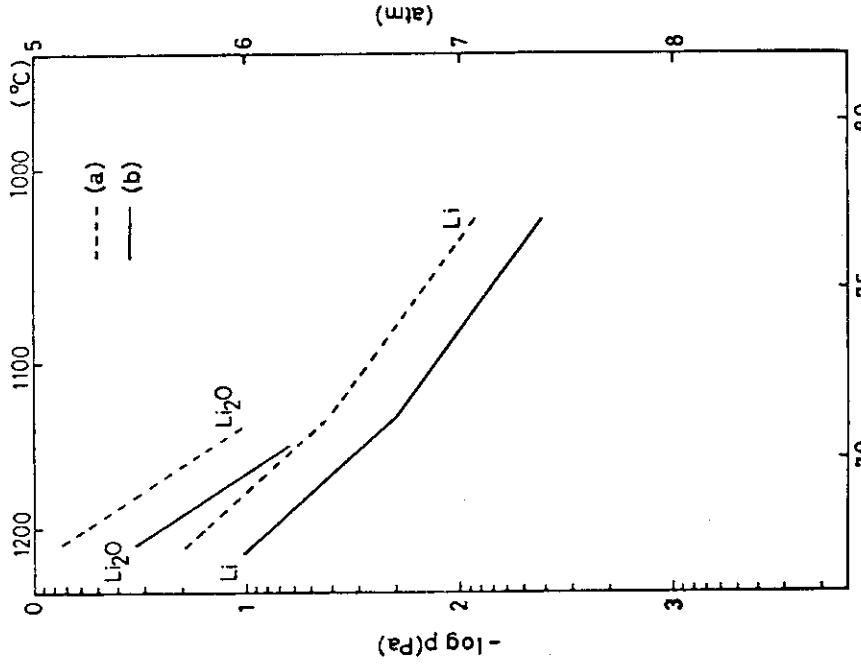

Fig.3.16 Partial pressure of Li(g) and Li_2O(g) over the condensed Li_5FeO_4 obtained by (a) the absolute method and (b) the reference method.

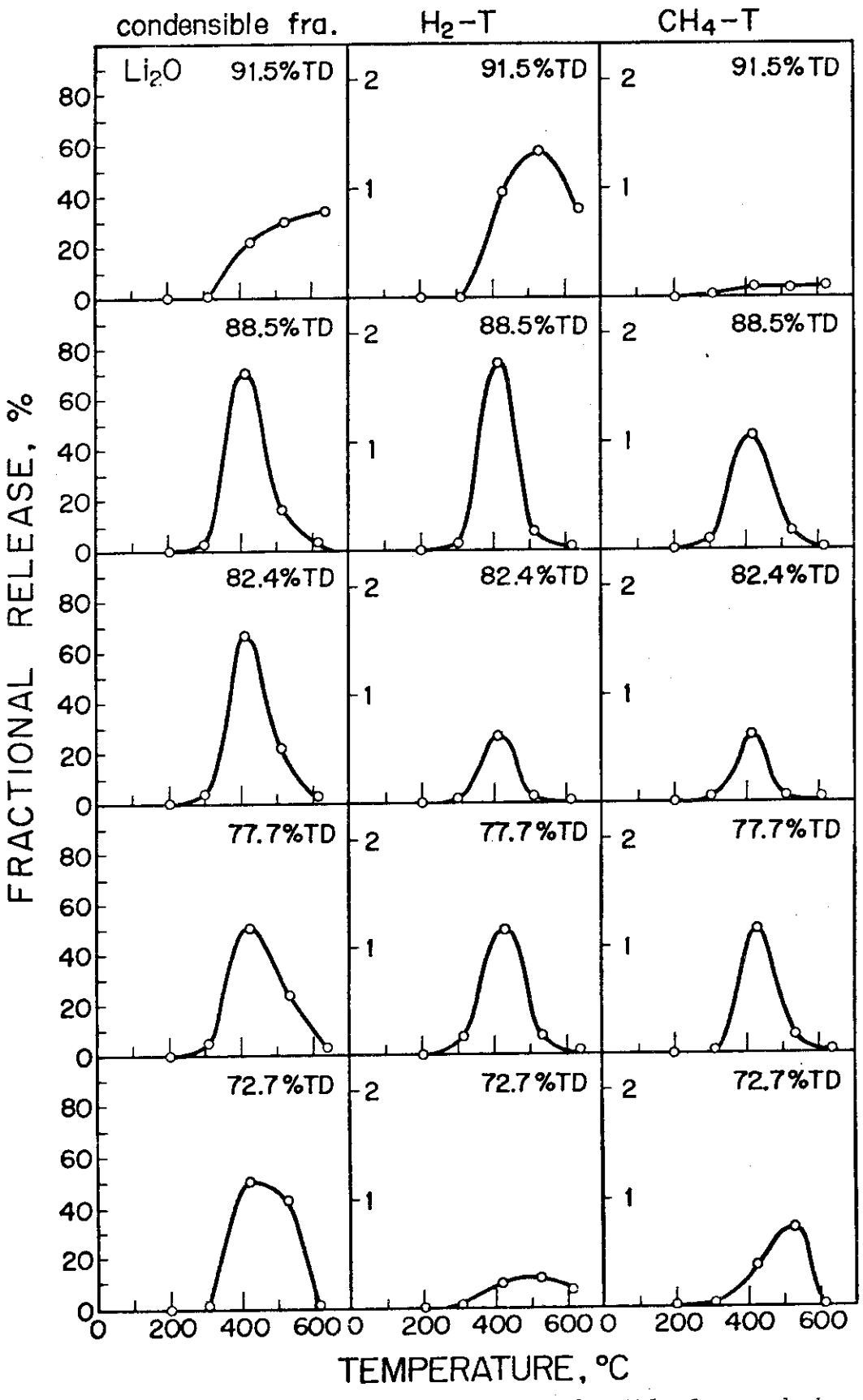

Fig.3.18 Tritium release spectra for the condensible form and the noncondensible form (H_2-T and CH_4-T) from neutron-irradiated Li_2O pellets.

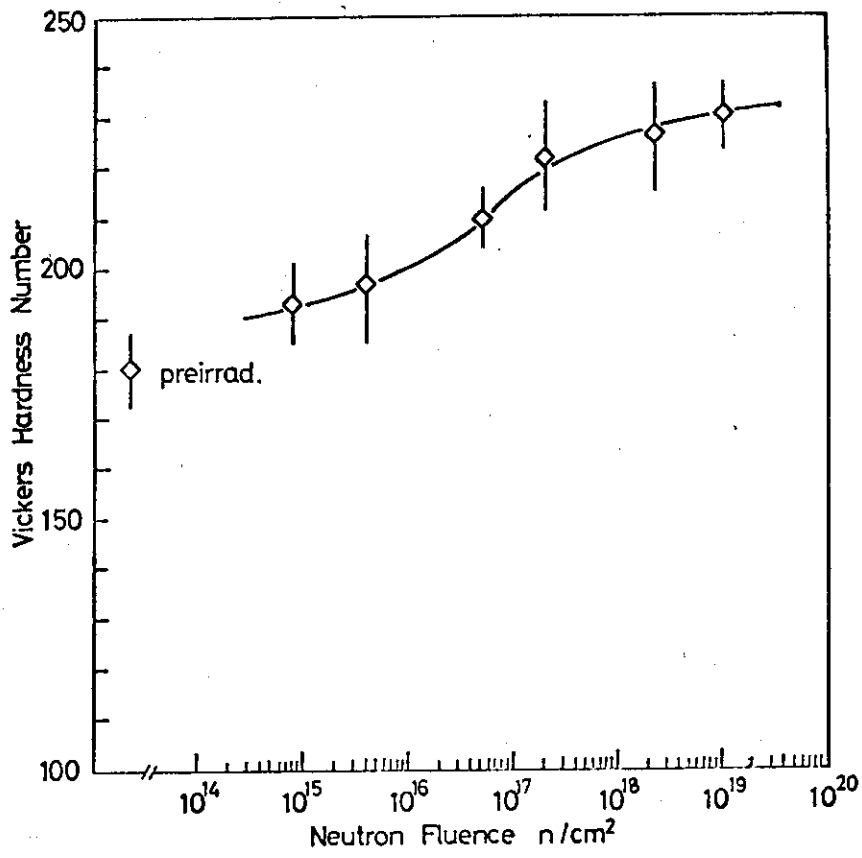

Fig.3.19 Vickers hardness of Li_2O pellets as a function of neutron dose.

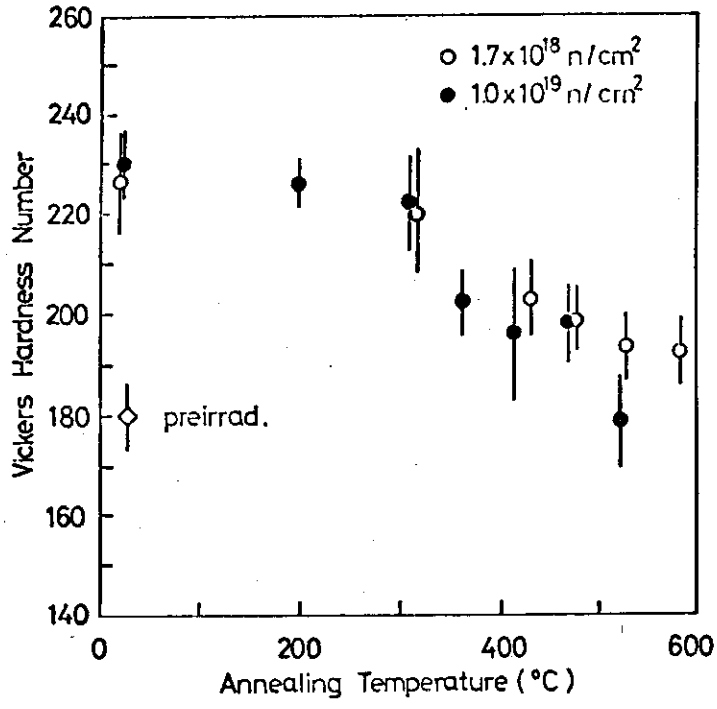

Fig.3.20 Microhardness recovery on annealing for Li_2O pellets irradiated to 1.7×10^{18} and 1.0×19^{19} n/cm^2.

4. Blanket Neutronics and Shielding

Main design bases for the blanket neutronics and shielding designs are as follows:

(1) To make the reactor compact, the composition of the portion of the blanket inside the torus (inner blanket) is selected to reduce sufficiently the radiation damage to the superconducting magnets employing as small space as possible. The inner blanket consists of effective neutron attenuators such as stainless steel and tungsten.

(2) The priority of obtaining the highest attainable tritium breeding comes next only to that of satisfying the shielding requirements for superconducting magnets. Major part of the blanket other than the inner blanket is called the outer blanket. It includes lithium oxide for tritium breeding and stainless steel as a neutron reflector. As the reflector material, originally used graphite was replaced by stainless steel in order to increase the attenuation of neutron flux even though the replacement caused a slight (~2 %) reduction of tritium breeding ratio which is about 0.9.

(3) The thickness of the bulk outer shield is determined from the requirement to reduce the induced gamma-ray dose to the level below which are allowed the hands-on maintenance outside the bulk shield.

(4) The outer shield is also designed to protect the superconducting magnets and other components from the enhanced neutron flux streaming through the neutral beam injection ports.

(5) No attempt to increase the nuclear heating in the blanket is made since no electric power is to be generated.

Figures 4.1a and 4.1b shows the attenuation of neutron and gamma-ray in the inner and outer blanket, shield and magnets, respectively.

The distribution of neutron flux in the superconducting magnets near a neutral beam port is shown in Fig. 4.2.

Some results obtained in the recent years for the blanket neutronics and shielding design include the evaluations of neutron streaming through injector ports to cryosorption pumps [1] and neutron streaming through a thin gap between adjacent blanket modules [2] using Monte Carlo calculations. A preliminary cross section sensitivity study was conducted to evaluate the uncertainties of the calculated tritium breeding ratio and some activation of the magnet caused by nuclear data uncertainties [3].

The nuclear heat deposition in the cryopumps for the reactor has been evaluated [1] using Monte Carlo method and the calculational model shown in Fig.4.3. The following conclusions have been obtained.

(1) Nuclear heat deposition in the cryopumps is small and the required refrigeration power for nuclear heating is acceptable.

(2) The total heat deposition in the cryopumps for the neutral beam injection system is particularly small amounting to less than 1/10 that for the main evacuating system.

(3) Nuclear heat deposition in the cryopumps is mostly due to gamma-rays.

The hot spot factor (the ratio of the maximum radiation heat deposition rate to the average) enhanced by the radiation streaming through a gap between the blanket modules have been evaluated [2]. The hot spots on the inner surface of the shield and in the toroidal field coil outside the shield were calculated using the Monte Carlo code MORSE-I [4]. This code can treat a calculational model composed

of not only quadratic surfaces but also toroidal surfaces. Figure 4.4 compares the 14 MeV neutron flux distribution along a gap 1 cm wide between the blanket modules and the distribution in the bulk shield. The former distribution was calculated by MORSE-I and the latter was derived from a one-dimensional discrete ordinates calculation using ANISN [5]. The hot spot factor on the shield inner surface was calculated to be about 5 while no hot spot was observed in the toroidal field coil.

The cross section sensitivity analysis [3] showed that the tritium breeding ratio was most sensitive to the cross sections of ^{7}Li and ^{16}O. The two of the most important reactions, $^{58}Ni(n,p)^{58}Co$ and $^{54}Fe(n,p)^{54}Mn$ with respect to the stainless steel activation in the toroidal field coils were shown to be very sensitive to the transport cross sections of iron.

REFERENCES

[1] IIDA, H., IDE, T. and SEKI, Y., Proc. of the 7th Symposium on Engineering Problems of Fusion Research, Oct.25-28, 1977, Vol.II, 1658, Knoxville (1977)

[2] IIDA, H. and YAMAUCHI, M., Proc. Meeting of Japan Atomic Energy Society, B35, Oct.7-10, 1978 (in Japanese)

[3] YAMAUCHI, M. and IIDA, H., JAERI-M 7915 (1978) (in Japanese)

[4] IIDA, H., to be published.

[5] ENGLE, W. W. Jr., K-1693, Computing Technology Center, Union Carbide Corporation (1967)

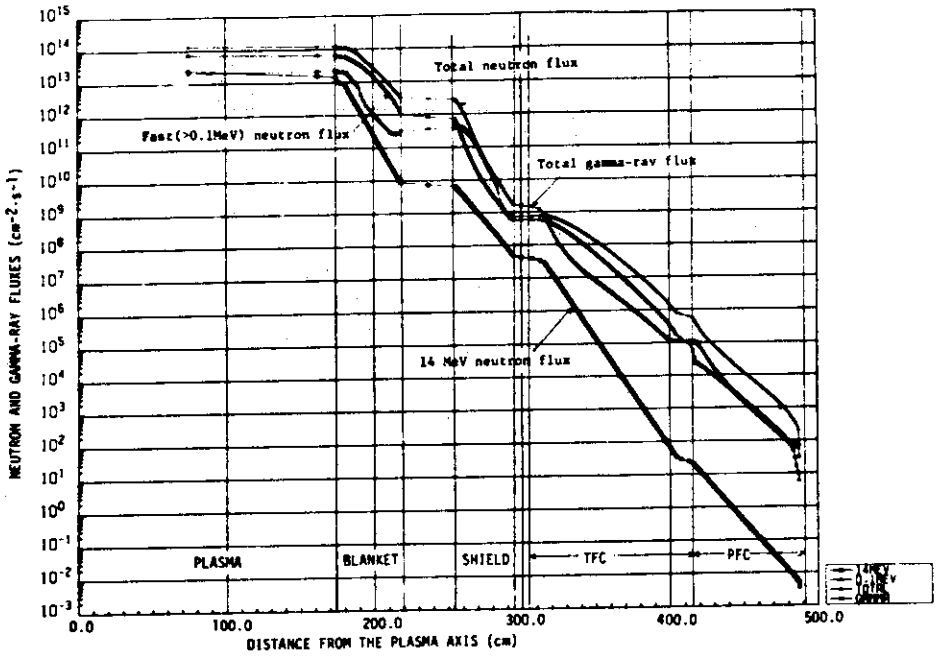

Fig. 4.1a Attenuation of neutron and gamma-ray fluxes in the inner blanket, shield, toroidal field coil and poloidal field coil

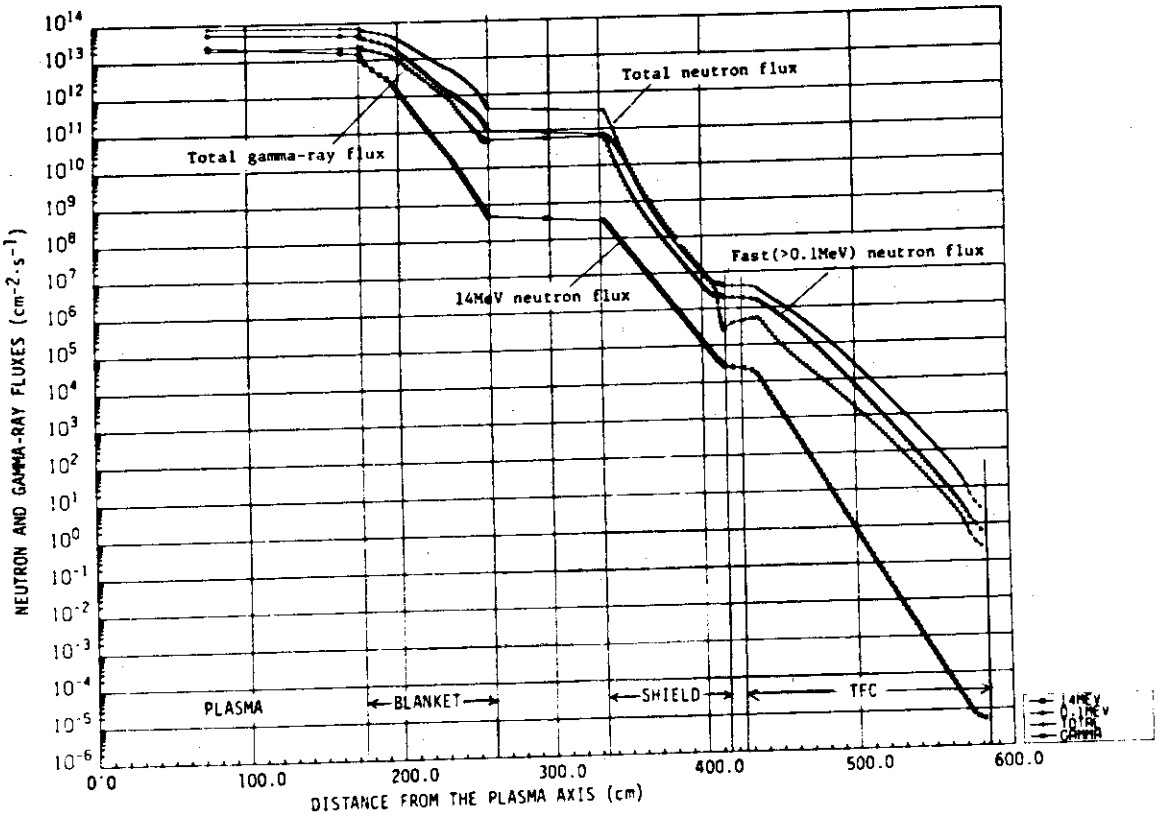

Fig. 4.1b Attenuation of neutron and gamma-ray fluxes in the outer blanket, shield and toroidal field coil

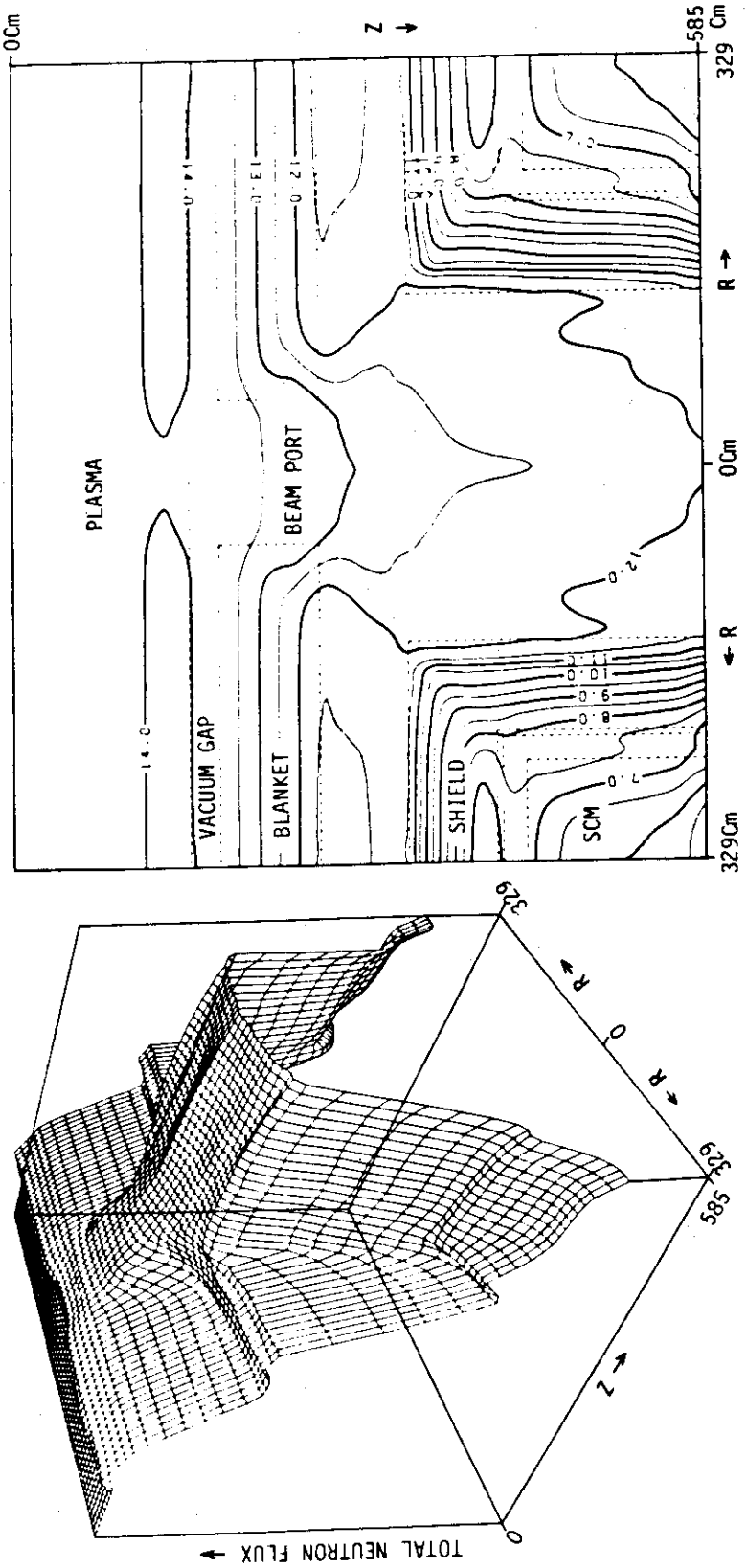

Fig. 4.2 The distribution of neutron flux in the superconducting magnet near a neutral beam injection port

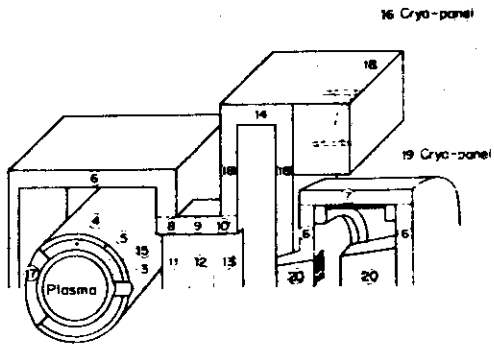

3	Carbon coating
4	Li_2O
5	Reflector (S.S.)
6~14	Heavy Concrete
15	End Wall (S.S.)
17	Stainless Steel
18	Heavy Concrete
20	Drift Tube & Neutralization Cell
16,19	Cryo-Panel

Fig. 4.3 Three dimensional model for the calculation of heat deposition in cryopumps

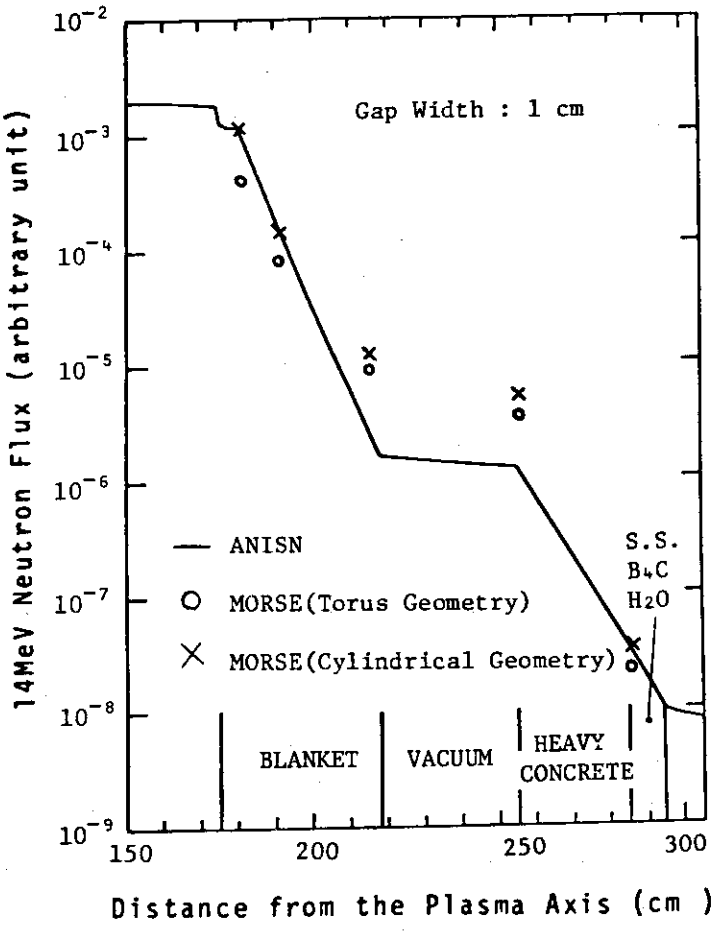

Fig. 4.4 Comparison of the distribution of 14 MeV neutron flux in the gap between adjacent blanket modules and the distribution in the bulk shield

5. Superconducting Magnets

5.1 Toroidal Field Magnets

The arrangement of the magnet is shown in Fig.5.1, and the detail coil structure is shown in Fig.5.2. The maximum toroidal field at the coil is 12.0 T, providing 6.0 T at the plasma axis (Fig.5.3). The total ampere-turns is 202.5 MAT. The bore of the coil is 7.3 × 11.2 m, and the coil shape is constant-tension D-shape, as shown in Fig.5.4, 16 coil design was chosen, considering the allowable ripple and the necessity for good access for the evacuation port or support structure of blanket and shield. The operating current is 25,000 amperes, and cryogenic stabilization is fulfilled. The dimensions of the superconducting cable are listed in Table 5.1.

The straight section length of the coil is about 8.1 m, and the inward centering force is 64,000 ton/coil. The centering force is supported by the wedged inner portion of 16 coils and center cylinder (Fig.5.5). The total hoop force which is supported by stainless steel disc is about 166,000 ton/coil. The stress distribution in the disc which is made of type 310S stainless steel is shown in Fig.5.6. Epoxy fibreglass insulator is inserted between the conductor and stainless steel structure material. Total heat load including eddy current loss, neutron and gamma-ray radiation heating and cryostat loss is 7.5 kW. The required liquefaction rate is 16,000 ℓ/h.

Safety aspects of the magnet are analyzed. Coil quench is detected by bridge method and coil is protected by external shunt method. In order to suppress a magnetic force in coil quench, 18 current suppliers are settled in parallel, corresponding to a disk number. As the result of earthquake EL CENTRO response analysis, maximum acceleration is enlarged by about three times.

Main parameters of the TF magnet are summarized in Table 5.2.

5.2 Poloidal Magnets

Superconducting magnets are used for both primary windings and vertical coils. It is assumed that the plasma current of 4.4 MA is induced in 10 sec and sustained for 110 sec by the primary winding. The magnetomotive force is 48 MAT for the primary winding and is 8.3 MAT for the vertical coils. The maximum field intensity of the poloidal magnet is about 5.6T.

Arrangement of coils are shown in Fig.1.2 and the detailed structure of a coil is shown in Fig.5.7. Copper stabilized NbTi stranded wires are placed in a case of 304SS and electromagnetic force is mainly supported by this case. The maximum stress in the case is about 24 kg/mm^2. In this design, liquid helium chamber made of FRP is used in order to decrease the eddy current loss in the chamber. Because of difficulty in removal of bubbles horizontally between the pancakes in the coolant, forced cooling is used though consumption of coolant becomes larger.

The coil current of the primary winding is 260 kA and is 110 kA in vertical coils. One of the difficult problems is development of high current high voltage current feeder.

Table 5.1 Characteristics of superconducting cable for each slot

Slot No.	1	2	3	4	5	6	7	8	9	10	11	12	13	14
Maximum Field (T)	3.3	3.3	4.0	4.8	5.7	6.5	7.2	7.9	8.6	9.3	10.0	10.6	11.3	12.0
Critical current per filament (A)	264	264	232	195	160	136	119	103	91	80	71	66	62	59
Number of filaments	49	49	55	66	80	94	108	124	141	160	180	194	206	216
Cross section of superconductors (mm^2)	2.20	2.20	2.47	2.96	3.59	4.22	4.84	5.56	6.32	7.17	8.07	8.70	9.24	9.69
Width of copper conductor (mm)	26	26	27	28	30	32	34	36	38	40	42	44	46	48
Cross section of copper conductor (mm^2)	105	105	108	110	115	121	126	131	136	140	144	150	156	162
Cu/SC ratio	47.7	47.7	43.7	37.2	32.0	28.7	26.0	23.6	21.5	19.5	17.8	17.2	16.9	16.7

Table 5.2 Main characteristics of toroidal field magnet

Magnet Structure	
Number of coils	16
Number of discs per coil	18
Number of slots per disc	14×2
Number of conductors per slot	2 (double conductors)
Dimensions of Magnet	
Major radius	6.75 m
Inner diameter	11.2×7.3 m
Outer diameter	14.4×10.0 m
Magnetic Field	
Magnetic field at plasma center	6T
Peak field at coil	12T
Maximum ripple at plasma	0.47%
Inductance	
Total	190H
Stored Energy	
Total	59.9 GJ
Per coil	4.74 GJ
Magnetomotive Force	
Total	202.5 MAT
Per coil	12.66 MAT
Magnetic Force	
Hoop force per coil	166,000 ton
Centering force per coil	64,000 ton
Lateral force per coil	1.87×10^{7} kg·m
Dimensions of Coil	
Thickness	0.92 m
Width	0.94-1.30 m
Length of straight section	7.8 m
Stainless steel Disc	
Thickness	5.0 cm
Width	94-130 m
Depth of slot	1.7 cm
Width of slot	3.0-5.2 cm
Depth of liq. He channel	1.0 cm
Width of liq. He channel	1.0 cm
Disc material	SUS 310S
Thickness of insulator between discs	0.1 cm
Number of Turns	
Total	8064
Per coil	504
Per disc	28

Table 5.2 Main characteristics of toroidal field magnet (continued)

Superconducting Cable	
Superconductor	Nb_3Sn
Stabilizer	Cu
Superconducting composite	Fine-multi twisted
Thickness	4.5 mm
Width	26-48 mm
Grades	13
Cu/SC ratio	48-17
Copper resistivity (maximum after irradiation)	3×10^{-10} Ωm
Insulator	Epoxy glassfiber
Current	
Operational current	25,100 A
Stabilization current	25,300 A
Critical current	25,500 A
Current Density	
At conductor	107-58 A/mm^2
Average at conductor	82 A/mm^2
Average at disc	15-11 A/mm^2
Cooling	
Method	Liq. He Pool Cooling
Temperature	4.2 K
Cool-down time	160 hr
Heat Load	
Superconductor loss	1.30 kW
Neutron and gamma ray heating	0.98 kW
Eddy current loss at structure material	0.15 kW
Cryostat loss	3.98 kW
Current lead loss	1.08 kW
Total	7.49 kW
Power Supply	
Number of suppliers	18
Dump resistor	0.3 Ω
Excitation time	5 hr
Induced voltage at excitation	19.4 V
Capacity of supplier	26kA×20V = 520kVA
Length of Conductor	
Per turn	39-33 m
Total	290 km
Weight	
Conductors of a disc	2.84 ton
Stainless steel disc (including conductors)	13.8 ton
Stainless steel discs and Helium can	298 ton
Toroidal coil	883 ton
Total	7150 ton

Table 5.3 Coil positions of the vertical field magnet

No.	R (m)	Z (m)	I
1	1.967	1.435	2.0 X 1.38 X 10^6 A
2	1.987	3.080	1.0 //
3	4.837	7.801	-1.0 //
4	12.621	4.059	-2.0 //

Table 5.4 Coil positions of the transformer

No.	R (m)	Z (m)	I
1	1.956	0.465	1.0 X 2.6 X 10^6 A
2	1.962	0.989	1.0 //
3	1.974	2.051	1.0 //
4	1.981	2.623	1.0 //
5	1.993	3.613	1.0 //
6	1.997	3.915	1.0 //
7	2.048	4.535	1.0 //
8	2.451	5.801	1.0 //
9	4.048	7.463	0.8 //
10	9.579	7.253	0.4 //

Table 5.5 Self inductance and coupling coefficient of poloidal coils

Upper Inductance (H)

Lower Coupling constant $k \equiv \frac{M}{\sqrt{L_1 L_2}}$

	Air core transformer	Vertical field coil	Plasma
Air core transformer	0.0378 1.00		
Vertical field coil	6.51×10^{-4} 0.926×10^{-2}	0.133 1.00	
Plasma	1.98×10^{-4} 0.258	2.95×10^{-4} 0.205	0.153×10^{-4} 1.00

Stored energy of air core transformer : 1.28 GJ
Stored energy of vertical field coil : 0.77 GJ

Table 5.6 Specification of superconducting wire

(1) Unit conductor		
Cross section	(mm^2)	11×25
Total length (Transformer)	(km)	83.1
(Vertical field coil)	(km)	68.3
Maximum magnetic field	(T)	5.6
Maximum current	(A)	5,680
Current density	(A/mm^2)	20.7
Maximum heat flux of conductor surface in case of quenching	(W/cm^2)	0.359
(2) Superconducting stranded wire		
Number		2
Cross section	(mm^2)	2×21
Number of strands		42
Current density	(A/mm^2)	71.2
(3) Multifilamentary superconducting wire		
Diameter	(mm)	1.1
Structure		NbTi-CuNi-Cu
Number of NbTi filaments		2033
Core diameter of NbTi filament	(μ)	10
Thickness of CuNi sheath	(μ)	2
Cu ratio (Cu: NbTi+CuNi)		2.04:1
Current density of NbTi	(A/cm^2)	0.423×10^5
Twist pitch	(mm)	30

Table 5.7 Electric loss in windings

Phase		I	II	III	IV	V	VI	Total
Time (s)		0.8	9.2	120	10	60	20	180
B ratio		1	1/45	1/400	1/12.5	0	1/16.7	
Small diameter coils	Stainless steel case (W)	762	40	0	40	0	0	
	Coupling loss (W)	281,766	3826	2.0	17,602	0	614	
	Hysteresis loss (W)	50,251	16,612	264	4,336	0	2,746	
	Total lossed power (W)	332,779	20,478	266	21,978	0	2,746	4297
	Total lossed energy (J)	266,223	188,398	31,920	219,780	0	67,200	773,521
Large diameter coils	Stainless steel case (W)	68	40	0	16	0	0	
	Coupling loss (W)	36,691	13,402	0	13,442	0	24	
	Hysteresis loss (W)	3,299	2,386	58	2,846	0	600	
	Total lossed power (W)	40,058	15,828	58	16,304	0	640	1,396
	Total lossed energy (J)	20,029	145,618	6,960	163,040	0	12,800	348,447

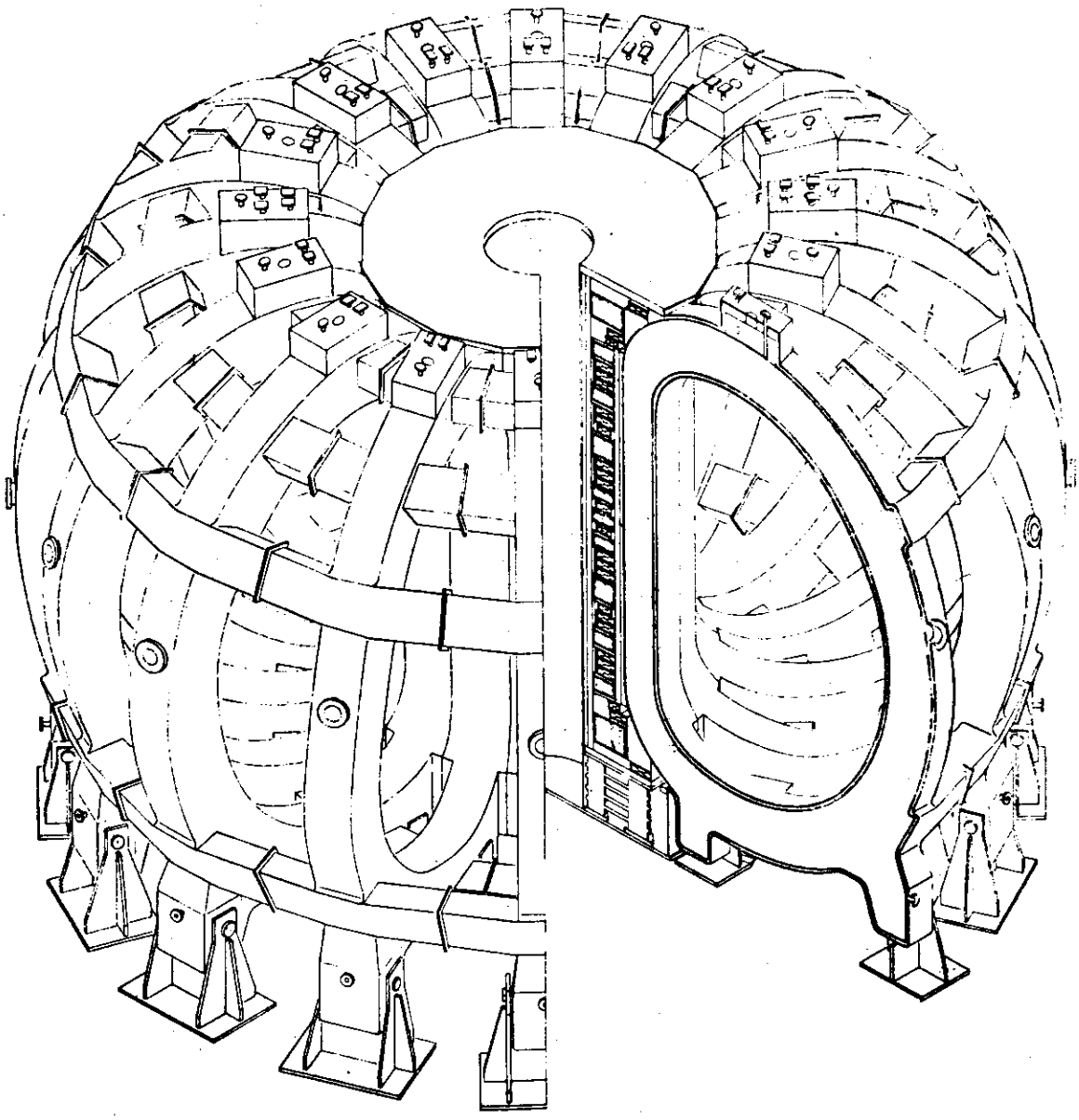

Fig.5.1 Overall View of Toroidal Field Magnet

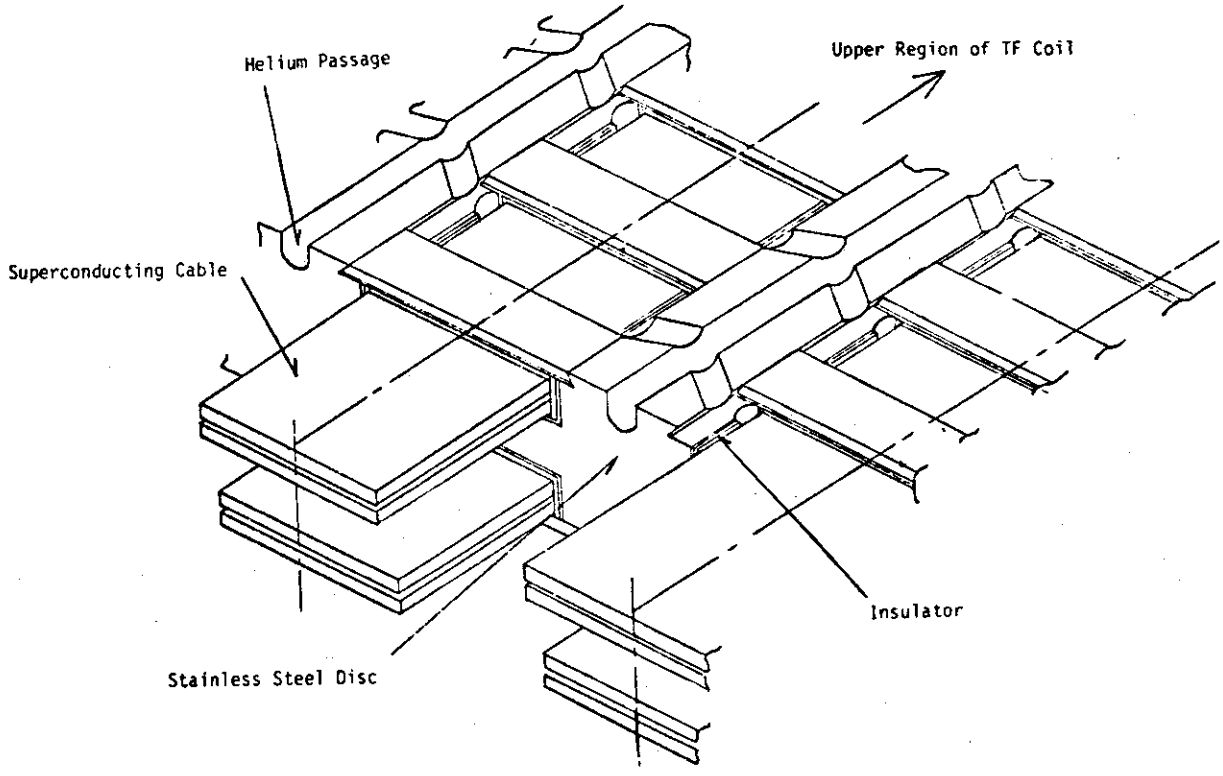

Fig.5.2 Perspective View of Stainless Steel Disc and Conductors

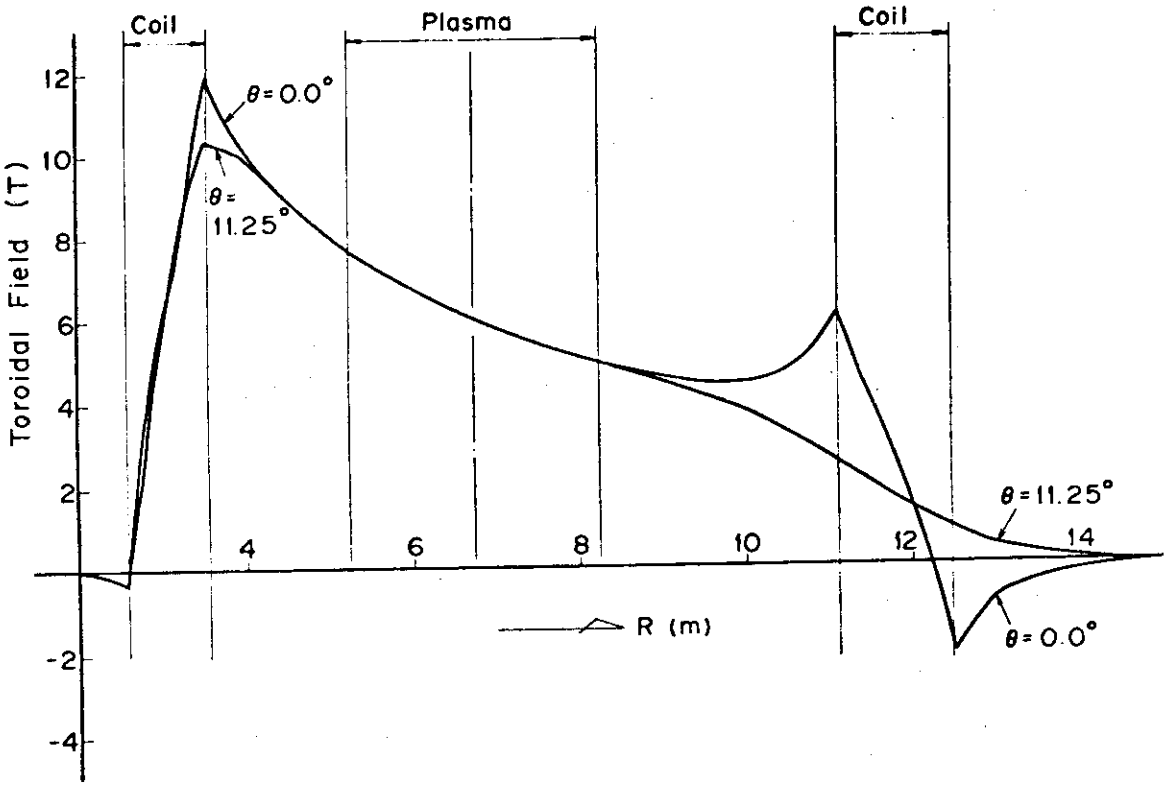

Fig.5.3 Spatial Distribution of Toroidal Field

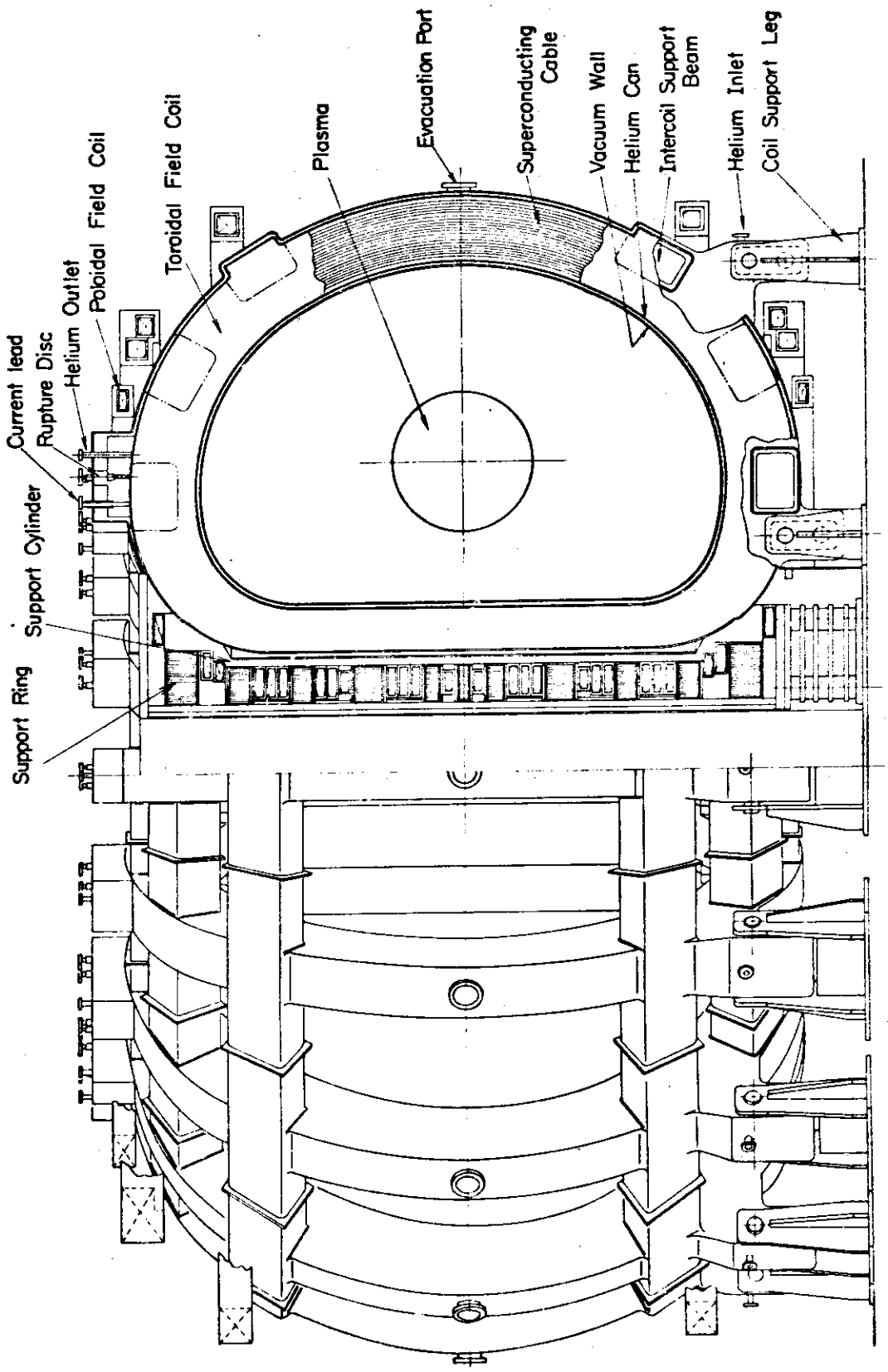

Fig.5.4 Side View of Toroidal Field Magnet

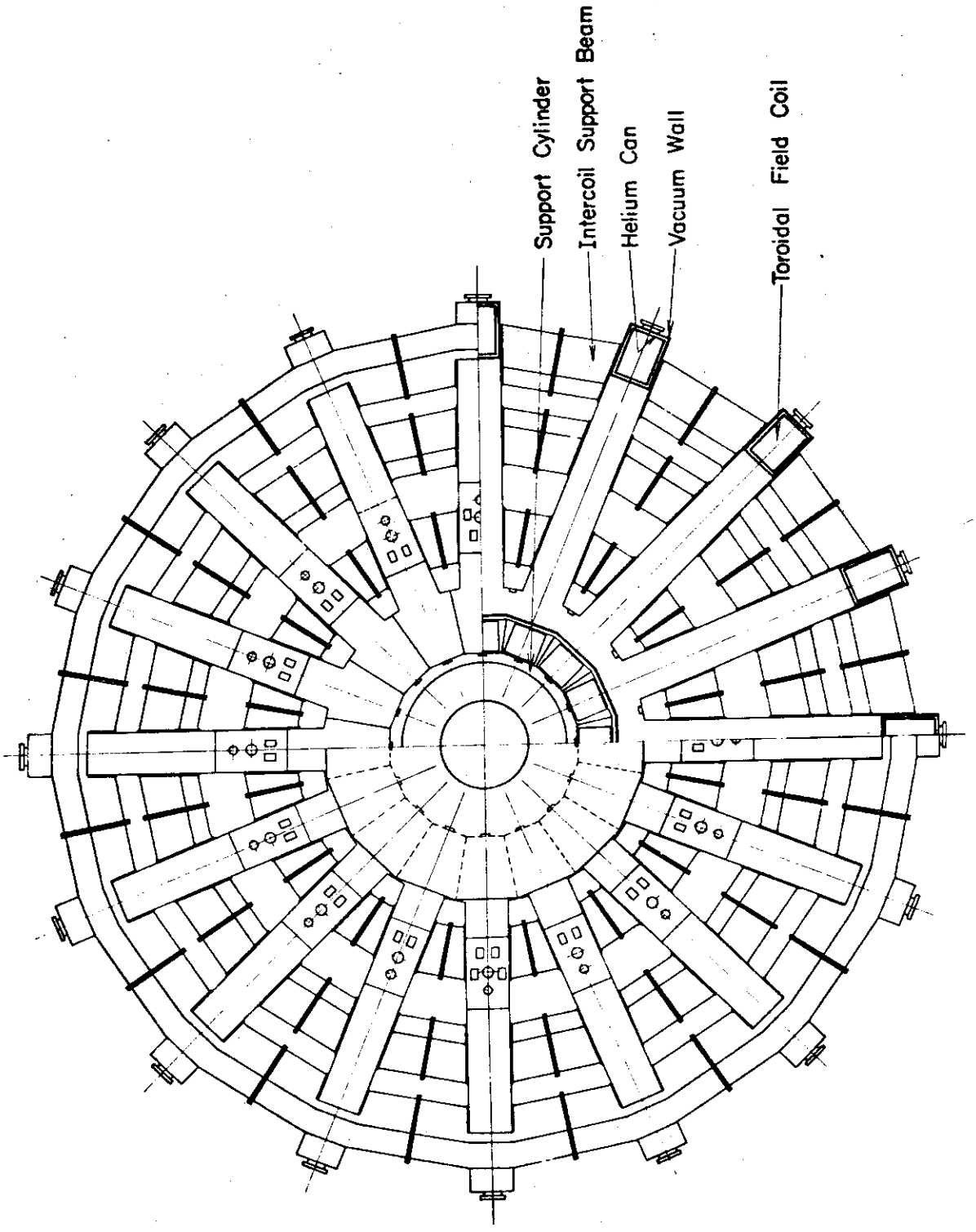

Fig.5.5 Plan View of Toroidal Field Magnet

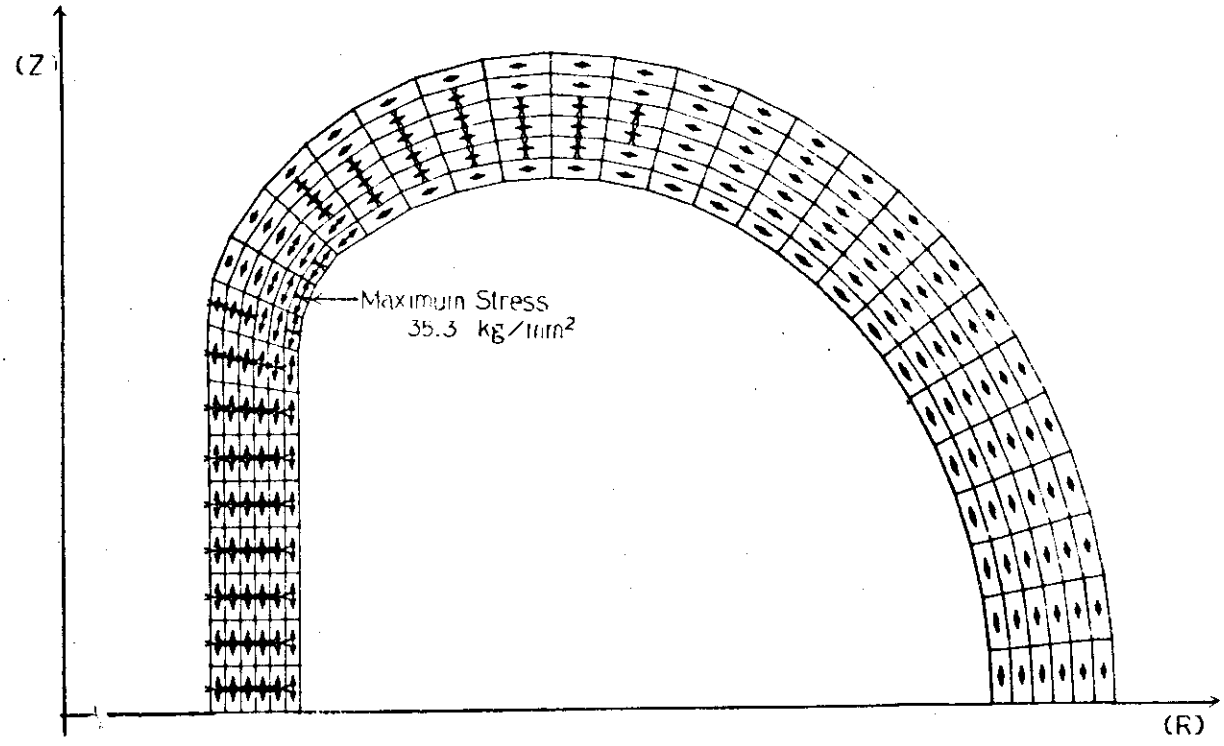

Fig.5.6 TF Coil Stress by Hoop Force

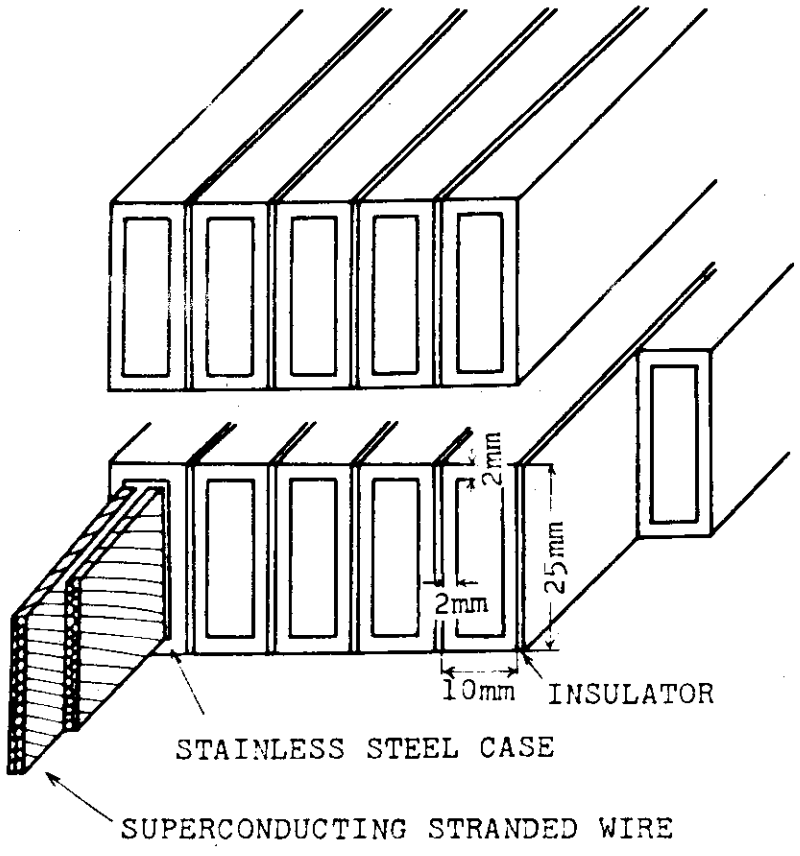

Fig. 5.7 View of coil windings

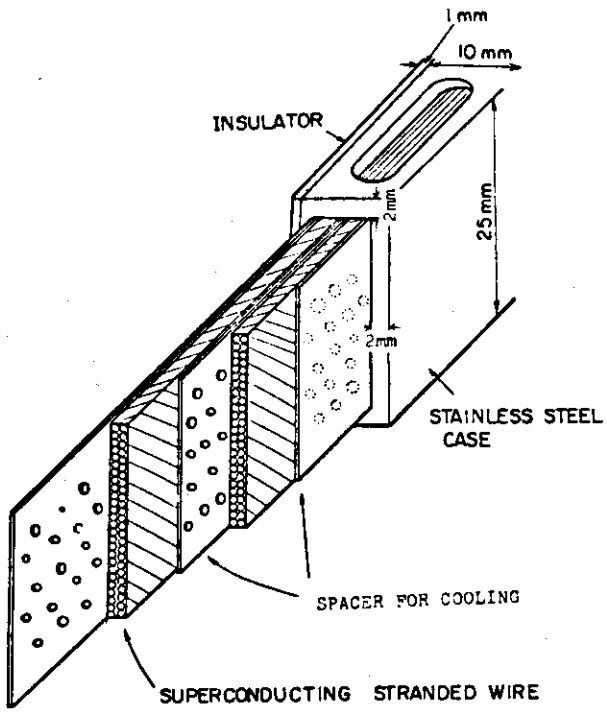

Fig. 5.8 View of unit conductor.

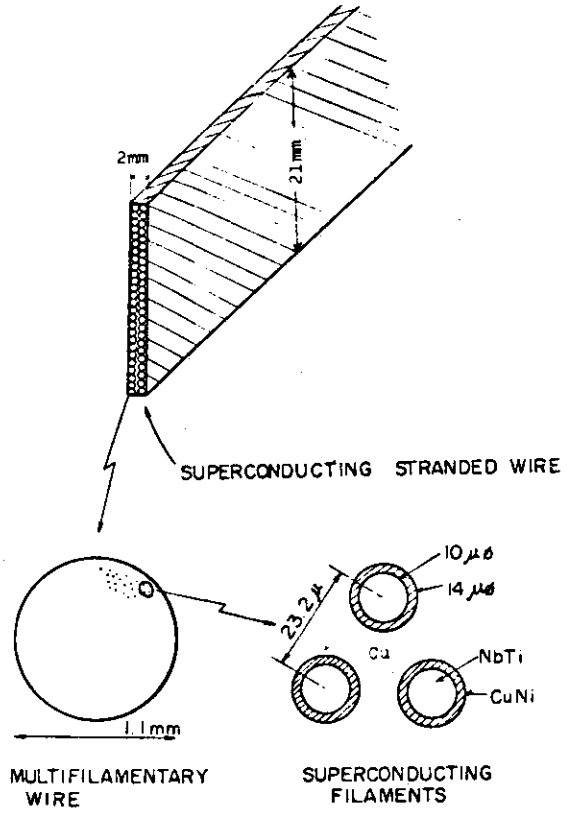

Fig. 5.9 Fine structure of superconducting standed wine.

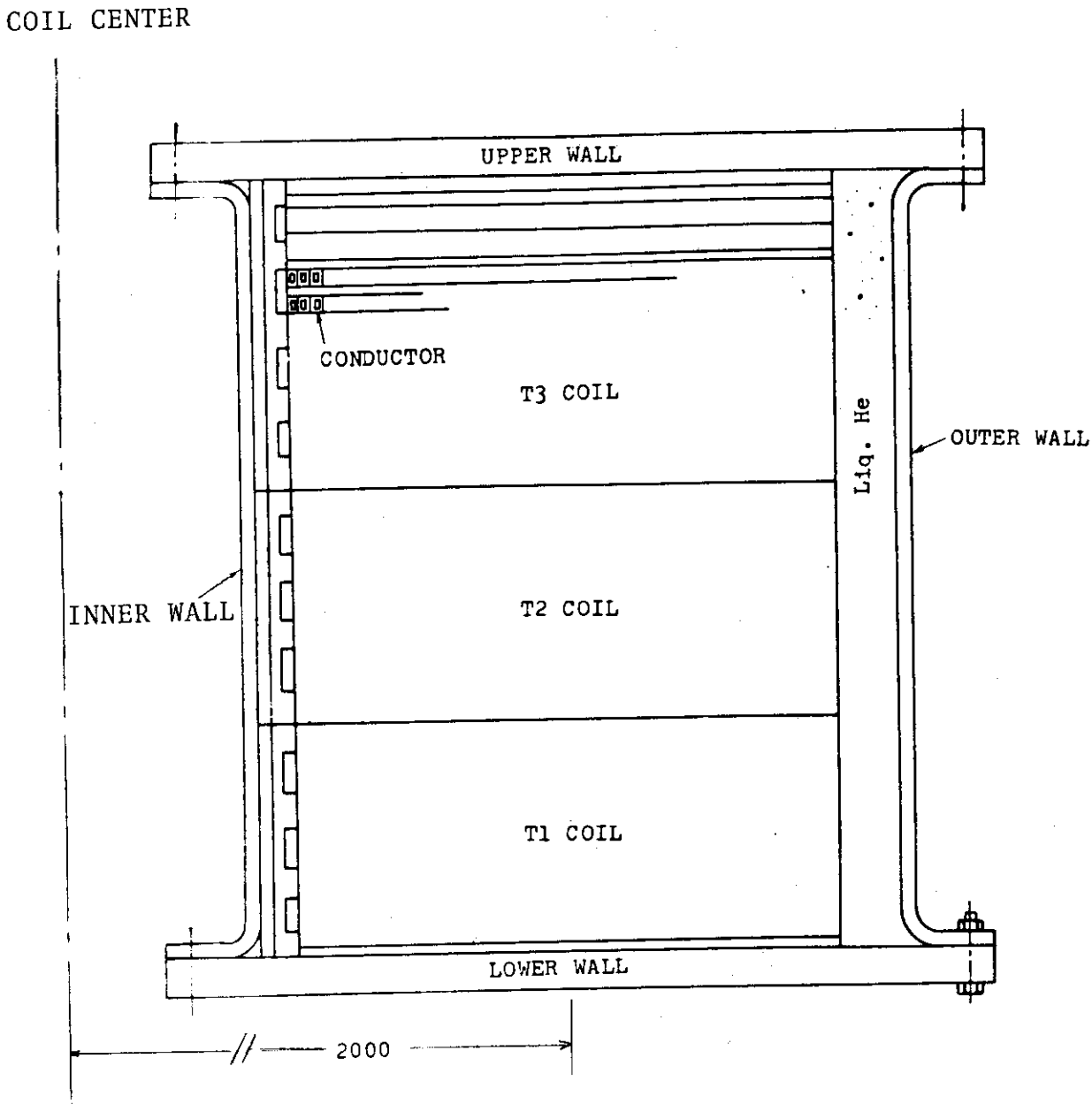

Fig. 5.10 Cross Section of Liquid Helium Can

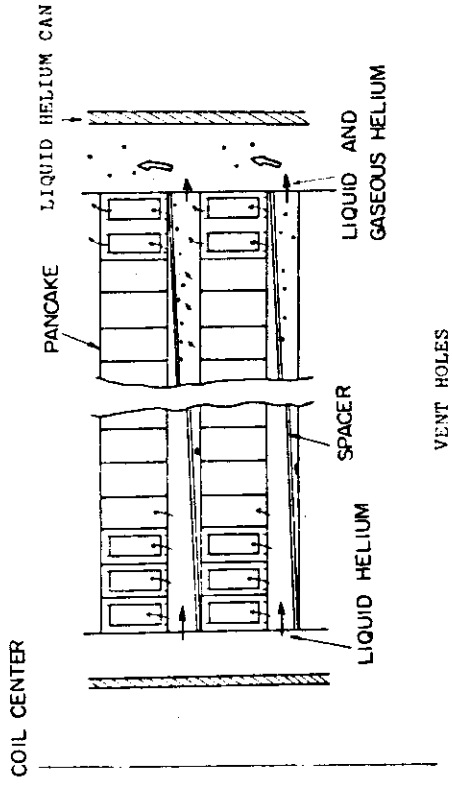

Fig. 5.11 Cooling passage of small diameter coils

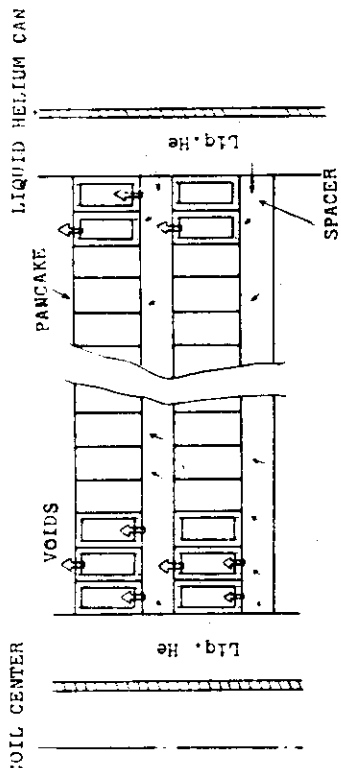

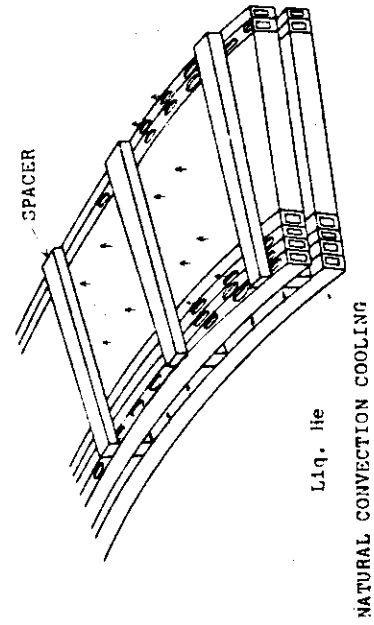

Fig. 5.12 Cooling passage of large diameter coils

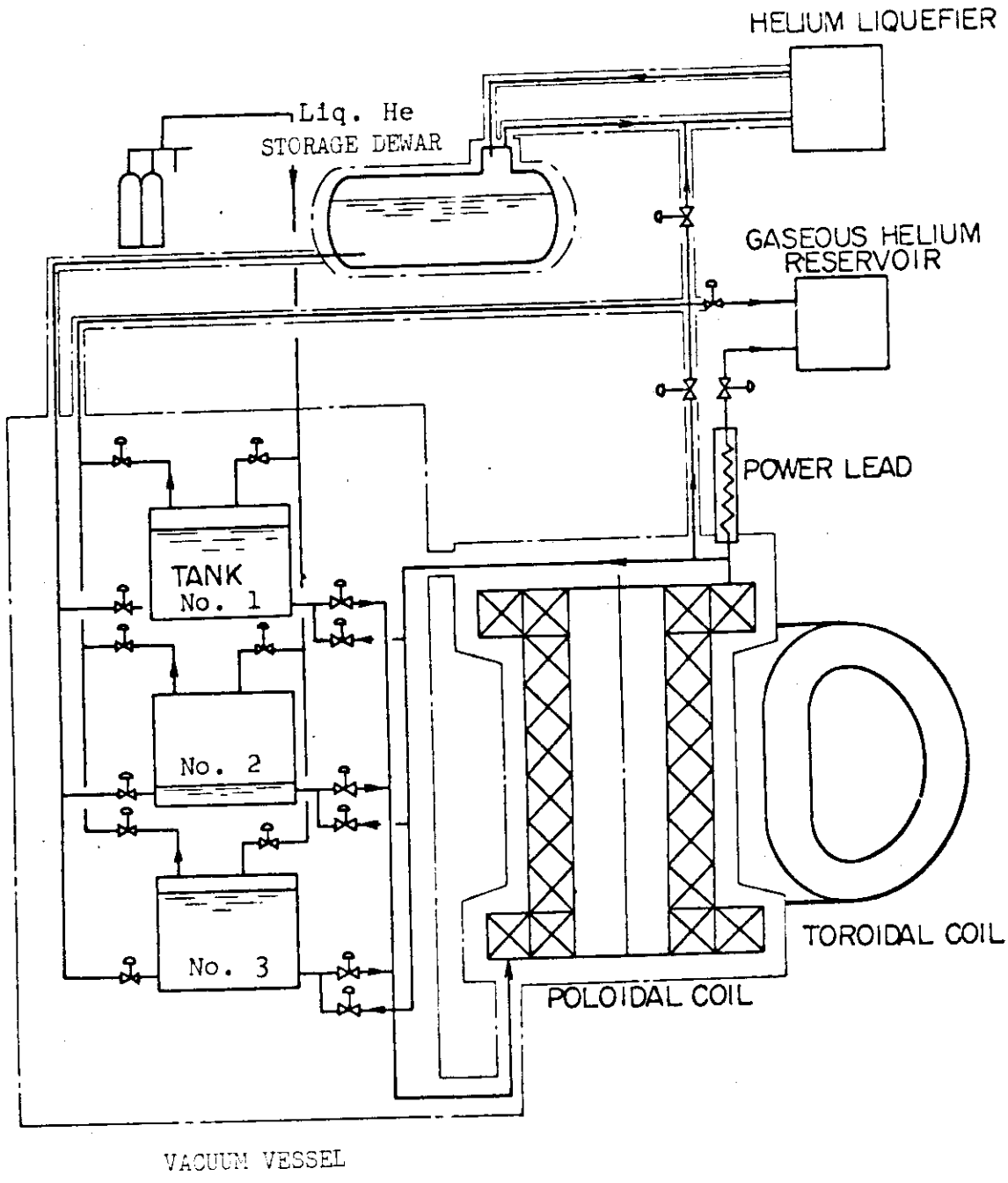

Fig. 5.13 Cooling system with three liquid helium tanks

6. Neutral Beam Injection System

Further heating of 32MW is required not only to heat the plasma up to 7 keV but also to sustain burning because the plasma is not in self-ignition. Neutral beam injection system of 200 keV D^0 beam of 110 sec. and repeated operation of every 180 sec is designed. Six ion sources with extraction current of 56 A D^+ beam is installed at four injection ports.

Though neutralization efficiency of D^+ ion of 200 keV is very low, D^+ beam is selected in this design because we do not have enough knowledge of negative ion sources. Application of hollow cathode discharge is proposed for ion sources expecting longer filament life and higer gas efficiency. When gas pressure is high in the acceleration space, heating of grids and source plasma chamber due to the secondary ions and electrons produced by ionization of residual gas becomes serious.

In-line direct converters are used to recover unneutralized beam energy and over all power efficiency of 35% is expected. Each injection system has a cryo-condensation pump with pumping speed of about 10^6 ℓ/s assuming the pressure of the converter space of 10^{-4} torr.

Table 6.1 Design parameters of the neutral beam injection system

Main Parameters	
Injection power (MW)	32
Injection energy (keV)	200
Number of injection ports	4
Duty cycle	110s/180s
Equivalent current efficiency	0.15
Power efficiency	0.35
Number of ion sources/port	6
Ion Source	
Ion current/ion source (A)	55
Extracted current density (A/cm^2)	0.15
Gas efficiency	0.6
Beam divergence	
Parallel to slits	0.4°
Perpendicular to slits	1.0°
Number of slits/ion source	56
Cross-section of slits (mm^2)	7×94
Number of electrodes	6
Electrode potentials referd to the first electrode (keV)	40 90 145 205 200
Transparency (%)	40.8
Neutralizing Cell	
Length (m)	3.5
Cross-section (mm^2)	130×780
Line density (torr-m) (90% of equilibrium cell)	0.48
Neutralization efficiency	0.17
Gas flow rate (torr.ℓ/s)	4.4
Direct Energy Converter	
Converter power output (MW)	150
Conversion efficiency	0.9
Pressure in direct converter (torr)	10^{-4}
Cryo-pump (Capacities/Port)	
Pumping speed (ℓ/s)	10^6
Gas flow rate (torr.ℓ/s)	100
Heat input to cryo-panel (W)	93
Heat input to LN_2 Baffle (kW)	7.6
Drift Tube	
Inlet pressure (torr)	10^{-4}
Outlet pressure (torr)	1×10^{-5}
Length (m)	2.5
Cross-section (mm^2)	150×780

7. Fuel Circulating System (FCS)

The fuel circulating system is shown in Fig.7.1. The main parameters of key components are given in Table 7.1. A schematic flow diagram of FCS and auxiliary systems is shown in Fig.7.2.

The vacuum system is composed of 16 cryosorption pumps, 8 auxiliary vacuum systems, 2 fuel recovery system and 2 rough pump system (Fig.7.3). 8 cryosorption pumps are alternately operated at an interval of 2 hr.

In the fuel gas refiner system(Fig.7.4), impurities are effectively removed by using Pd-alloy membranes.

For the isotope separation system, the diffusion method through Pd-alloy membrane was adopted. This method can separate hydrogen isotopes in their atomic states. The system consists of 1st and 2nd cascades for removing protium and separating deuterim, respectively. The numbers of separators are 47 for the 1st cascade and 46 for the 2nd cascade. The effective surface area for the 1st and the 2nd cascades are 2,541 and 21,617 cm^2, respectively. An isotope separator is shown in Fig.7.5.

From the standpoint of the tritium containment and safety, a three-stage containment system of tritium fuel are settled to control tritium release to environment as low as possible. Basic design parameters of the system are summarized in Table 7.2. Some processing systems of tritium bearing gases are required for such a containment system, a schematic flow diagram of these processing systems is shown in Fig.7.6.

FCS components and piping are designed to minimized leakage into the secondary containment which encloses most of the primary containment. The secondary containment is of glovebox type with an inert gas atmosphere, provided Glovebox Atmosphere Purification System (Fig.7.7) of flow rate 70 m^3/min. The tertiary containment system consists of the rooms enclosing secondary system and tritium bearing gas processing system, a 3 m^3/min Atmosphere Cleanup System and à 150 m^3/min Emergency Containment System.

Table 7.1 Summary of Fuel Circulation System

Main Vacuum System		
Gas Lord (at 300°K)		158 Torr·l/s
Number of Pumping Ports		8
Number of Cryosorption Pumps (for on-line regeneration)		8 (16)
Pumping Speed of Each Cryosorption Pump		3.3×10^5 l/s
Pumping Speed of Secondary Pumps ;		
Turbomolecular Pump for Auxiliary System		4.1×10^3 l/s
Mechanical Booster Pump for Recovery System		40 l/s
Rotary Pump for Rough Pumping System		790 l/s
Fuel Gas Refine System (Permeation System through Pd-Alloy Membrane)		
Number of Separators		12
Dimension of Separator		360 mm^D x 1300 mm^L
Effective Surface Area of Each Separator		820 cm^2
Operating Pressures :	upstream	$\sim$ 1 Kg/cm^2
	downstream	< 1 Torr
Operating Temperature		420 °c
Isotope Separation System (Permeation System through Pd-Alloy Membrane)		
Number of Separators ;	1st Cascade	47
	2nd Cascade	46
Dimension of Separator ;	1st Cascade	140 mm^D x 1.6 m^H
	2nd Cascade	170 mm^D x 1.6 m^H
Effective Surface Area of Each Separator ;		
	1st Cascade	2541 cm^2
	2nd Cascade	21617 cm^2
Operating Pressure ;	High Pressure Side	$\sim$ 6 Kg/cm^2
	Low Pressure Side	$\sim$ 1 Kg/cm^2
Operating Temperature		420 °c

Table 7.2 Parameters of Tritium Containment Systems

Secondary Containment System	
Volume of Gloveboxes	7×10^2 m^3
Pressure in Glovebox	-25 mm Aq
Cover Gas	He (≤99.9 %)
Tritium Inreakage Rate	1×10^{-3}cm^3(STP)/sec
Basic Tritium Level	2×10^{-2} μCi/cm^3
Number of Gloves	1,400
GAPS Flow Rate	70 m^3/min
Method of Tritium Removal	Catalytic Reactor / Dryer
Tertiary Containment System	
Volume of Rooms	4.2×10^4 m^3
Pressure in Room	-15 mm Aq
Room Leak Rate	0.1 vol.%/day
Basic Tritium Level ;	
at Reactor Operation	2×10^{-5} μCi/cm^3
at Maintainance	2×10^{-7} μCi/cm^3
ECS Flow Rate	150 m^3/min
ACS Flow Rate	3 m^3/min

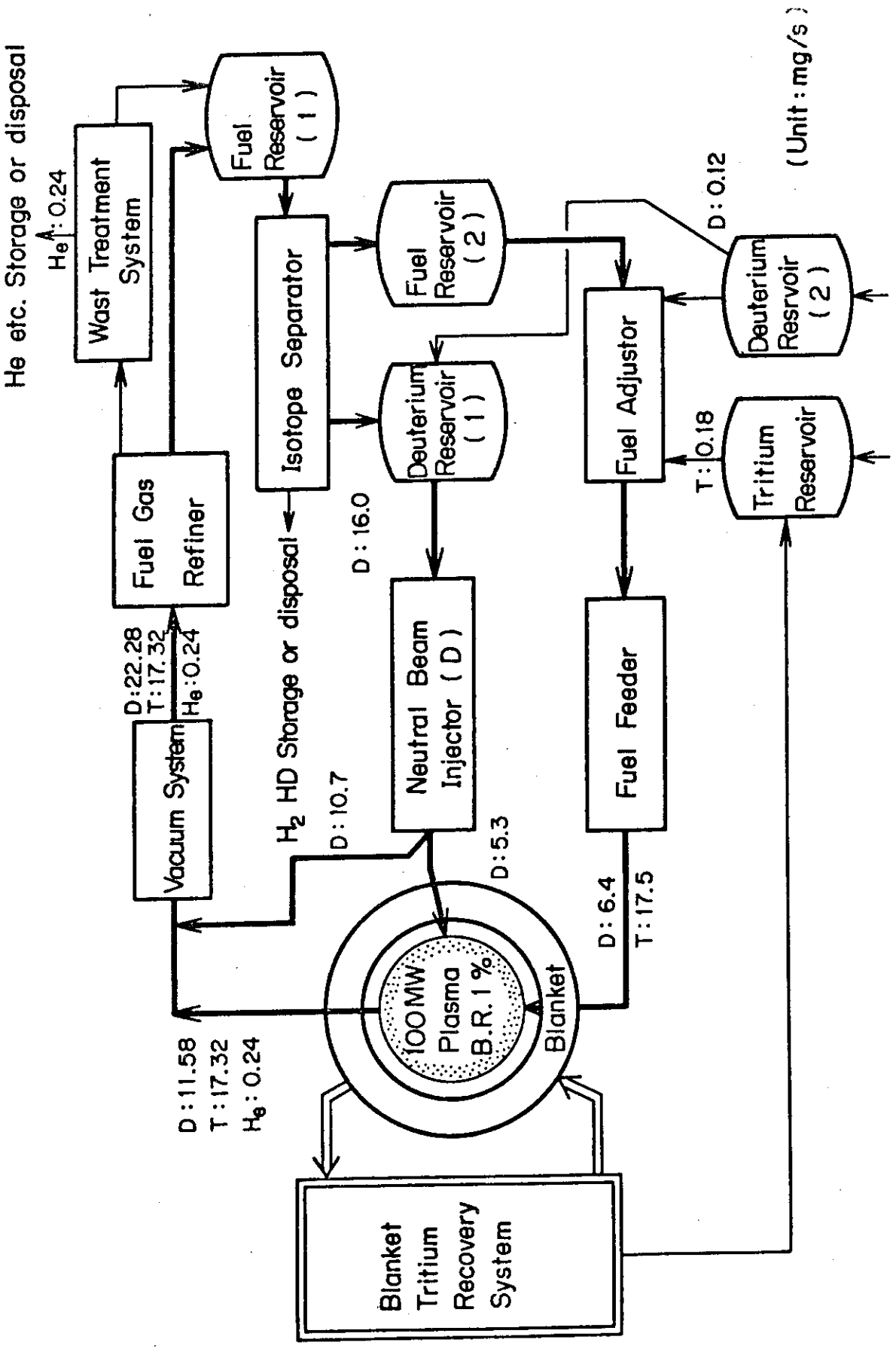

Fig.7.1 Fuel Circulating System Flow Diagram

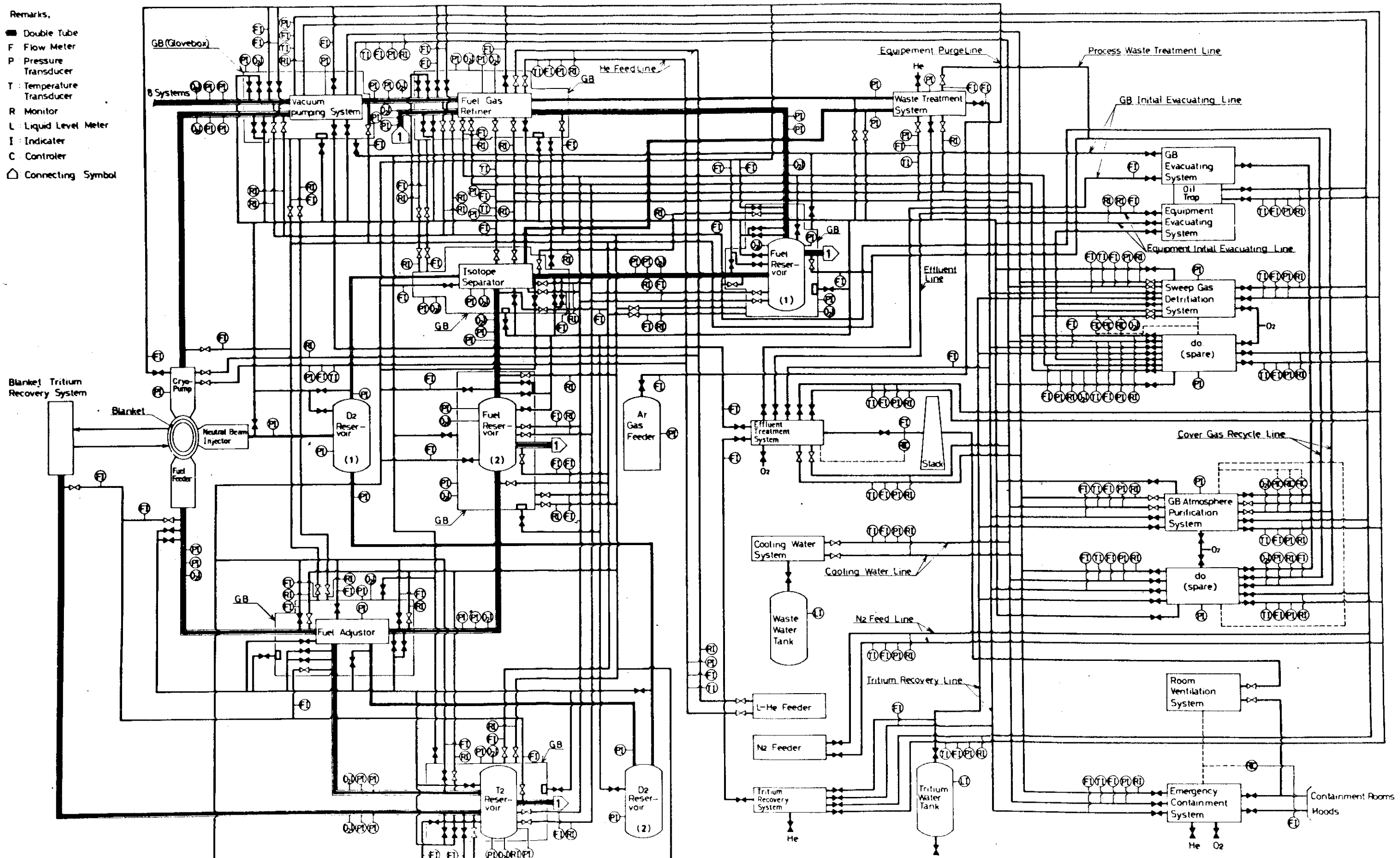

Fig.7.2 Conceptual Flow Diagram of FCS and Auxiliary System

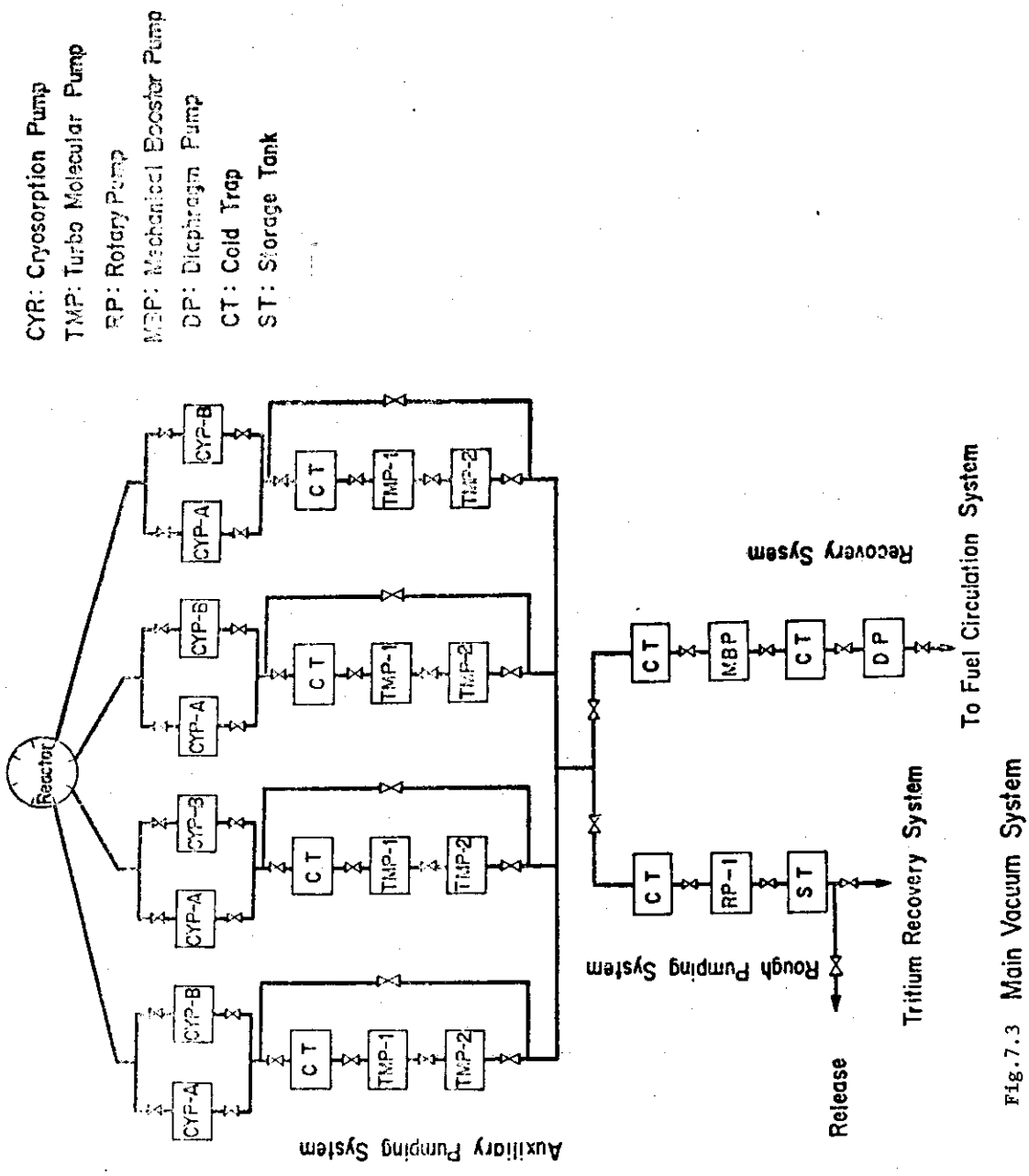

Fig.7.3 Main Vacuum System

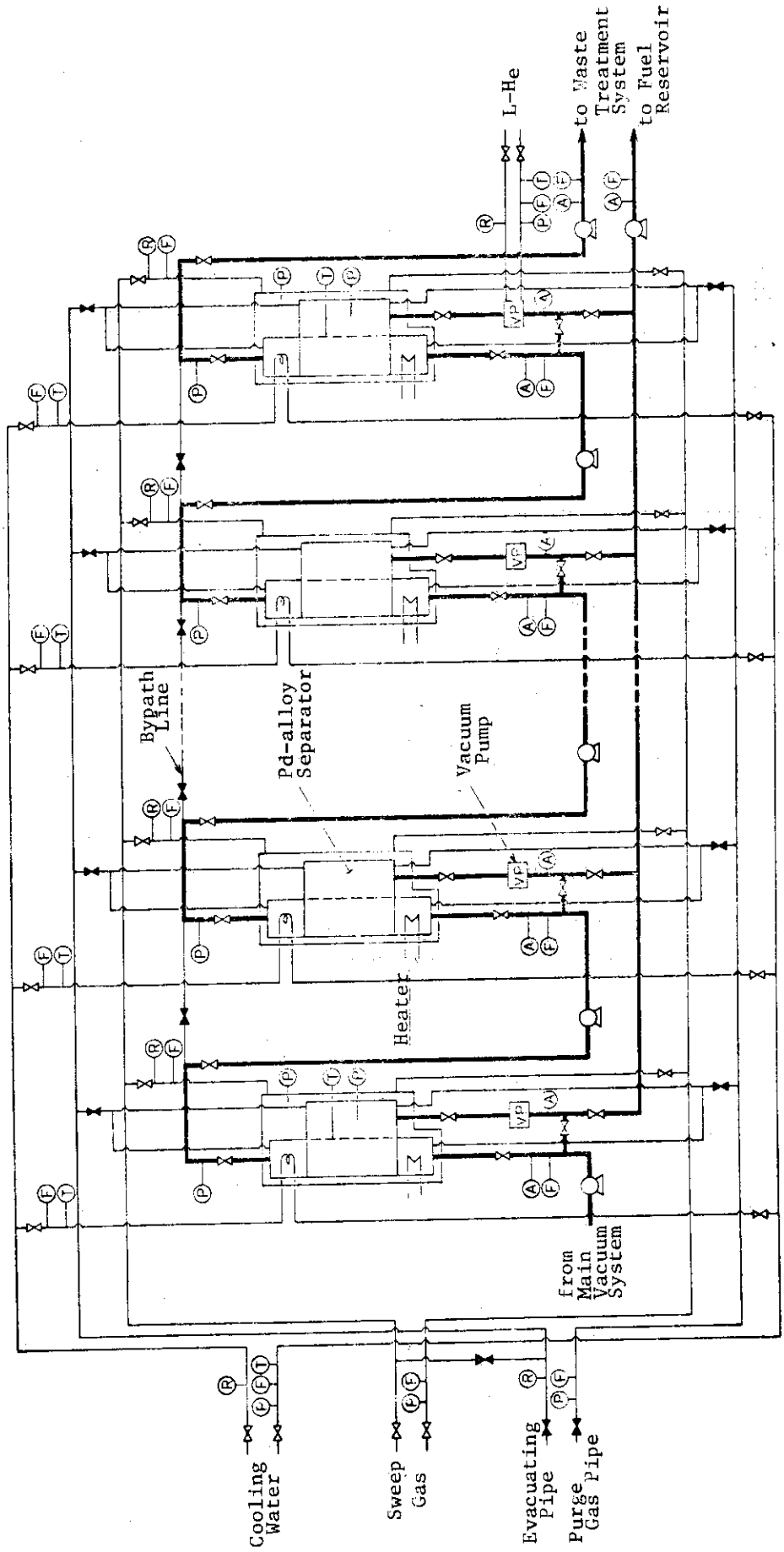

Fig.7.4 Conceptual Flow Diagram of Fuel Gas Refiner

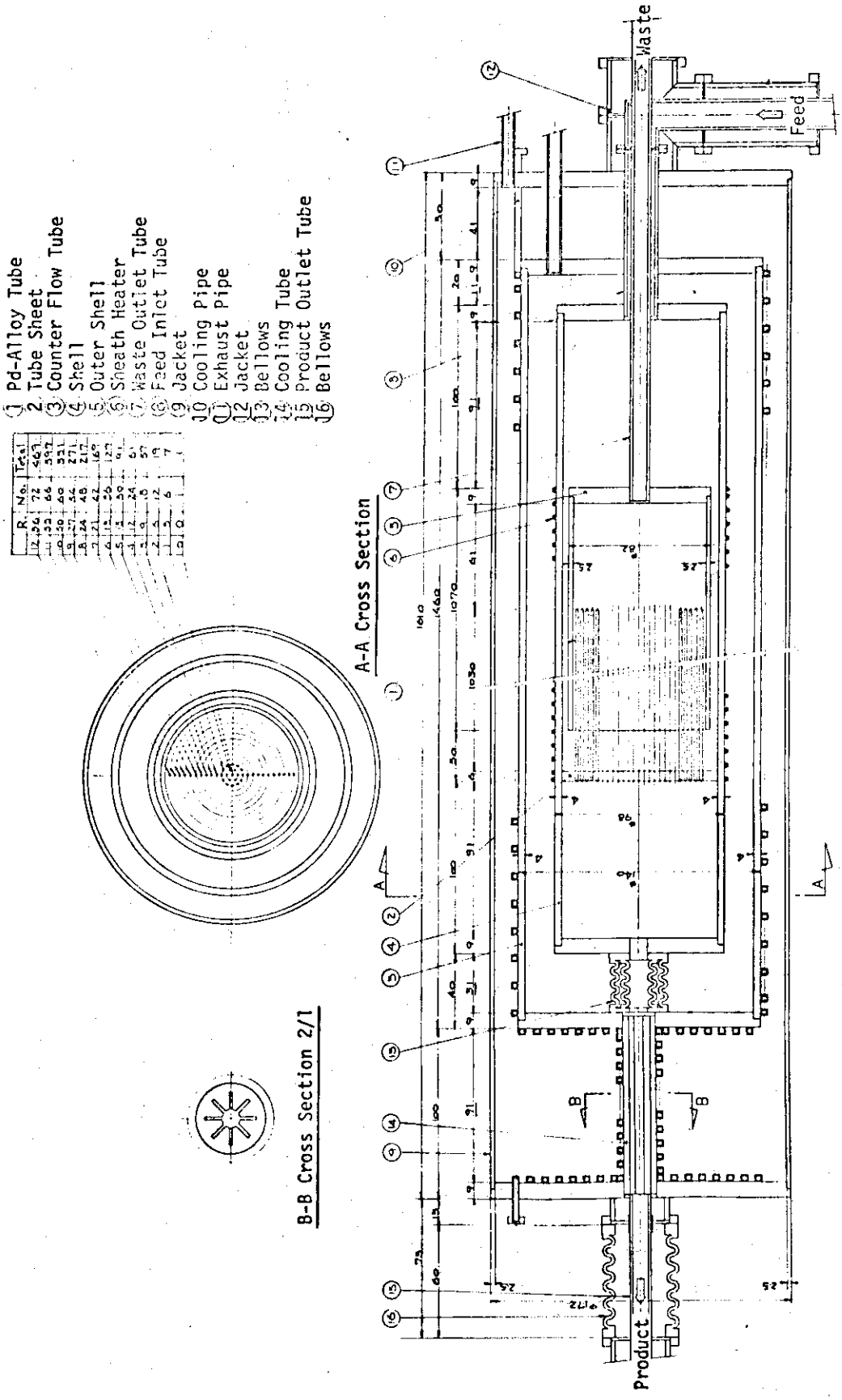

Fig.7.5 Structure of Hydrogen Isotope Separator

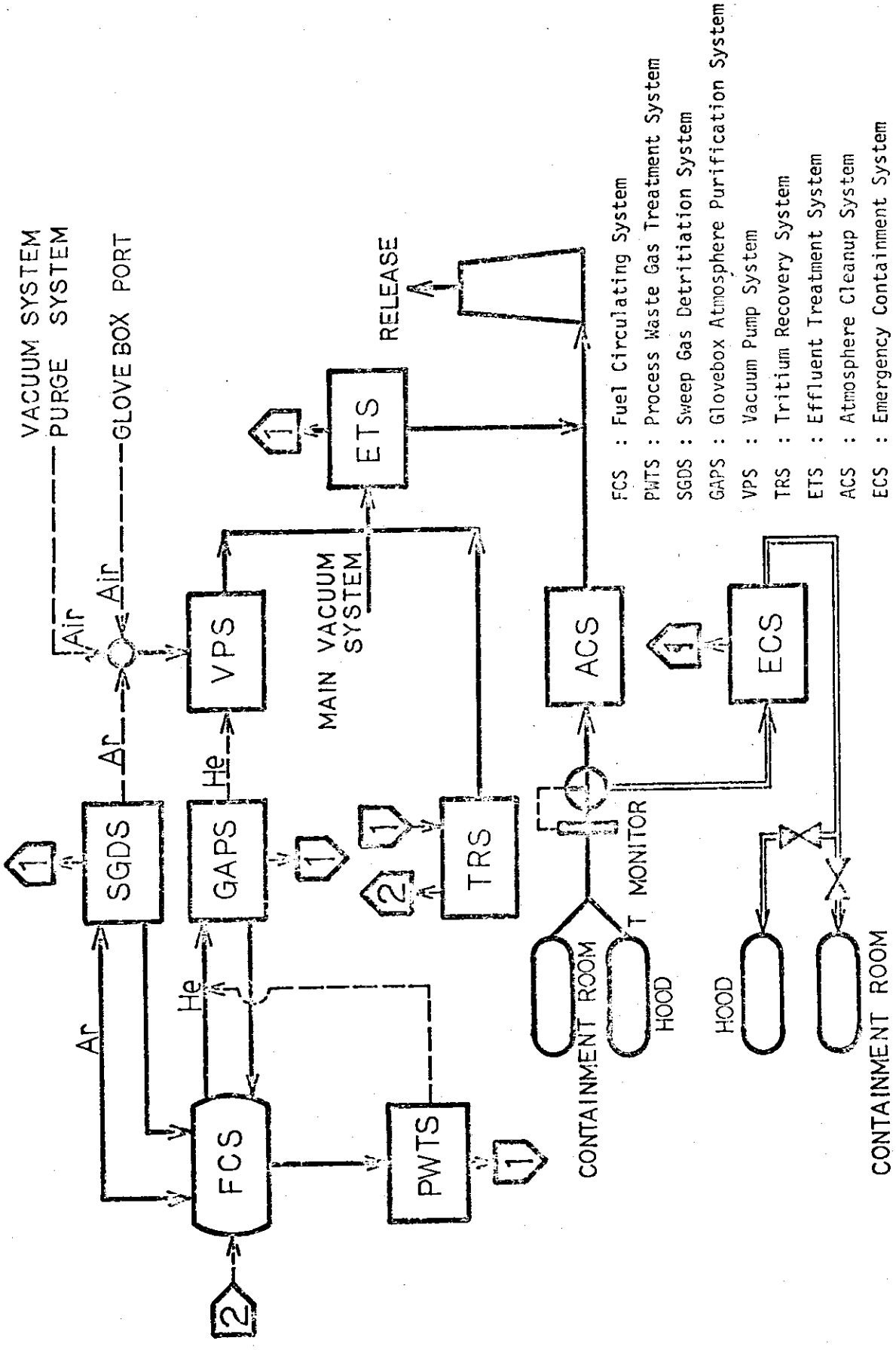

Fig. 7.6 Schematic Diagram of Tritium Containment Concept

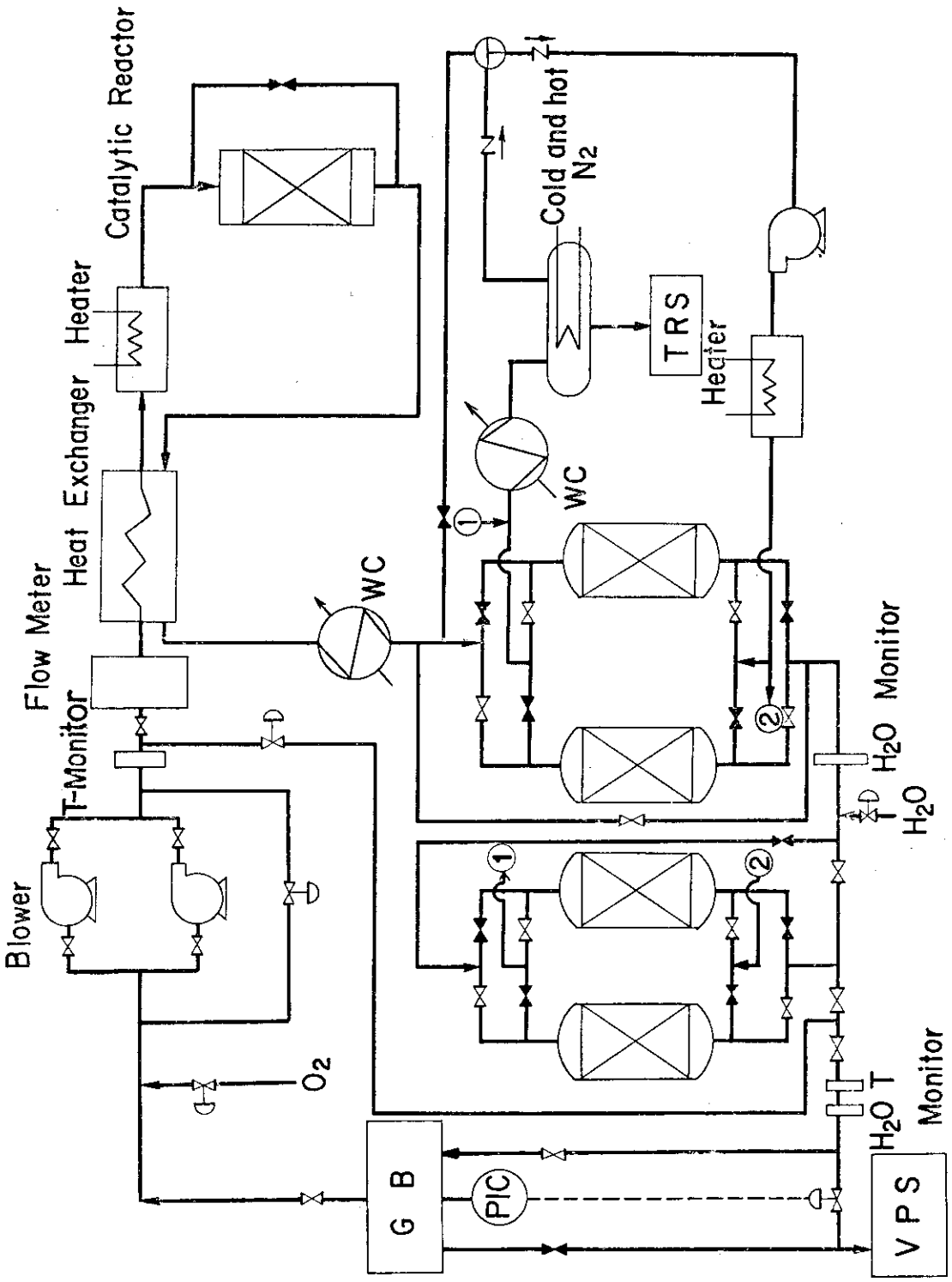

Fig.7.7 Glovebox Atmosphere Purification System (GAPS)

8. Reactor Cooling and Tritium System

Reactor cooling and tritium system of JXFR at the stage of first preliminary design was reviewed from the safty point of view, and additional design works were performed.

Fig. 8.1 shows the main cooling system. Main cooling system has 4 loops. The main components are Heat Reservoir, Intermediate Heat Exchanger and so on. Fig. 8.2 shows the Heat Reservoir. Fig. 8.3 show the Intermediate Heat Exchanger. Fig. 8.4 shows the Tritium Removal System. Fig. 8.5 shows the Catalyst Oxdizer.

In normal operation, tritium gas generated in the blanket permeates through the wall of the hot leg pipes. Fig. 8.6 shows the heat balance and the tritium permiation in the main cooling system. The rate is 120 Ci/day. Therefore, to reduce this rate, we proposed the Jacket Sweep Method. Fig. 8.7 shows the system. Fig. 8.8 shows the Jacket Tritium Processing System (JTPS). By mean of this method, we reduced the tritium release. Table 8.1 shows the result.

Potential maximum tritium release in accident is due to a guillotine rupture of the main cooling outlet header. Tritium release for this accident was estimated based on the analysis of pressure transients in the reactor. Estimated results given in Table 8.2 shows the strong dependance of estimation on the method to simulate the tritium release behavior.

Table 8.1 Tritium release in normal operation

Items	Release Rate (Ci/day)
Permeation through primary loops	0.014 (with jacket) 120 (without jacket)
Permeation through IHX tubes	0.20
Leakage from primary loops	0.085 *

* Coolant leakage was assumed to be 0.01%/day

Table 8.2 Tritium release following the rupture of main cooling outlet header

Analytcal models to simulate the tritium release behavior	Tritium releases from vacuum vessel to reactor room (Ratio of released tritium to the total inventry in vacuum vessel)
Assuming full mixing of tritium with helium gas in vacuum vessel	90 ~ 100 %
Assuming temporary confinement of tritium in the neighborhood of cryo-panels while helium gas is flowing towards cryo-panels	20 ~ 30 %
Assuming temporary confinement of tritium and emergency shutdown of gate valves	0 ~ 10 %

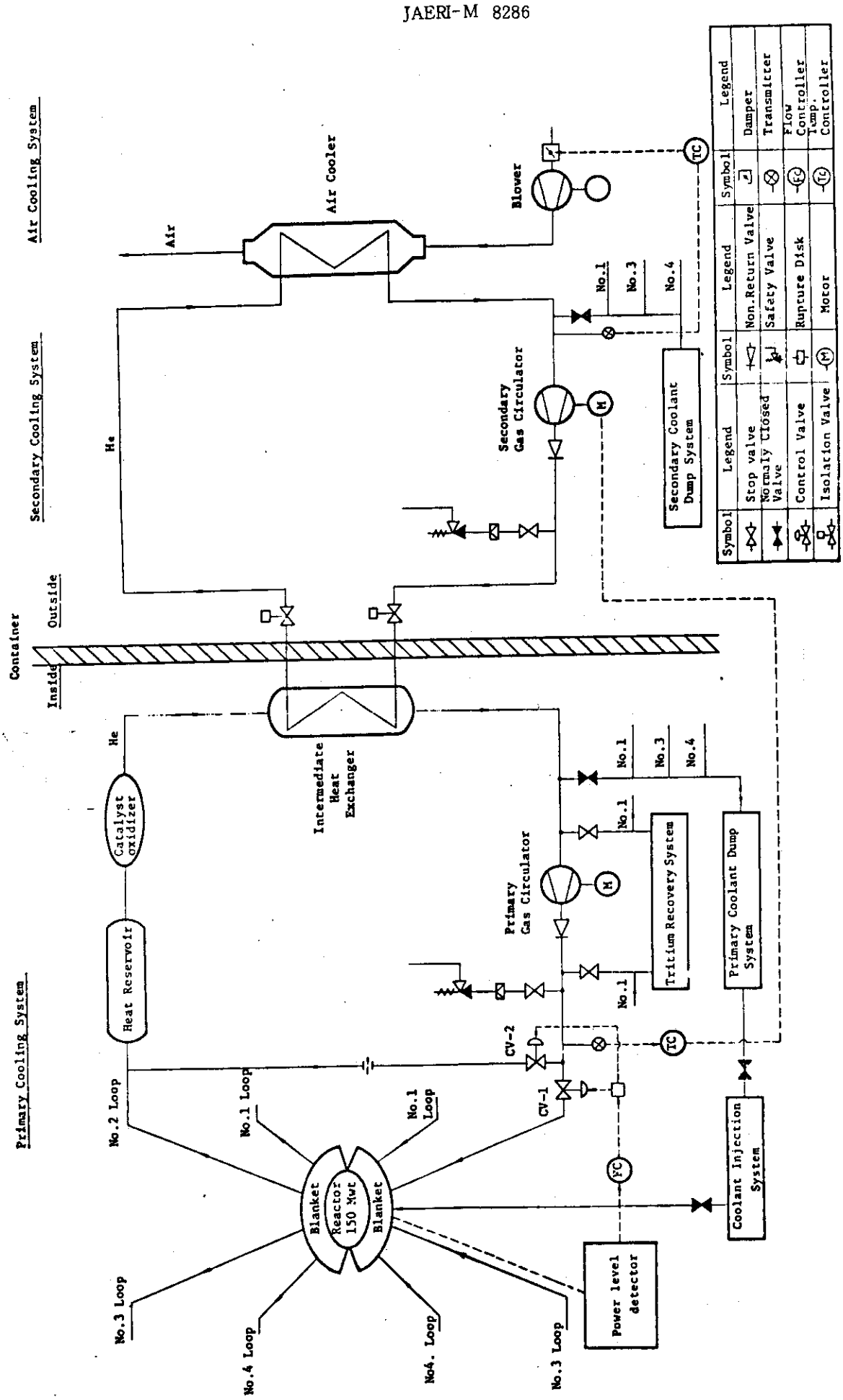

Fig. 8.1 Main Cooling System

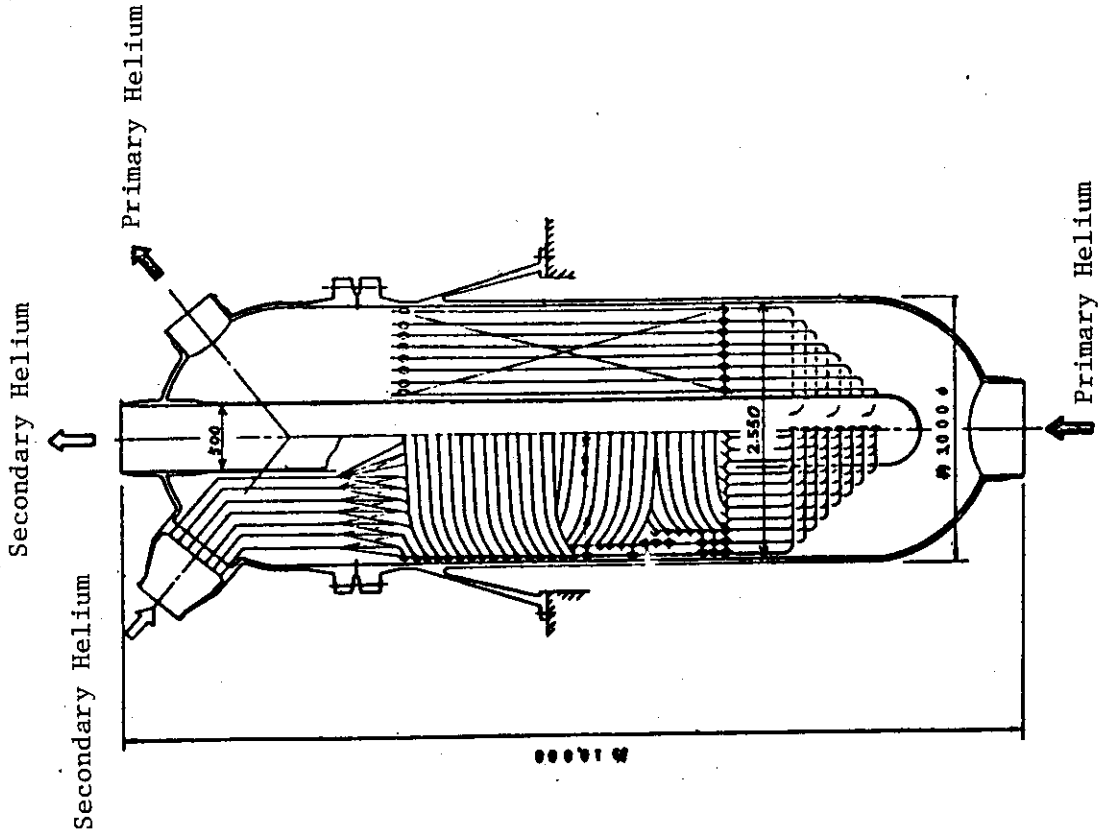

Fig. 8.3 Intermediate Heat Exchanger

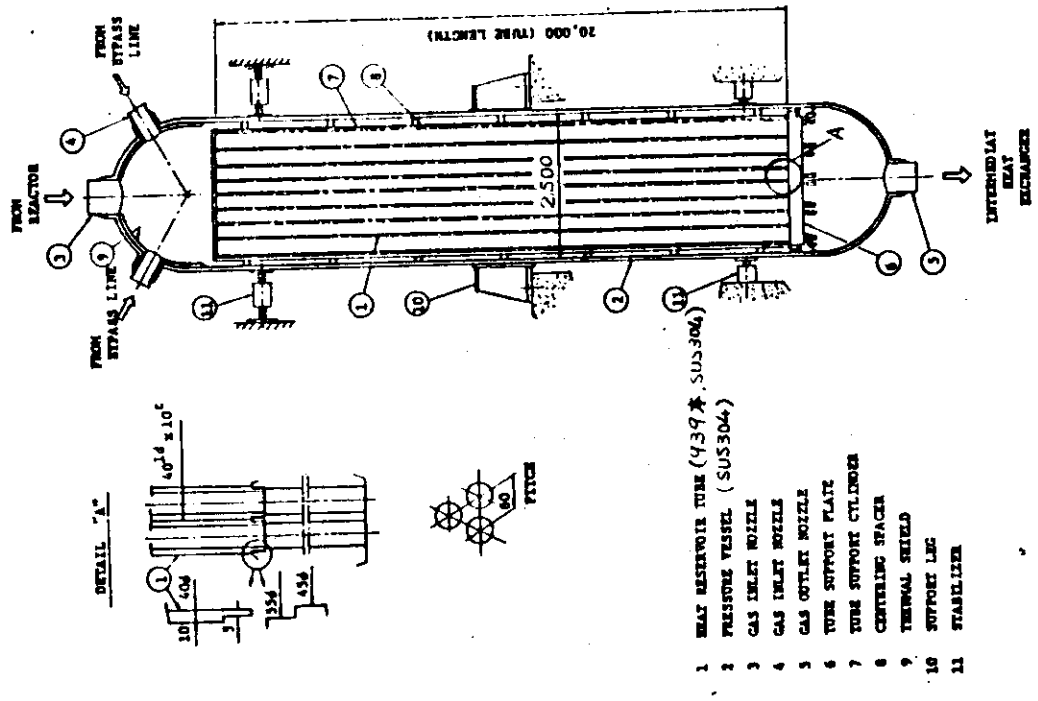

Fig. 8.2 Heat Reservoir

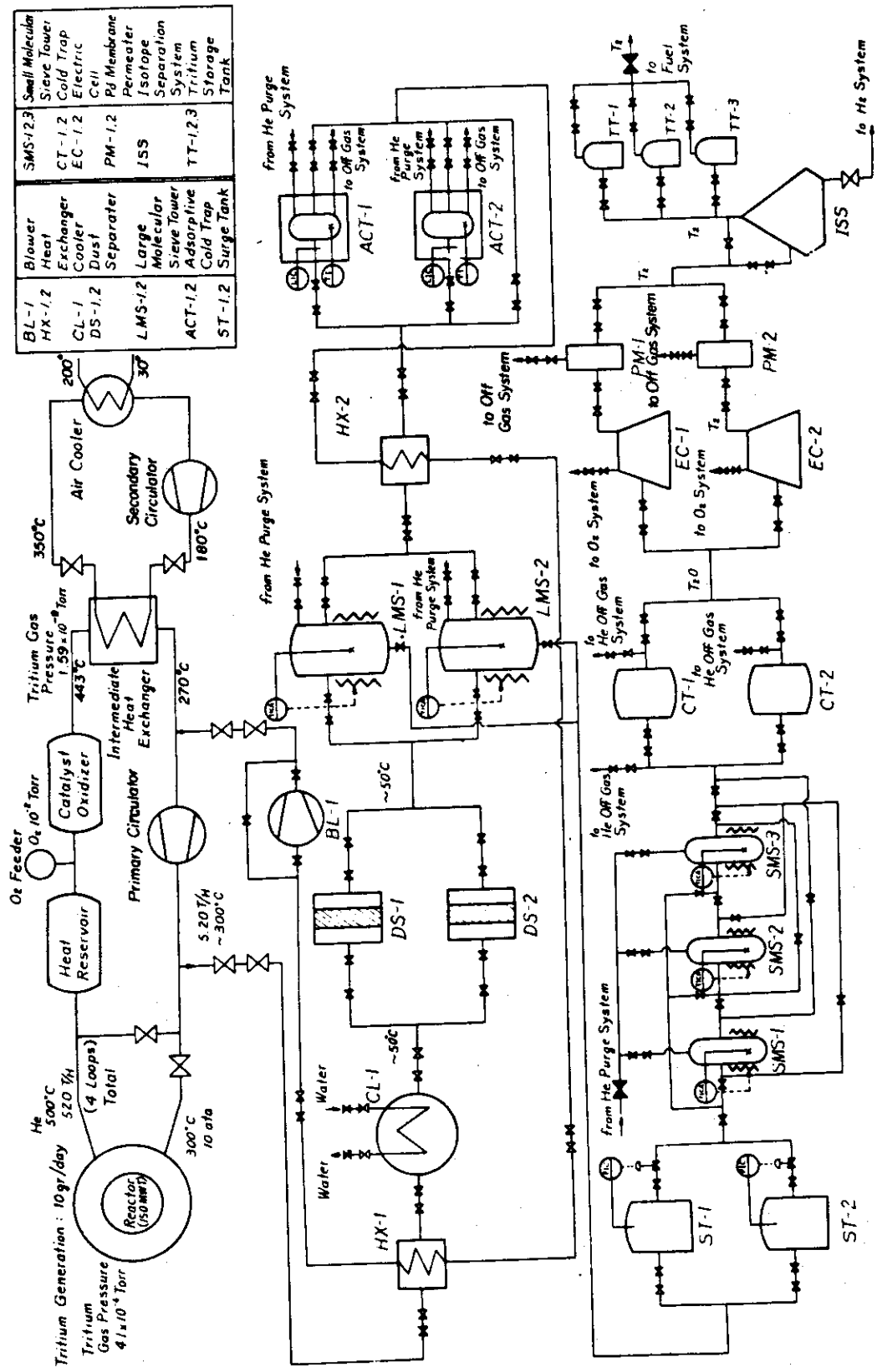

Fig. 8.4 Tritium Removal System

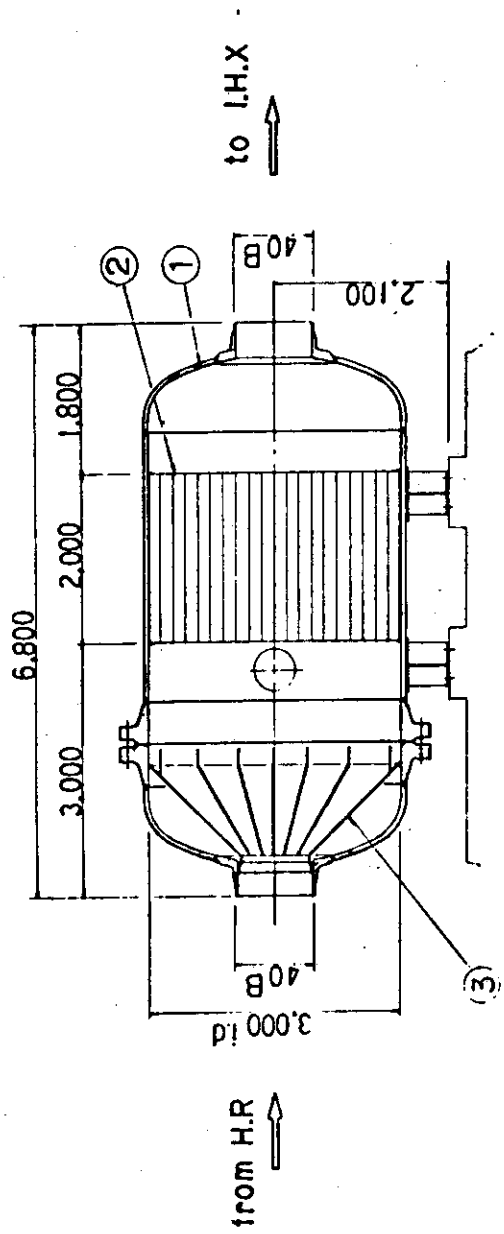

Fig. 8.5 Catalyst Oxidizer

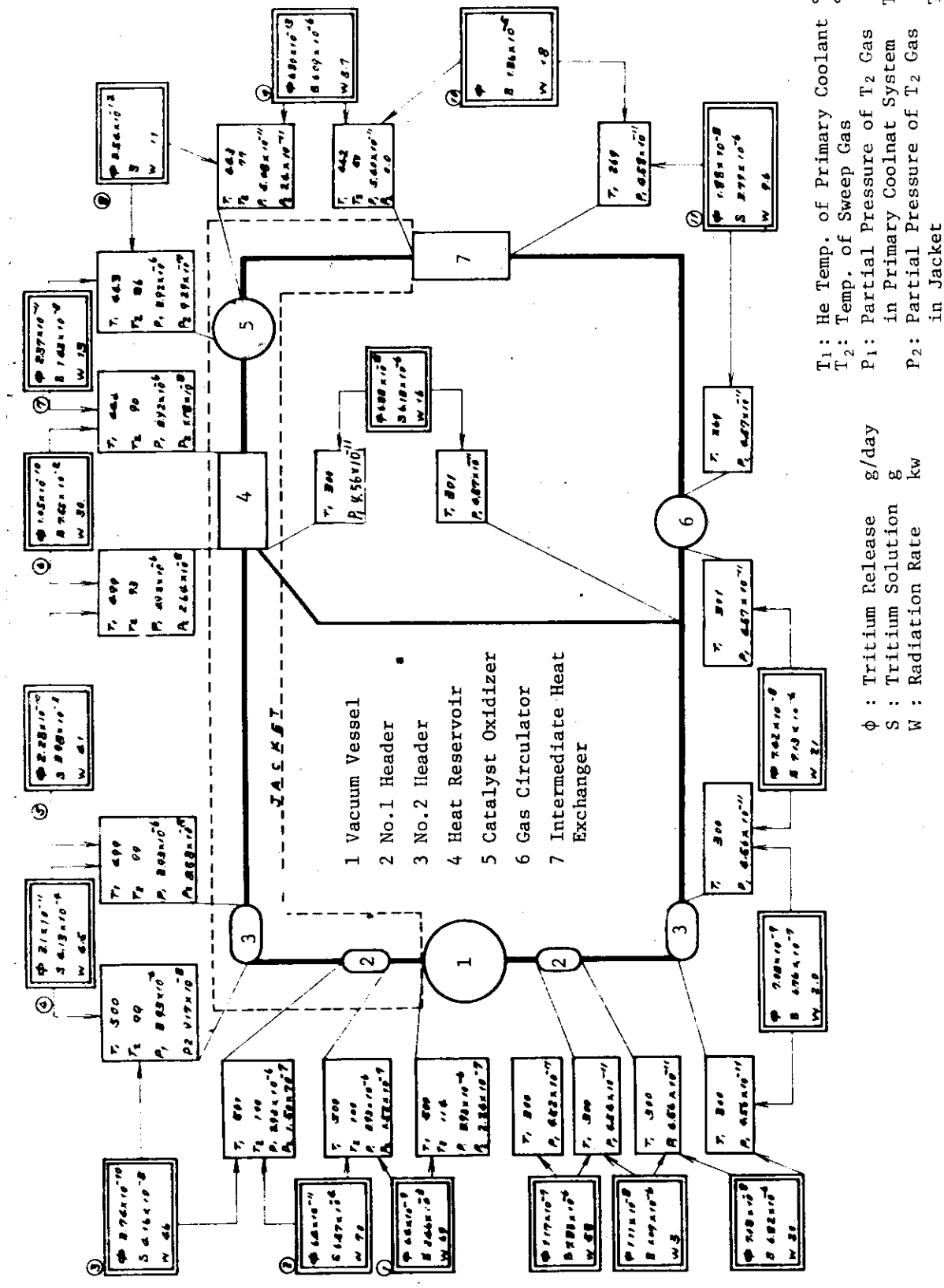

Fig. 8.6 Heat balance and Tritium Permeation in the Main Cooling System

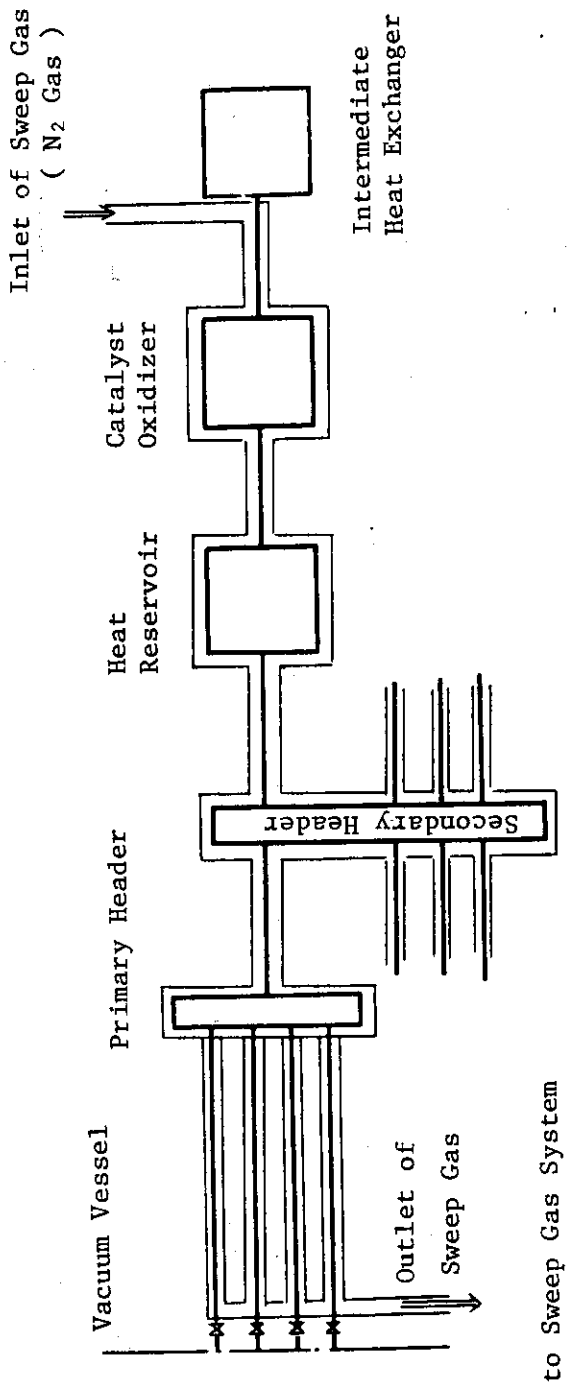

Fig. 8.7 Jacket Sweep System

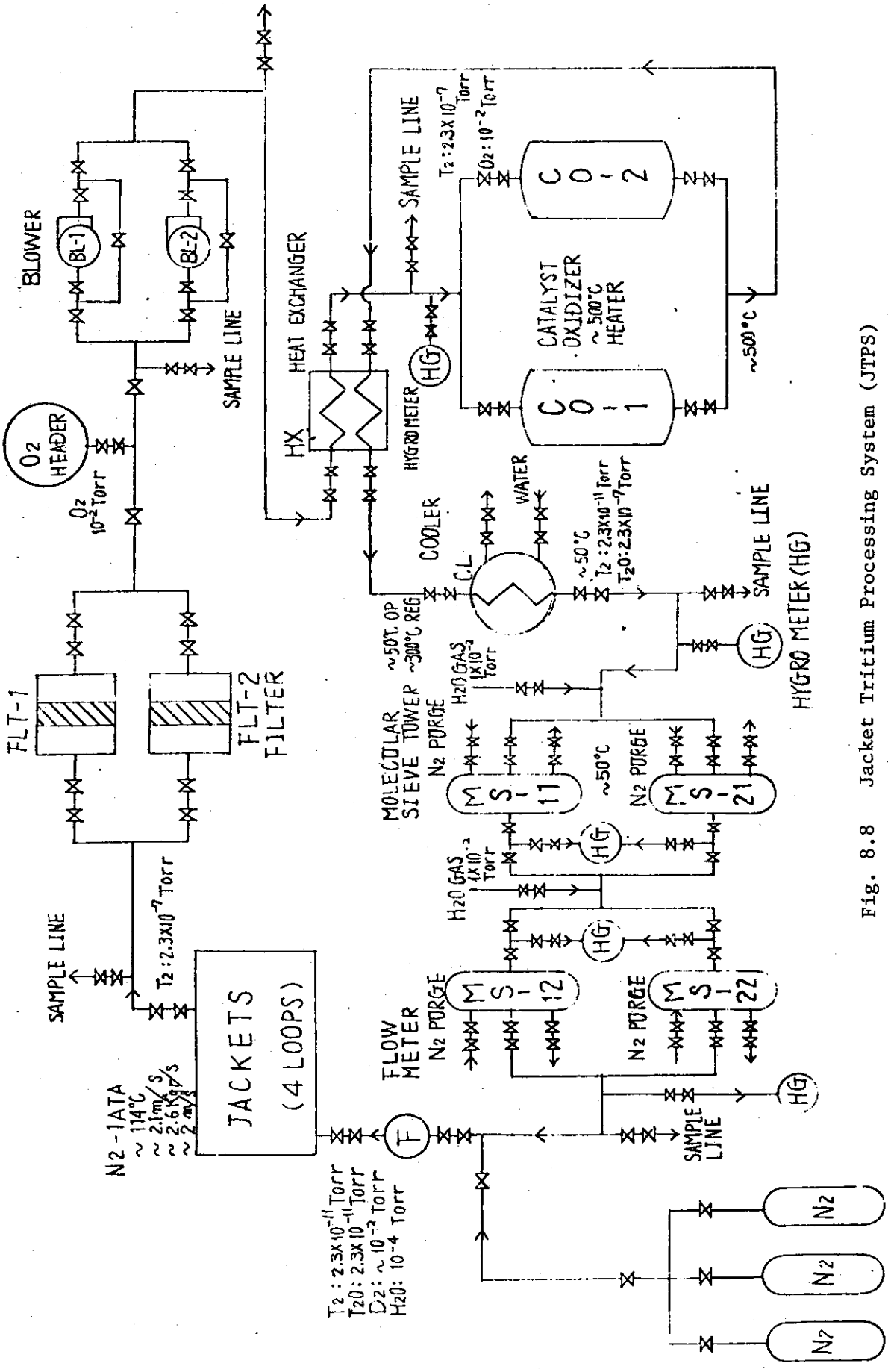

Fig. 8.8 Jacket Tritium Processing System (JTPS)

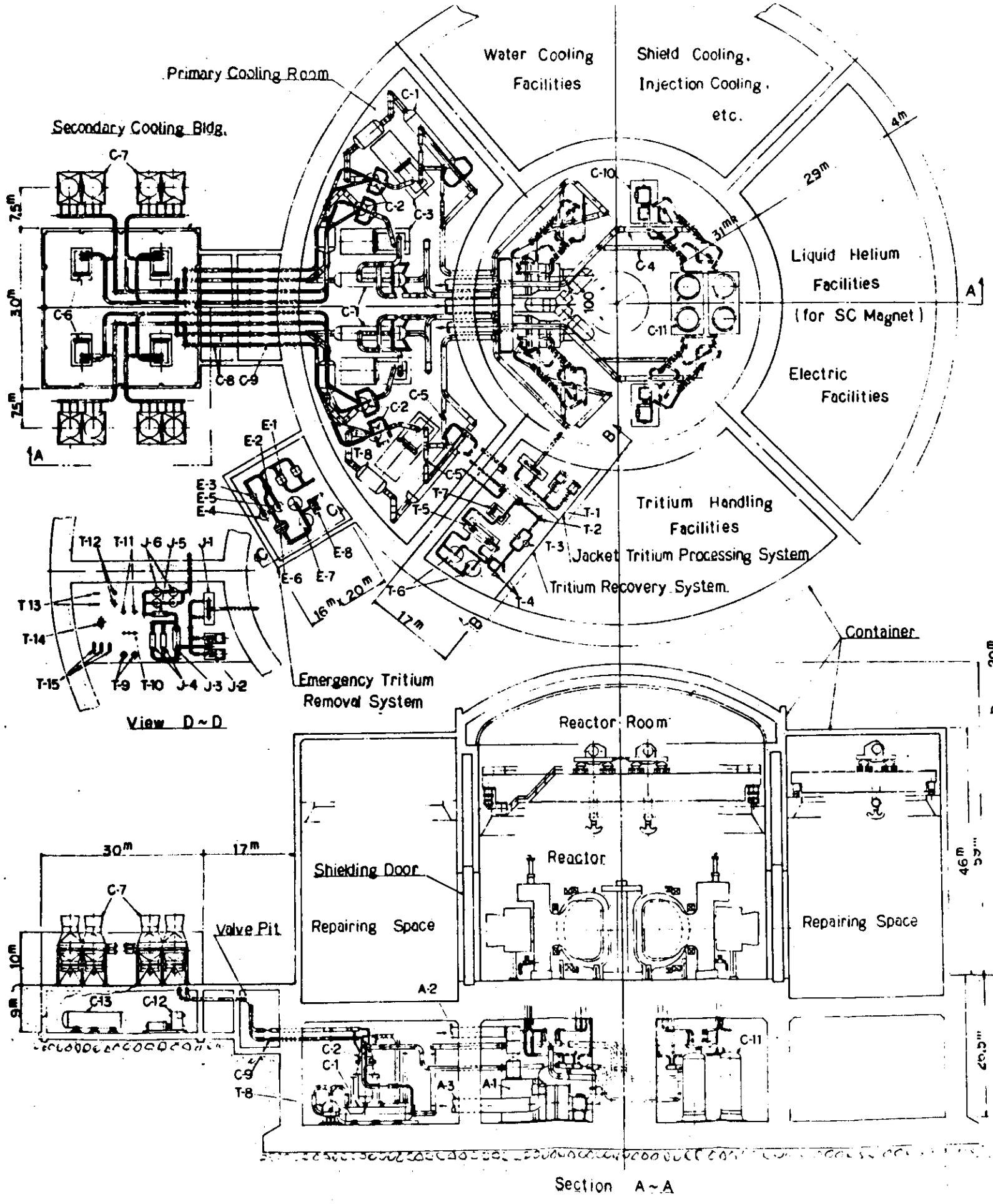

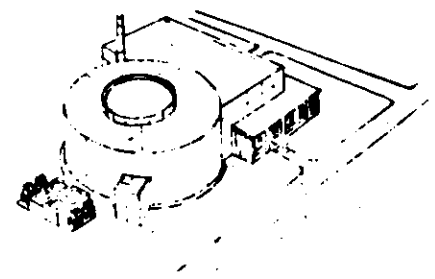

Plant Layout

Main Cooling & Auxiliary Systems

C-1 Heat Reservoir	C-8 Secondary Piping
C-2 Inter. Heat Exchanger	C-9 Isolation Valve
C-3 Primary Gas Circulator	C-10 Primary Dump Comp.
C-4 Primary Piping	C-11 Primary Dump Tank
C-5 Flow Control Valve	C-12 Secondary Dump Comp.
C-6 Secondary Gas Circulator	C-13 Helium Supply Tank
C-7 Air Cooler & Blower	

Tritium Recovery System

T-1 No.1 Heat Exchanger	T-9 Surge Tank
T-2 Cooler	T-10 Small M.S Tower
T-3 Dust Separater	T-11 Cold Trap
T-4 Large M.S Tower	T-12 Electric Cell
T-5 No.2 Heat Exchanger	T-13 Pd Membrane Permeater
T-6 Adsorptive Cold Trap	T-14 Isotope Separation System
T-7 Blower	T-15 Tritium Storage Tank
T-8 Catalyst Oxidizer	

Jacket Tritium Processing System

J-1 Filter	J-4 Catalyst Oxidizer
J-2 Blower	J-5 Cooler
J-3 Heat Exchanger	J-6 M.S Tower

Emergency Tritium Removal System

E-1 Filter	E-5 Catalyst Oxidizer
E-2 Heat Exchanger	E-6 Cooler
E-3 Heater	E-7 Adsorption Column
E-4 Cracker	E-8 Blower

Air Cooling System of Primary Cooling Room

A-1 Air Cooler Unit	A-3 Air Outlet Duct
A-2 Air Inlet Duct	

0 5 10 20m

Fig. 8.9 Main Cooling System Layout

9. Repair and Maintenance

The basic policy of the overhauling method is that a damaged segment of the reactor is exchanged for a new or checked one. On the other hand, the damaged segment is transported to the repair shop beside the reactor room, then it is repaired and stored. Plant layout of JXFR is shown in Fig.9.1.

Each segment is installed on a carriage which can be movable in radial direction. Eight shield doors, in order to pull out the segments, are furnished at the wall of the reactor room. Circular railways are set along the outside of the reactor room, and a "rotating carriage" moves on the rail. A damaged segment pulled out to the outside through a shield door is mounted on the rotating carriage. The rotating carriage transports the segment in front of a repair shop which is laid out just beside the railway. Then the segment is drawn into the repair shop, and a complete segment is sent out from the shop instead of the damaged one. The complete segment is sent into the reactor room by the reverse order of the damaged one.

The overhaul procedure for case of the blanket trouble is shown in Table 9.1. Then Fig.9.2 represents the time required from shutdown to reoperation of the reactor.

Table 9.1 Overhaul Procedure for Blanket Trouble

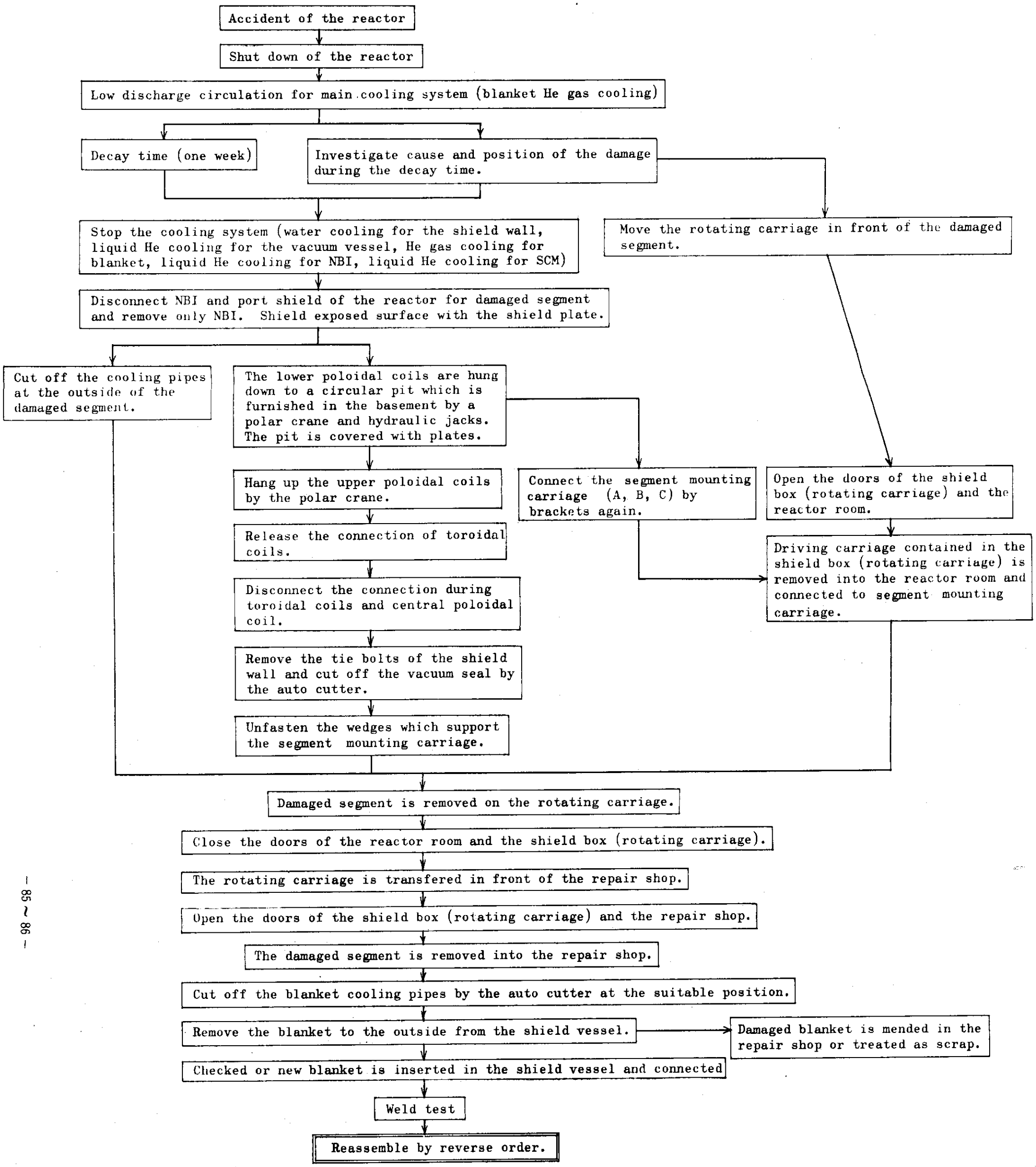

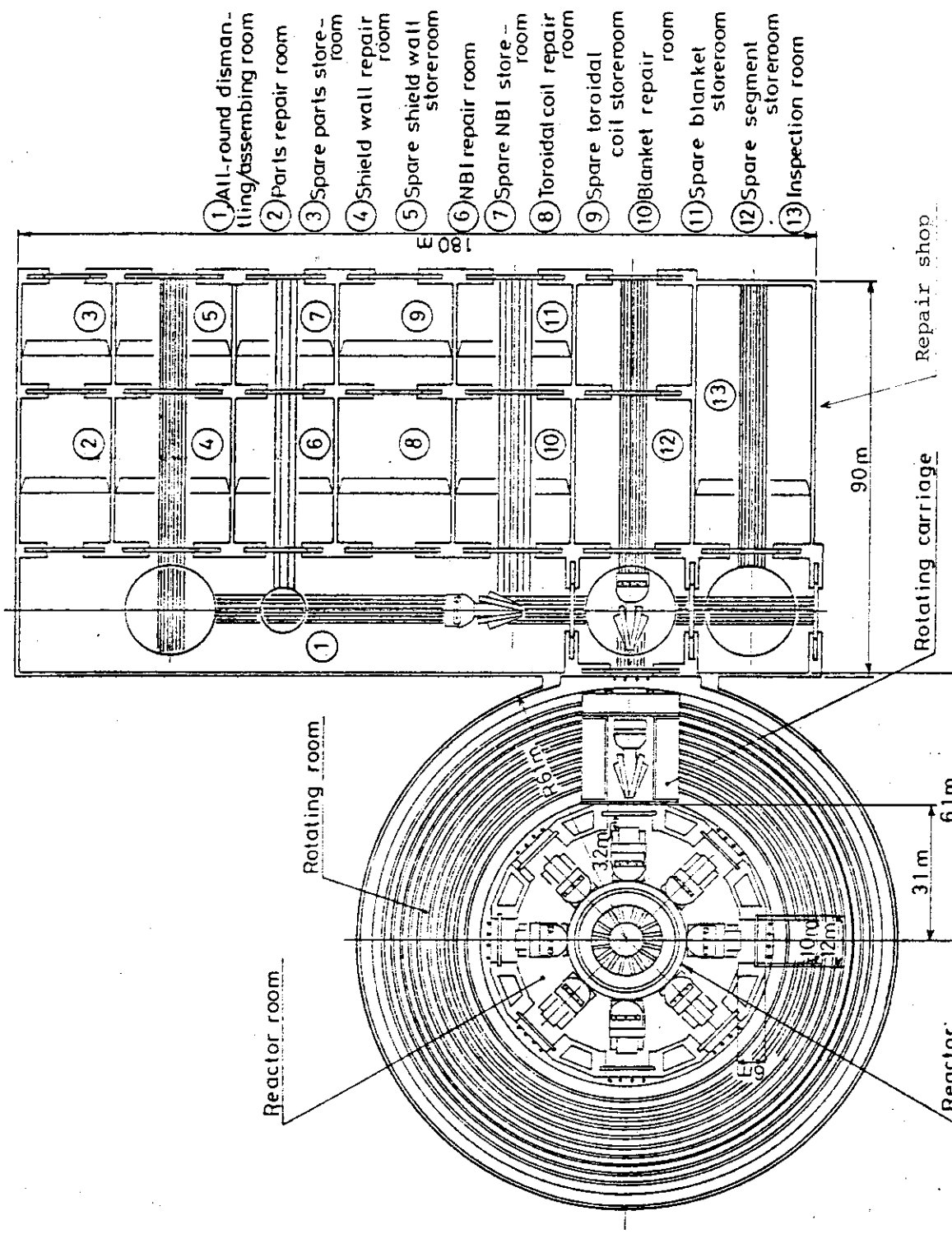

Fig. 9.1 PLANT LAYOUT

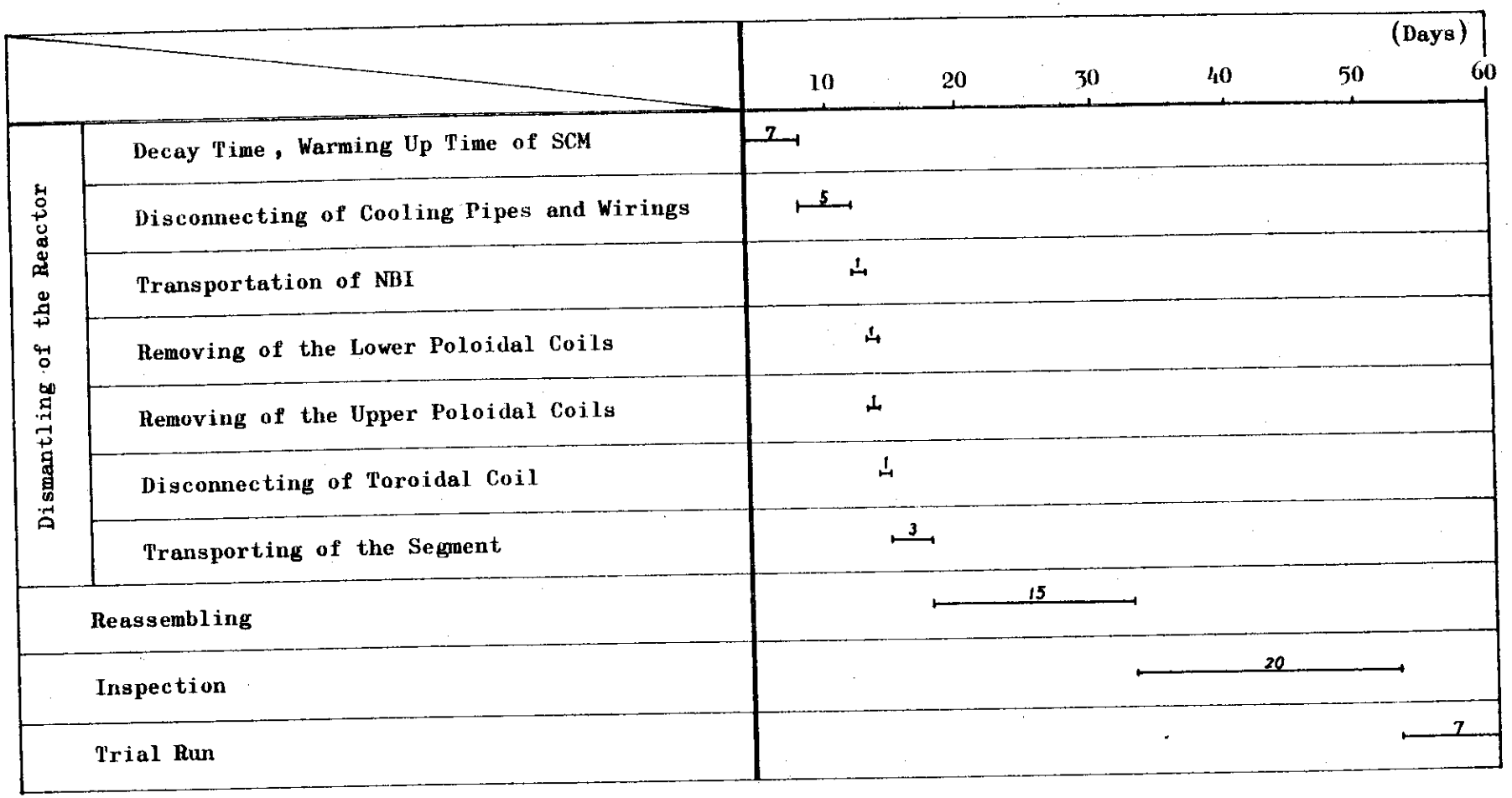

Fig.9.2 The Time Required from Shut Down to Reoperation of the Reactor

Appendix: Feasibility Study of JXFR-Upgrade

A.1 Introduction

The purpose of the JXFR design is to develop realistic solutions to a technological feasibility reactor which could be built in the near future with reasonable confidence, assuming a moderate beta value of 2.5 % for a circular plasma cross section.

If a higher beta value is available, two choices in the JXFR with fixed reactor dimension come in hand. One is to lower the toroidal field strength. This eases not only the magnet design but also the over all reactor structural design. The other is to raise power density. Since the former choice can be accomplished by easing the present design, it was not studied. Only the feasibility of the latter choice was studied. As a result it is shown that the present JXFR design can cope with the higher power density without changing most of the major component designs.

Preliminary results on the three major design items concerned with an enhancement of fusion power from 125 MW of JXFR to 450 MW are briefly described in the following. Main design parameters are listed in Table A.1.1. Figure A.1.1 shows a cross sectional view of the reactor which differs structurally from JXFR by the additional tube walls placed between protection walls and blankets.

Table A.1.1 Design parameters of JXFR-upgrade

Power	
Fusion power (MW)	450
Thermal power (MW)	500
Electrical power (MW) ,Gross	140
Net	60
Net thermal efficiency	18%
Wall loading (MW/m^2)	1.1
Operation mode	
Operation period (s)	180
Burn time (Flat top) (s)	120
Duty factor	0.667
Plant availability	0.75
Load factor	0.5
Reactor dimensions	
Major radius (m)	6.75
Plasma radius (m)	1.5
First wall radius (m)	1.75
Plasma volume (m^3)	300
Plasma	
Mean temperature (keV)	10
Mean ion density ($10^{14}cm^{-3}$)	1.4
Mean electron density ($10^{14}cm^{-3}$)	1.6
Effective charge	1.6
Confinement time (s)	3.7
Injection power (MW)	40
Toroidal field (T)	5.5
Safety factor	2.3
Poloidal beta	2.5
Toroidal beta	0.04
Plasma current (MA)	5.1

(continued)

Blanket structure	
Blanket module/Reactor	8
Blanket cells/Blanket module	284
Injection and evacuation hole/Blanket module	1
Nominal max. 1-st wall temp. (°C)	450
Materials	
Structural material	316SS
Blanket fertile material	Li_2O
Reflector material	Stainless steel & W
Tube wall material	Stainless steel
Protection wall material	Refractory material
Neutronics	
Neutron current at 1-st wall (n $cm^{-2}s^{-1}$)	3.4×10^{13}
Neutron wall loading (MW m^{-2})	0.8
First wall displacement damage rate (dpa y^{-1})	5.0
Max. helium production rate in 1-st wall (appm y^{-1})	56
Max. hydrogen production rate in 1-st wall (appm y^{-1})	170
Tritium breeding ratio	0.9 (1.0)
Nuclear heating per DT neutron (MeV n^{-1})	16.1
Total induced activity at one hour after shutdown (Ci) (after one year operation)	3.3×10^{8}

(continued)

Toroidal field magnet	
Number of coils	16
Bore, width/height (m)	7/11
Magnetomotive force (MAT)	186
Max. field strength (T)	11
Stored energy (GJ)	50
SCM material	Nb_3Sn
Neutral beam injector	
Deuterium beam energy (keV)	200
Injection power (MW)	50
Cooling system	
Number of loops	4
Coolant, pressure (kg cm^{-2})	He, 20
Inlet/outlet temp. (°C)	300/600
Flow rate (kg/s)	318
Secondary system	He
Third system	Steam turbine
Tritium inventory (kg)	
Fuel recirculating system	0.6
Tritium recovery system including blanket	0.2
Total inventory including storage	1.0

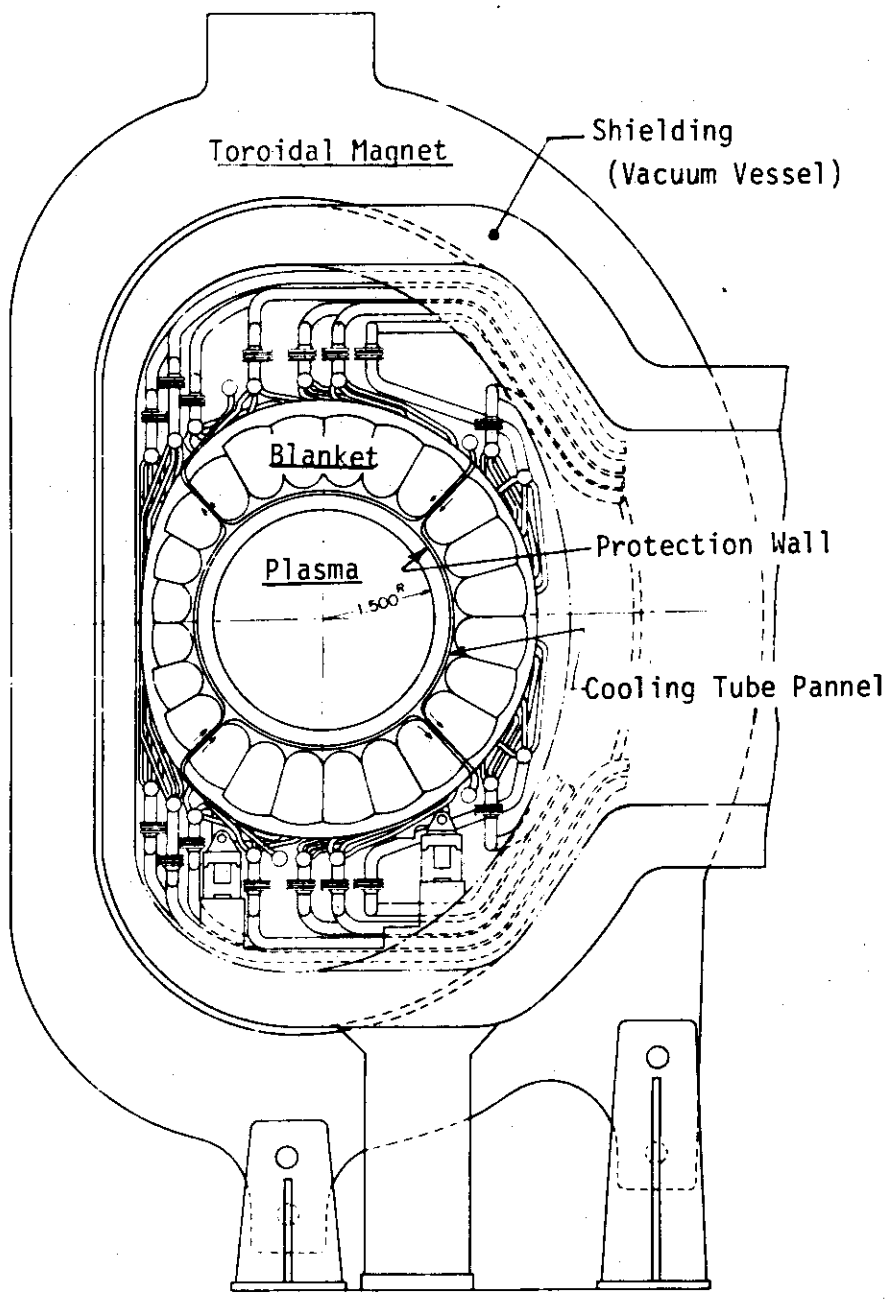

Fig. A.1.1 Cross section of the reactor

A.2 Plasma

In order to enhance the thermal power of JXFR to about 500 MW with the same dimension and toroidal field strength, the toroidal beta was increased to 4 %. The plasma parameters listed in Table A.1.1 were obtained from MHD equilibrium and power balance calculations. The safety factor of JXFR is reduced to 2.3 and the poloidal beta is increased to 2.5 near which current reversal occurs. The exponent α characterizing the functional form of toroidal current density is 1.25. The flux function, plasma pressure and current density profiles along the mid-plane are shown in Figs. A.2.1 to A.2.3. The magnetic axis is peaked slightly more to the outside than that of the JXFR plasma.

The impurity assumed is carbon of 2 %. The radiation loss due to ionization, recombination and excitation is estimated to be about half the bremsstrahlung loss. The required injection power to bring the plasma up to a self-ignition state at 10 keV during ten seconds is about 50 MW. At 10 keV, the required energy confinement time given by the same definition as in experiments is 2.4 seconds, while the empirical scaling of $\tau_E^*=5\times10^{-15}na^2$ gives 1.8 seconds, though the trapped-ion scaling given in WASH-1295 meets the required value. If the na^2 scaling law is applicable to future reactor plasmas, an improvement over the present value of about 1.5 times is required.

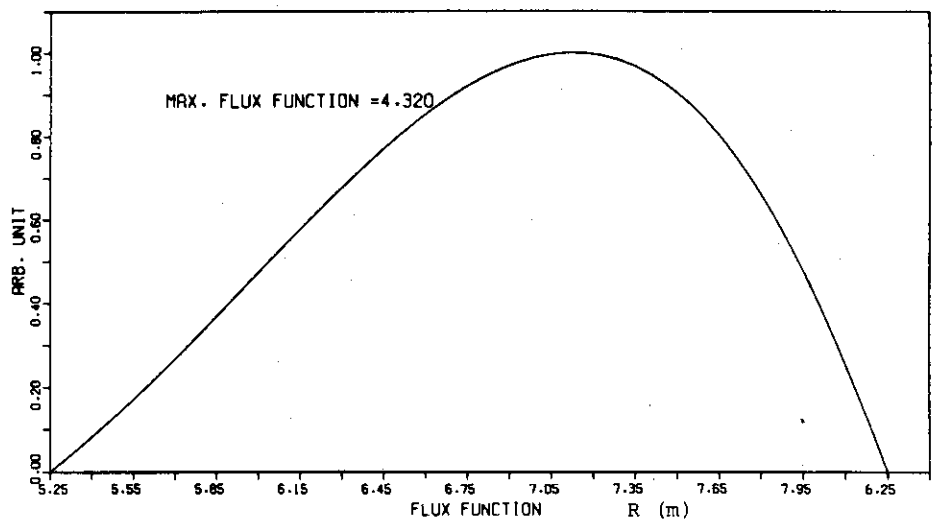

Fig. A.2.1 Flux function profile along the mid-plane

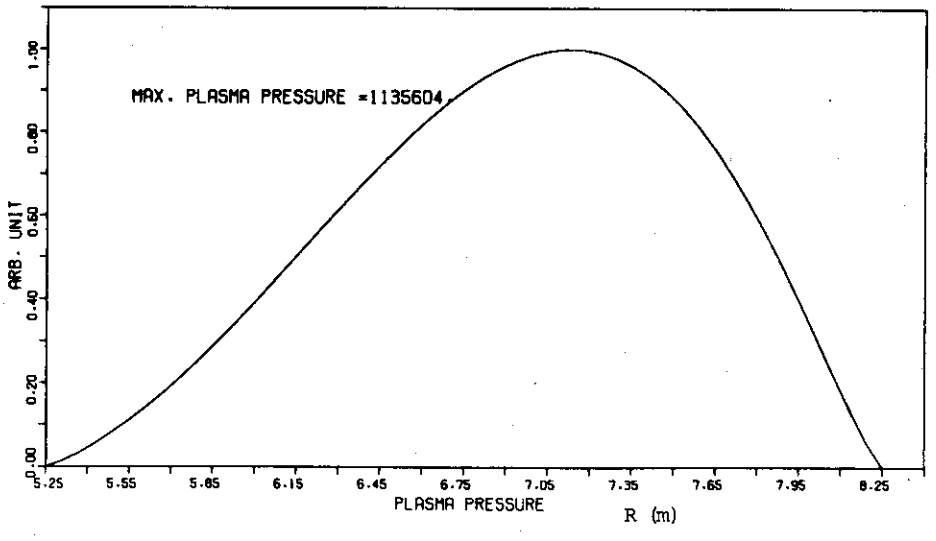

Fig. A.2.2 Plasma pressure profile along the mid-plane

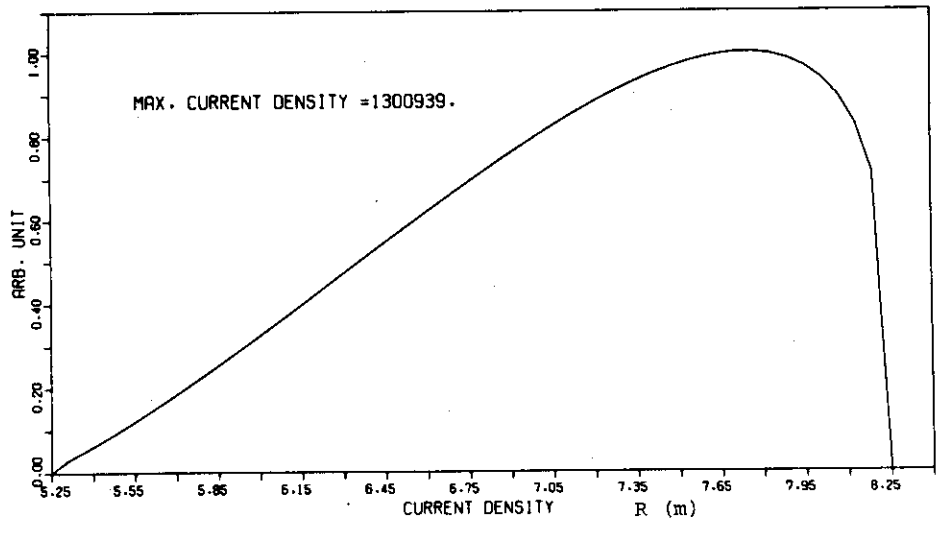

Fig. A.2.3 Toroidal current density profile along the mid-plane

A.3 Thermal and Hydraulic Design

Even when the wall loading is increased by nearly four times, a reasonable thermal and hydraulic design is shown to be feasible if helium coolant pressure of 20 kgf/cm^2 can be employed. In this case the installation of a cooling tube wall becomes a necessity.

(1) Temperature Calculation for Tube Walls

There are several combinations of a tube wall and the protection wall. They are shown in Fig.A.3.1. Calculated results for the Type-B and Type-E configurations will be discussed in the following. The heat load in the tube wall is about 30% of the total reactor power. Figure A.3.2 shows the cross-section of the Type-B cooling tube. The radiative heat flux ratio on the tube surface is shown in Fig.A.3.3. Figure A.3.4 shows the temperature distribution in the cooling tube when the helium coolant is 400°C. When the coolant is 300°C, the temperatures shown in the figure will be lowered by 100°C. The cross-section of the Type-E cooling tube and protection wall is given in Fig.A.3.5. The temperature distribution for this case is shown in Fig.A.3.6. The temperature in the cooling tube and hence the thermal stress on the tube becomes lower for the Type-E configuration than for the Type-B case.

(2) Temperature Distribution in the Blanket Vessel

The temperature distribution for the coolant inlet temperature 300°C and the outlet temperature 600°C, is shown in Fig.A.3.7.

(3) Evaluation

As far as the heat removal is concerned, the design is shown to be feasible.

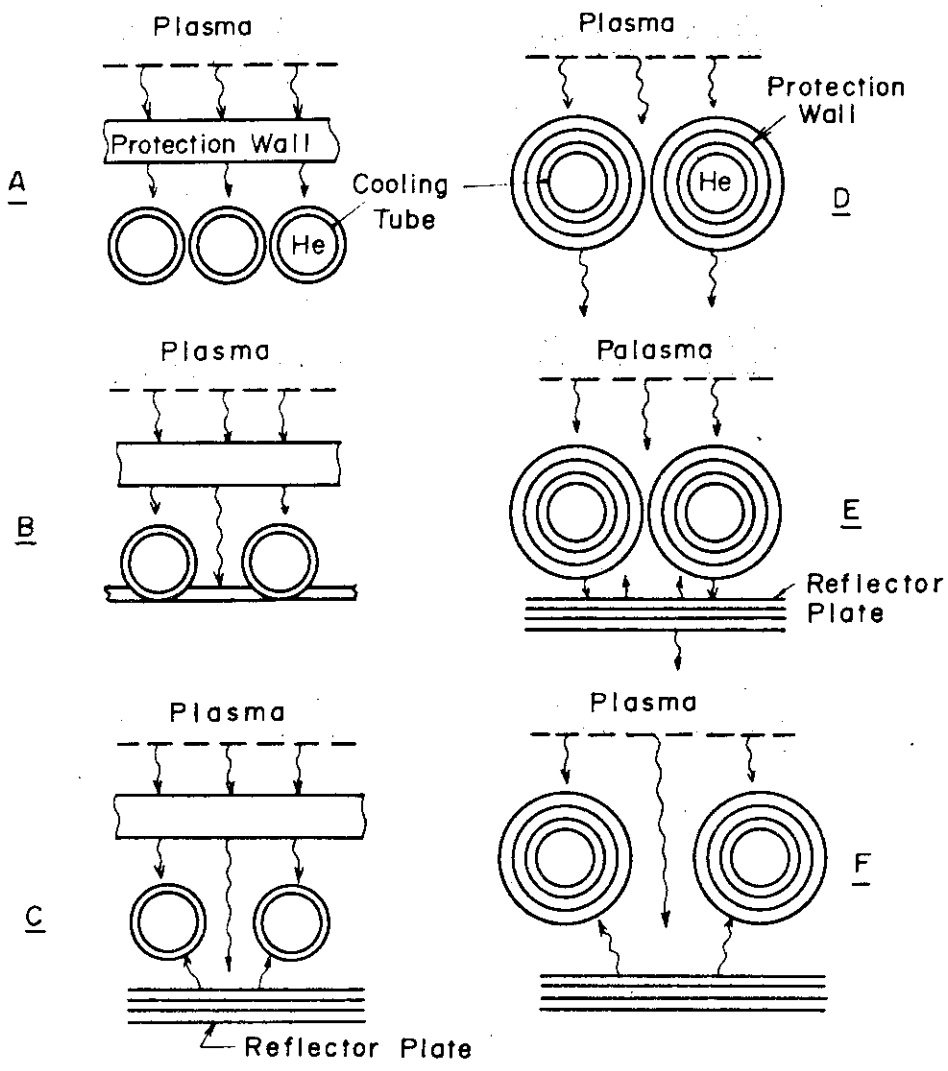

Fig.A.3.1 Possible configurations of the cooling tubes and protection wall

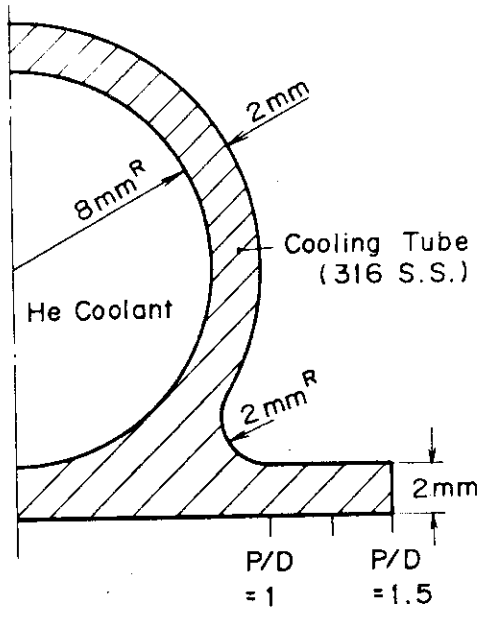

Fig.A.3.2 Cross-section of the Type-B cooling tube

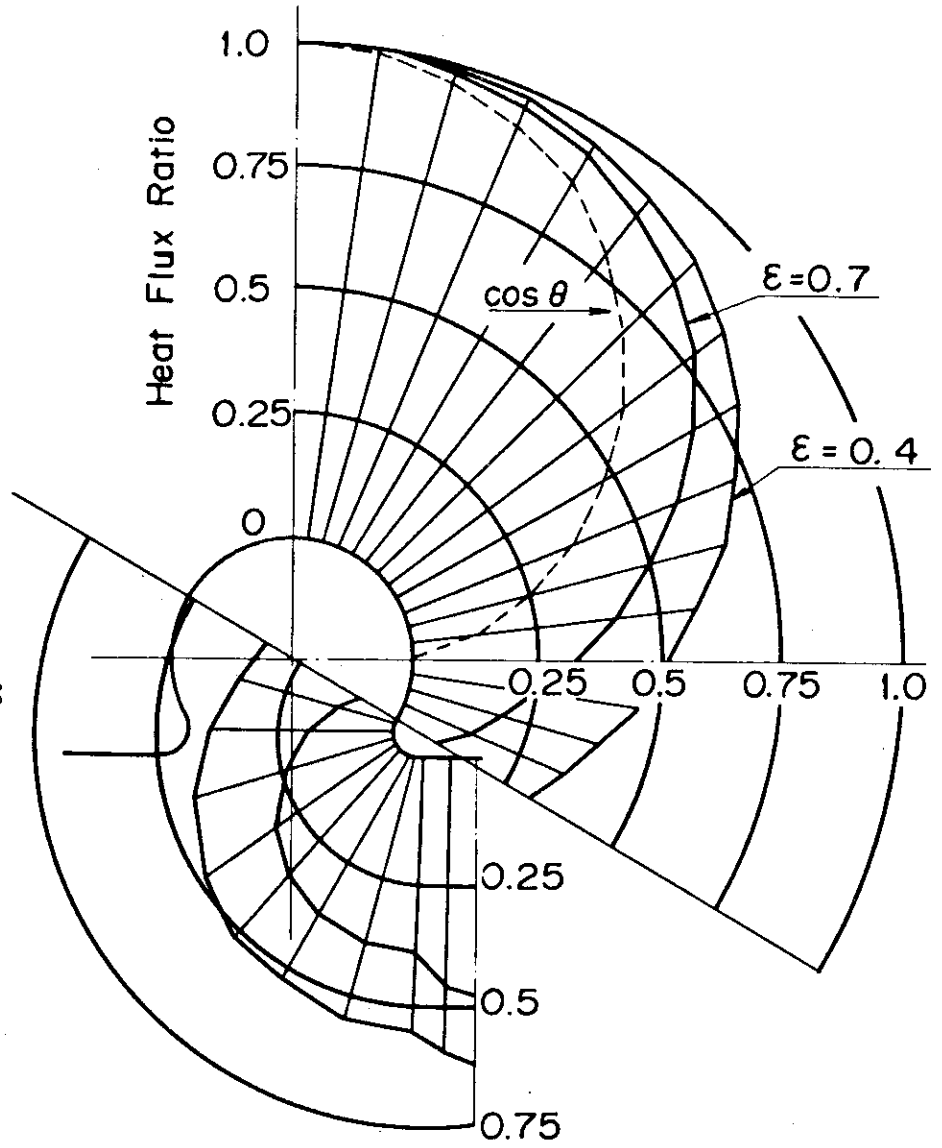

Fig.A.3.3 Radiative heat flux ratio on the tube surface

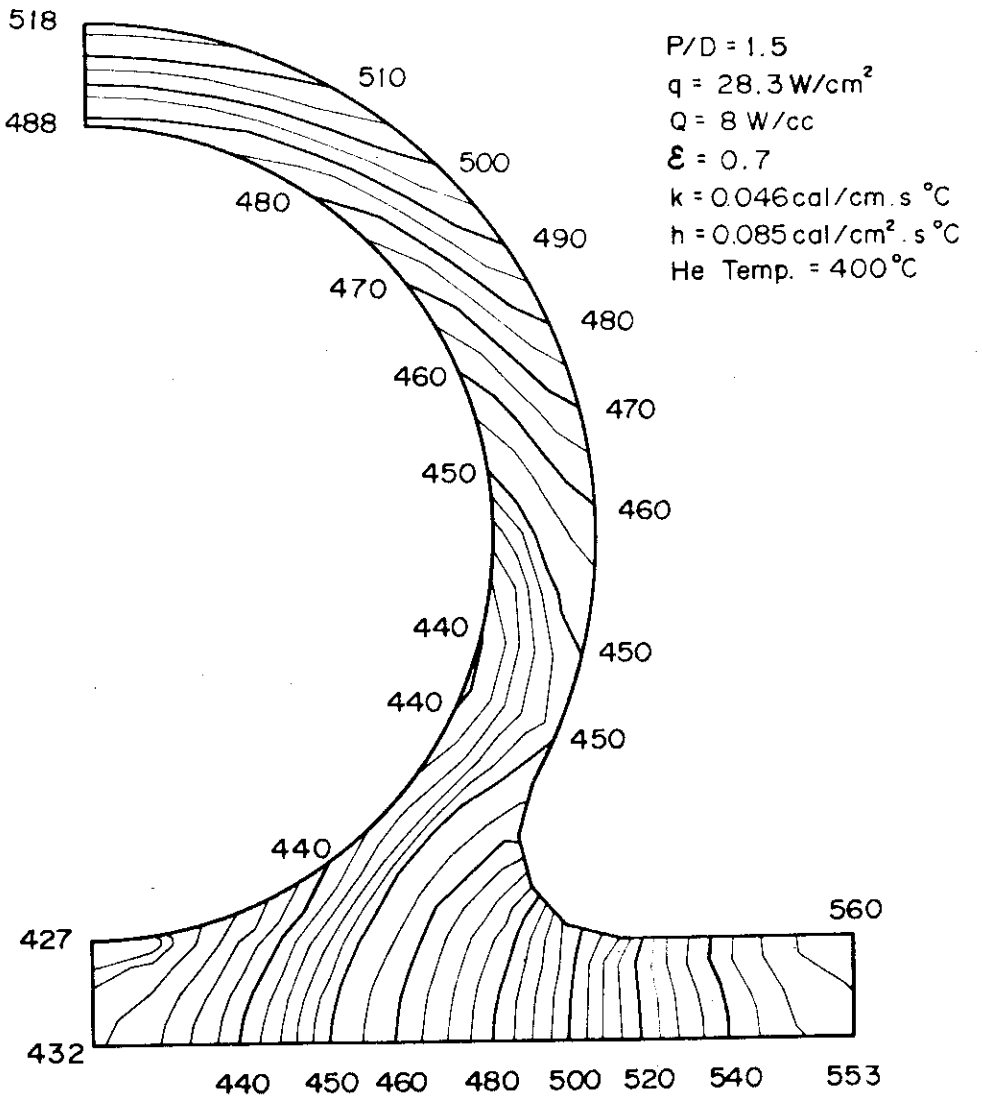

Fig.A.3.4 Temperature distribution in the cooling tube

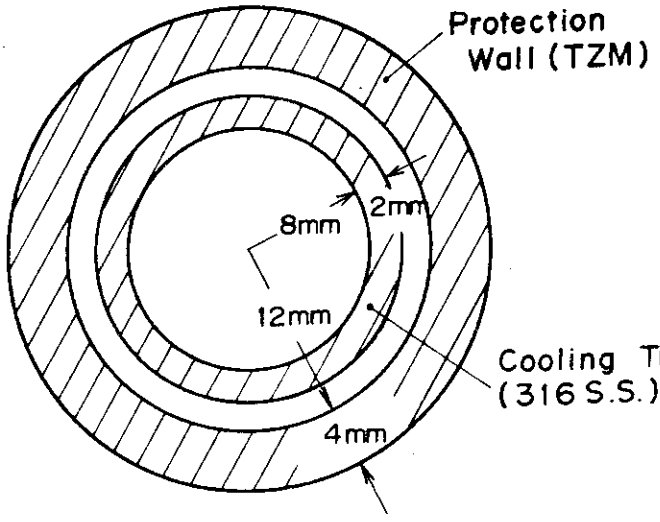

Fig.A.3.5 Cross-section of the cooling tube and protection wall

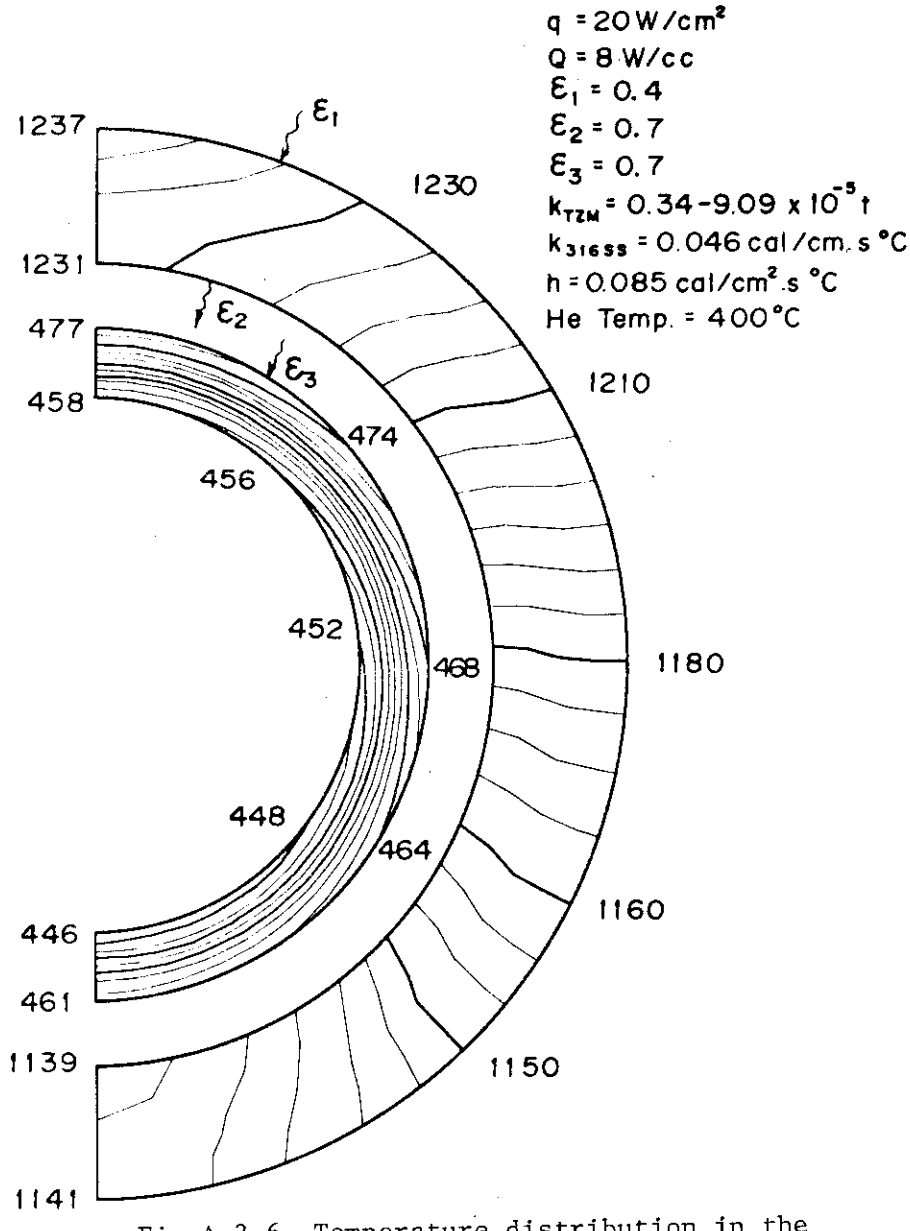

Fig.A.3.6 Temperature distribution in the cooling tube wall and protection wall

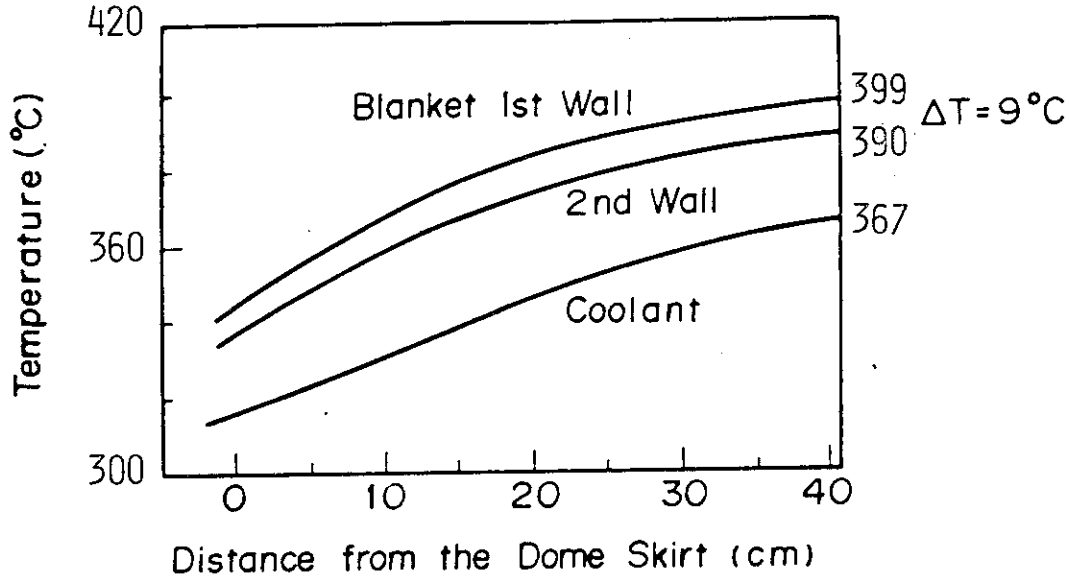

Fig.A.3.7 Temperature distribution in the blanket vessel wall (wall loading, 1MW/m^2)

A.4 Neutronics

When the neutron wall loading is increased four fold from 0.2 $MW \cdot m^{-2}$ to 0.8 $MW \cdot m^{-2}$, neutron and gamma fluxes and hence nuclear heating rate in the blanket, shield and magnets increase proportionally. Also the radiation dose around the reactor becomes 4 times larger. When the load factor of the reactor increases from 0.3 to 0.5 in addition to the above increase of the neutron wall loading, the cumulative fluence effects such as radiation damage effects and long lived induced activity will become 6.7 times larger.

Assuming the reactor life of 10 years, the integrated neutron wall loading over the lifetime for the first wall becomes 4 $MW \cdot m^{-2} \cdot y$. This is well below the estimated limit of ~10 $MW \cdot m^{-2} \cdot y$ for a stainless steel first wall. Tritium breeding ratio will be reduced somewhat due to the reduction of ^{7}Li $(n,n'\alpha)t$ reactions by the addition of cooling tubes to the protection wall, which will be placed in front of lithium oxide region of the blanket. Increased nuclear heating in the blanket will require proportional increase of heat removal capability of the primary cooling system, which seems to be of little problem. The nuclear heating in the SCM will still remain less than other sources of heat intrusion into the SCM.

The following shielding design bases have been adopted to cope with the power and load factor increase.

The shielding of the prototype reactor consists of the primary shield placed inside the toroidal field coils and the secondary shield which will also serve as the reactor building.

The requirements for the primary shield are:

(1) The protection of the superconducting magnets,

(a) by restricting the maximum dpa in copper stabilizer to 9.8×10^{-5},

with annealing every two years,

(b) by restricting the maximum neutron fluence to the Nb_3Sn superconductor to less than 10^{18} $n \cdot cm^{-2}$ during the lifetime of 10 years,

(c) by reducing the maximum nuclear heating rate in the SCM to less than 0.001 $W \cdot cm^{-3}$ and restricting the total nuclear heating in the SCM as low as practicable in view of cryogenic capacities,

(d) the radiation damage to the super insulations such as epoxy resin should be kept below the allowable level.

(2) Hands-on maintenance of the personnel should be permitted outside the primary shield one week after the shutdown of the reactor.

The requirements for the secondary shield are to reduce the following dose rates to allowable values:

(1) Dose rates during the reactor operation at the site boundary and at the outside secondary shield,

(2) Dose rate of the same places when one module is extracted from the whole reactor for repair and maintenance.

Results of the shielding calculations for the inner and outer shields of the superconducting magnets (SCM) are compared with the design criteria in Table A.4.1. Results of the biological shielding design are given in Table A.4.2.

Table A.4.1 Results of bulk shielding design of superconducting magnets for the prototype reactor

Items*)	Design criteria	Values at inner SCM	Values at outer SCM**)
Maximum dpa in copper ($dpa \cdot y^{-1}$)	4.9×10^{-5}	4.1×10^{-5}	9.0×10^{-8}
Maximum neutron fluence ($n \cdot cm^{-2}$)	1.0×10^{18}	5.4×10^{17}	2.5×10^{15}
Maximum nuclear heating rate ($W \cdot cm^{-3}$)	1.0×10^{-3}	2.8×10^{-4}	1.7×10^{-7}
Total nuclear heating in SCM (W)	——— +)	3060	
Maximum dose in Mylar++) (rad)	1.2×10^{8}	1.9×10^{9}	3.8×10^{6}

*) Load factor and reactor lifetime are assumed to be 50% and 10 years, respectively.

**) To take the effect of neutron streaming through the injection ports the values for outer SCM should be multiplied by 20~50.

+) As low as practicable for cryogenic capacities.

++) Epoxy resin or some other radiation resistent superinsulation must be used.

Table A.4.2 Maximum biological dose rates at various positions under various conditions for the prototype reactor

Conditions of the reactor and the types of radiations	Positions: In the reactor room (mrem/h)	Outside the concrete wall (mrem/h)	At 500m from the reactor (mrem/y)
Operation			
neutron	1.1×10^{6}	3.6×10^{-3}	2.3×10^{-2}
gamma-ray	5.4×10^{3}	5.0×10^{-3}	2.7×10^{-2}
total	1.1×10^{6}	8.6×10^{-3}	5.0×10^{-2}
One week after shutdown			
(i) Scheduled shutdown induced gamma-ray	10	-	-
(ii) One module extracted for repair induced gamma-ray	5×10^{8}	5×10^{-4}	-

ACKNOWLEDGEMENT

The authors are greatly indebted to Drs. S. Mori and Y. Obata for their encouragement. They also thank deeply to Dr. S. Nasu for the valuable information on solid blanket material (Li_2O).

They would like to acknowledge deeply the people from the industries who have participated in the design. They are:
Fuji Electric Co., Ltd. for the design of electric power supply system,
Hitachi, Ltd. for the design of plasma control and instrumentation,
Kawasaki Heavy Industries, Ltd. for the design of blanket structure and its cooling system with tritium recovery system,
Mitsubishi Industries Group (Mitsubishi Electric Co., Ltd., Mitsubishi Atomic Power Industries, Inc. and Mitsubishi Heavy Industries, Ltd.) for the design of magnets, shielding and fuel circulating system,
Sumitomo Heavy Industries, Ltd. for the design of repair and maintenance system, and
Tokyo Shibaura Electric Co. for the design of magnets and plasma heating facilities.

List of the publications related to the design

(1) Sako, K., et al. : "Conceptual design of a gas cooled Tokamak reactor," JAERI-M 5502 (in Japanese), (1973).

(2) Sako, K., et al. : Proc. of IAEA Workshop on Fusion Reactor Design Problems, Culham, 1974, 27 (Special Supplement of Nuclear Fusion, 1974).

(3) Ohta, M. et al. : "A consideration of ignition and shutdown of the JAERI Tokamak reactor", JAERI-M 5569, (1974)

(4) Yamato, H. and Ohta, M. : Proc. of the First Topical Meeting on the Technology of Controlled Nuclear Fusion", San Diego, 1974, Vol. 2, 309 (CONF-740402)

(5) Seki, Y., et al. : ibid., 77.

(6) Sako, K., et al. : Proc. of the 5th Conf. on Plasma Physics and Controlled Nuclear Fusion Research, Tokyo, 1974, Vol. 3, 535 (IAEA, Vienna, 1975).

(7) Iwai, K. and Seki, Y. : "Evaluation of gas production in the molybdenum structures of a fusion reactor" (in Japanese), JAERI-M 5855, (1974)

(8) Seki, Y., et al. : "Induced activity of the copper coil in D-T burning experiment" (in Japanese), JAERI-M 5862, (1974).

(9) Seki, Y, : "Evaluation of shielding design of superconductiog magnet (I)" (in Japanese), JAERI-M 6046, (1975).

(10) Sako, K. : "Design study of a heat reservoir system for the Tokamak reactor" (in Japanese), JAERI-M 6099, (1975).

(11) Tone, T. and Yamato, H. : "Preliminary study on power balance in the plasma of an experimental fusion Reactor" (in Japanese), JAERI-M 6453, (1976).

(12) Iida, H., et al. : "Neutronics of the blanket in a JAERI experimental fusion reactor" (in Japanese), JAERI-M 6460, (1976).

(13) Ide, T., et al. : "Evaluation of neutron streaming through injection ports in a Tokamak-type fusion reactor," JAERI-M 6475, (1976).

(14) Yamato, H., et al. : "Basic plasma parameters of an experimental fusion reactor", JAERI-M 6484, (1976).

(15) Seki, Y. : "Gas production rates in lithium exide of fusion reactor blanket", J. Nucl. Sci. Technol, 12, 12, 769 (1975)

(16) Seki, Y., et al. : "Evaluation of shielding design for super-

conducting magnets (Ⅰ) " (in Japanese), JAERI-M 6540 (1976).

(17) Iida, H., et al. : "Induced activity and dose rates in the JAERI experimental fusion reactor (JXFR)" (in Japanese), JAERI-M 6639, (1976).

(18) Fusion Reactor System Laboratory : "Preliminary design of an experimental fusion reactor (Interim Report)" (in Japanese), JAERI-M 6670, (1976).

(19) Ide, T., et al. : "Calculation of the neutron radiation damage in D-T fusion reactor materials" (in Japanese), JAERI-M 6672, (1976).

(20) Tone, T., et al., : Proc. of the 2nd Topical Meeting on the Technology of Controlled Nuclear Fusion, Richland, 1976, Vol. Ⅱ, 975 (CONF-760935)

(21) Ioki, K., et al. : ibid., Vol. Ⅳ, 1273.

(22) Ide, T., et al. : ibid., Vol. Ⅰ, 395.

(23) Sako, K., et al. : ibid., Vol. Ⅰ, 607.

(24) Ichikawa, H., et al. : ibid., Vol. Ⅳ, 1259.

(25) Seki, Y. : "Neutronics design of fusion reactors and applications of blanket neutronics experiment to the design" (in Japanese), JAERI-M 6726, (1976).

(26) Seki, Y., et al. : "Evaluation of shielding design for superconducting magnets (Ⅱ)"(in Japanese), JAERI-M 6783, (1976).

(27) Maki, K., et al. : "Study on plasma ignition of JAERI experimental fusion reactor" (in Japanese), JAERI-M 6876, (1977).

(28) Sako, K., et al. : Proc. of the 6th Conf. on Plasma Physics and Controlled Nuclear Fusion Research, Berchtesgaden, 1976, Vol. Ⅰ, 239 (IAEA, Vienna, 1977).

(29) Fusion Reactor System Laboratory : "Design study of pumping system for tokamak fusion power reactor" (in Japanese), JAERI-M 6922

(30) Fusion Reactor System Laboratory : "Design study of superconducting poloidal magnets for tokamak fusion power reactor " (in Japanese), JAERI-M 6802 (1977).

(31) Fusion Reactor Systemem Laboratory : "Design study of electrical power supply system for tokamak fusion power reactor"(in Japanese), JAERI-M 6803 (1977)

(32) Fusion Reactor System Laboratory :"Design study of superconducting troidal fuell magnet for tokamak fusion power reactor" (in Japanese), JAERI-M 6921 (1977)

(33) Fusion Reactor System Laboratory : "Design study of repair and maintenance for tokamak fusion power reactor" (in Japanese), JAERI-M7198 (1977)

(34) Fusion Reactor System Laboratory : "Design study of cooling system for tokamak fusion reactor" (in Japanese), JAERI-M 7199 (1977)

(35) Fusion Reactor System Laboratory : "Design study of superconducting poloidal magnets for tokamak experimental fusion reactor" (in Japanese), JAERI-M 7200 (1977)

(36) Fusion Reactor System Laboratory : "Design study of superconducting inductive energy storages for tokamak fusion reactor" (in Japanese), JAERI-M 7201 (1977)

(37) Fusion Reactor System Laboratory : "Design study of neutral beam injector for tokamak experimental fusion reactor" (in Japanese), JAERI-M 7262 (1977)

(38) Fusion Reactor System Laboratory : "Design study of fuel circulation system for tokamak experimental fusion reactor" (in Japanese), JAERI-M 7293 (1977)

(39) Fusion Reactor System Laboratory : "Design study of superconducting toroidal field magnet for tokamak experimental fusion reactor" (in Japanese), JAERI-M 7298 (1977)

(40) Maki, K.*, Tone, T. and Yamato, H.**: "Studies on Plasma Shutdown of JAERI Experimental Fusion Reactor", JAERI-M 7635 (April 1978) (in Japanese).

(41) Maki, K.*, Tone, T. and Yamato, H.**: "Studies on Plasma Ignition of JAERI Demonstration Fusion Reactor", JAERI-M 7676 (May 1978) (in Japanese).

(42) Seki, Y. and Maekawa, H.: "Cross-Section Sensitivity Analysis of U-235 and U-238 Fission Rates Measured in a Graphite-Reflected Lithium Assembly", Nucl. Sci. and Eng. 66 (1978) 243.

(43) Iida, H., Seki, Y. and Ide, T.*: "Induced Activity and Dose Rate in a Fusion Reactor with Molybdenum Blanket Structure", J. Nucl. Sci. Tech. 14 (1977) 68.

(44) Sako, K. and Minato, A.*: "Blanket structure design for JAERI experimental fusion reactor", Proc. of the 7th Symposium on Engineer-

ing Problems of Fusion Research, Knoxville, 1977, Vol.II, 1490.

(45) Iida, H., Ide, T.* and Seki, Y.: "Nuclear Heat Deposition in Cryosorption Pumps of a Fusion Reactor", Proc. of the 7th Symposium on Engineering Problems of Fusion Research, Knoxville, 1977, Vol.II, 1658.

(46) Fusion Reactor System Laboratory:"Preliminary Safety Analysis of the Reactor Cooling System for Tokamak Experimental Fusion Reactor",JAERI-M 7772, (Sept. 1978).

(47) Fusion Reactor System Laboratory: "Repair and Maintenance Design for Tokamak Experimental Fusion Reactor", JAERI-M 7825, (Oct. 1978).

(48) Fusion Reactor System Laboratory: "Safety Analysis of Superconducting Toroidal Field Magnet for Tokamak Experimental Fusion Reactor", JAERI-M 7963, (Feb. 1979).

(49) Fusion Reactor System Laboratory: "Safety Analysis of Fuel Circulating System for Tokamak Experimental Fusion Reactor", JAERI-M 7964,(Dec. 1978).

(50) Fusion Reactor System Laboratory: "Safety Analysis of Superconducting Poloidal Magnets for a JAERI Experimental Fusion Reactor", JAERI-M 8140, (March, 1979).